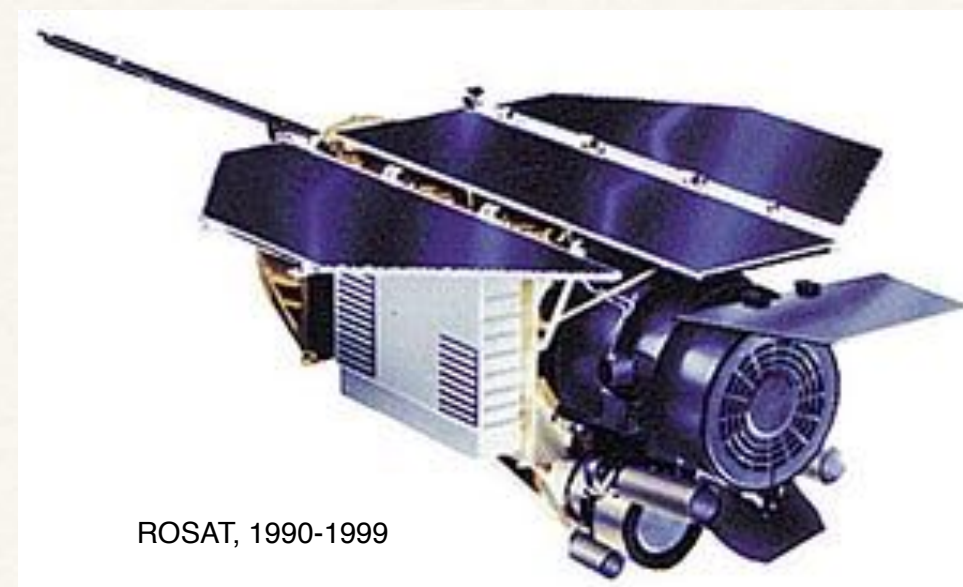


2024.07

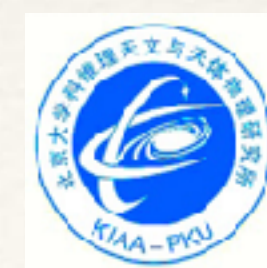


Detection of X-ray extended galaxy clusters with ROSAT and XMM-Newton data

Weiwei Xu
NAOC

Orcid: 0000-0002-9587-6683

Main collaborators: Thomas Reiprich, Florian Pacaud, Miriam Ramos-Ceja, Linhua Jiang, Bin Luo, Ran Li, W. N. Brandt



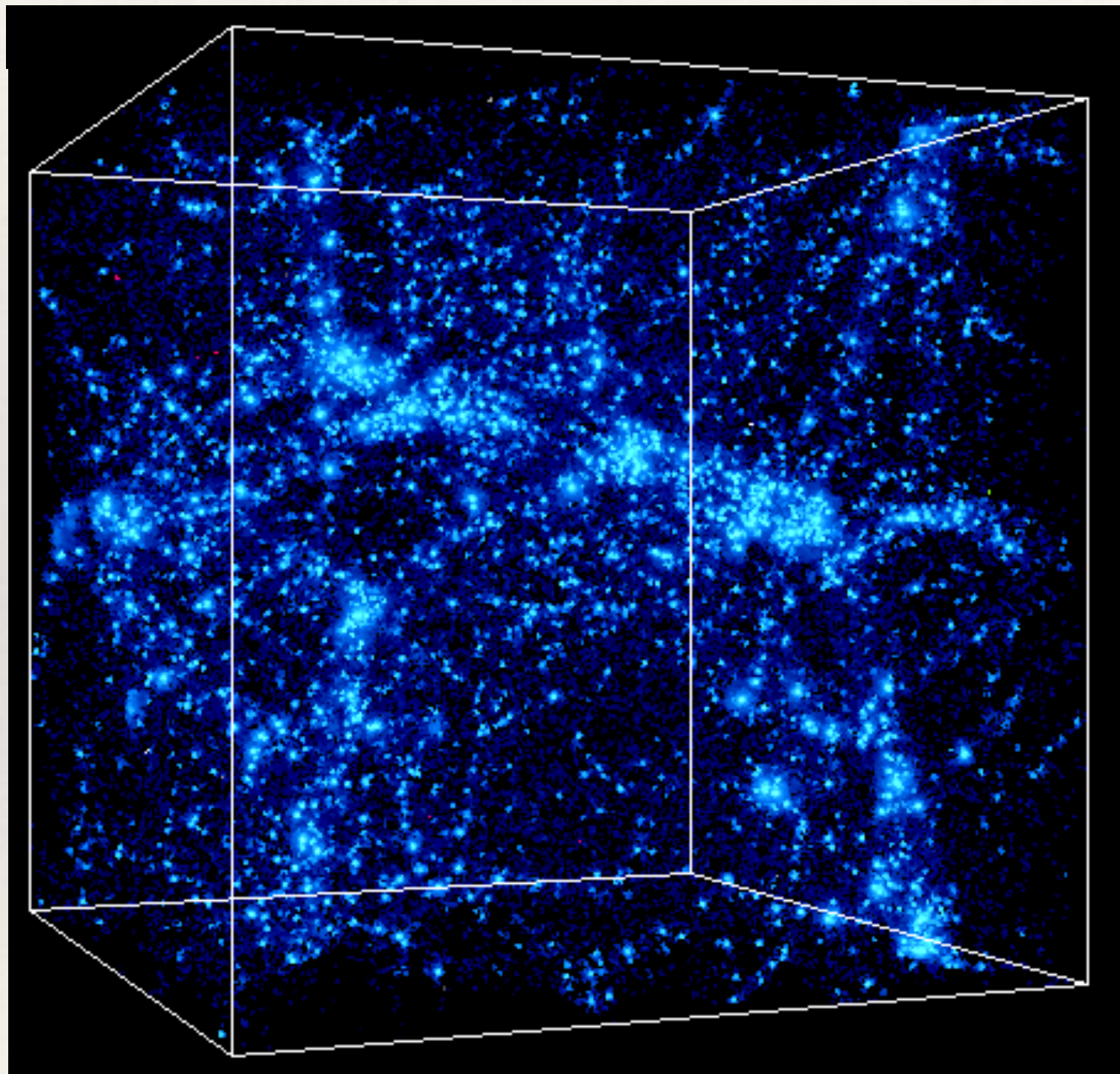
Outline

1. Overview of X-ray galaxy clusters
2. Detection of X-ray extended galaxy clusters
 - ❖ RXGCC (RASS-based extended X-ray Galaxy Cluster Catalog)
 - ❖ XVXGC (XMM-SERVS X-ray eXtended Galaxy Cluster catalog)
3. Summary

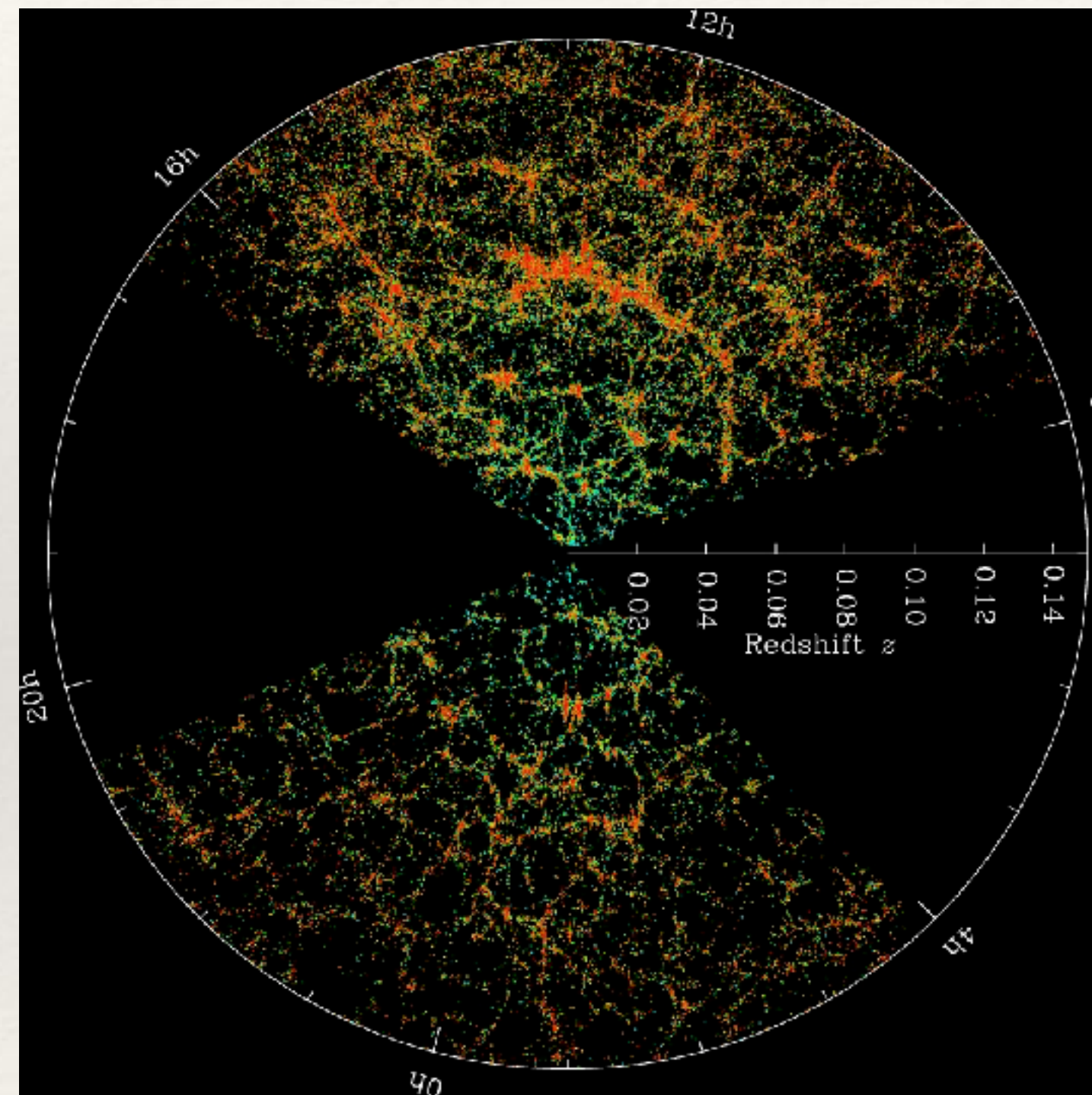
1. Overview of X-ray galaxy clusters

Simulations and Observations of clusters

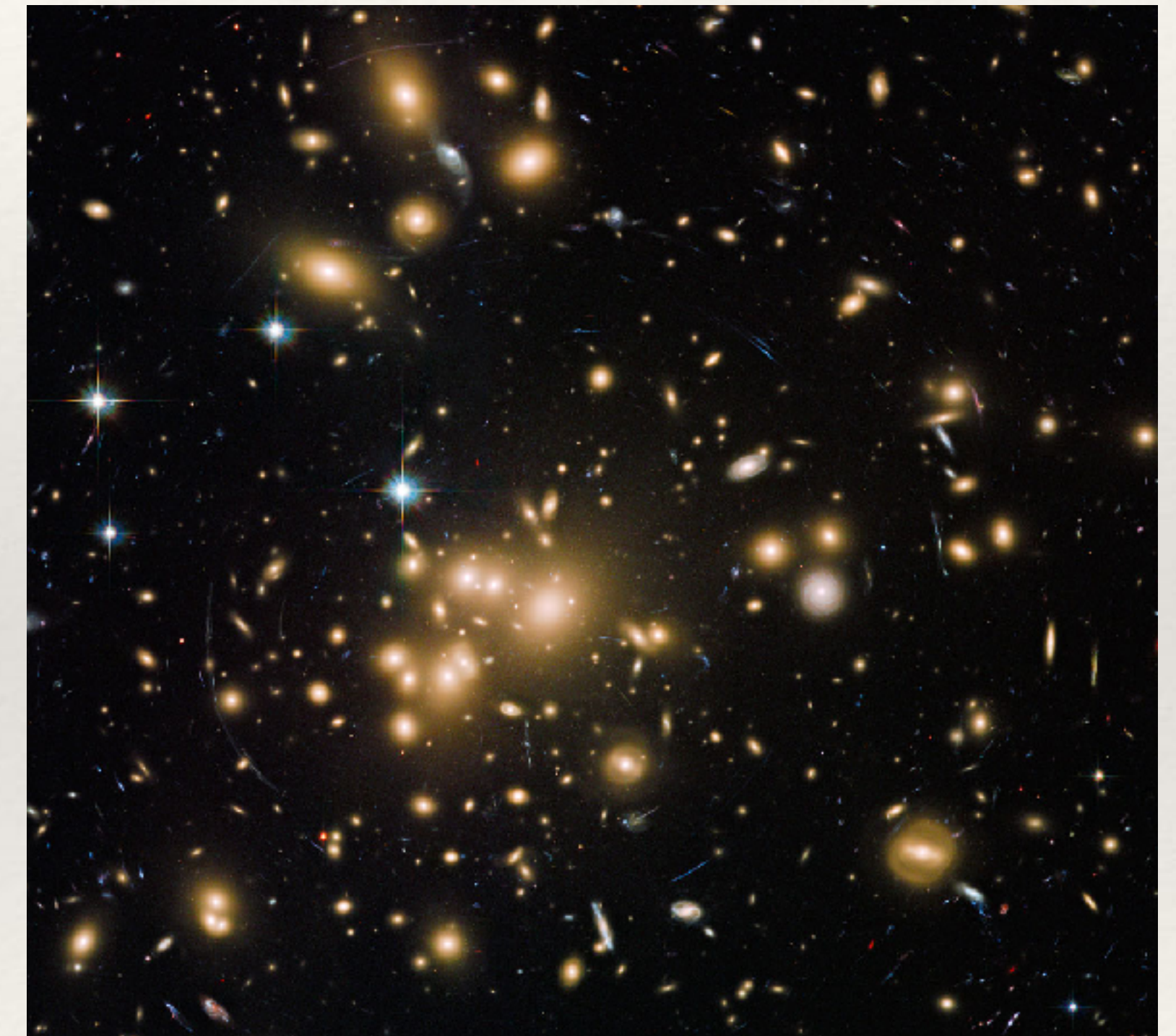
- ❖ In both simulation and observation, the spatial distribution of galaxies are not uniform.
- ❖ Galaxy clusters, the largest gravitational-bounded structure, are usually located at the nodes of filaments.



simulation (KICP)



SDSS



Abell 1689, HST (ESA/Hubble)

Cosmological constraints

Two major routes to constrain cosmological parameters:

- geometrical tests, using *absolute distance* (d_A)
 - ❖ f_{gas} (e.g., Sasaki 1996, Pen 1997)
 - ❖ cluster distance from X-SZ (e.g., Silk & White 1978)
- experiments of growth of structures

gas mass ($\propto d^{5/2}$) and total mass ($\propto d$)

$$f_{\text{gas}}(z) \propto d(z)^{3/2}$$

$$y \propto \int dx n_e(x) T(x)$$

$$d_A \propto \left(\frac{y_{\text{obs}}}{y_{\text{pred}}} \right)^2$$

$$y_{\text{pred}}(z) \propto d(z)^{1/2}$$

$$y_{\text{obs}} = y_{\text{SZ}}; y_{\text{pred}} = y_{\text{X}}; y_{\text{obs}} = y_{\text{pred}}$$

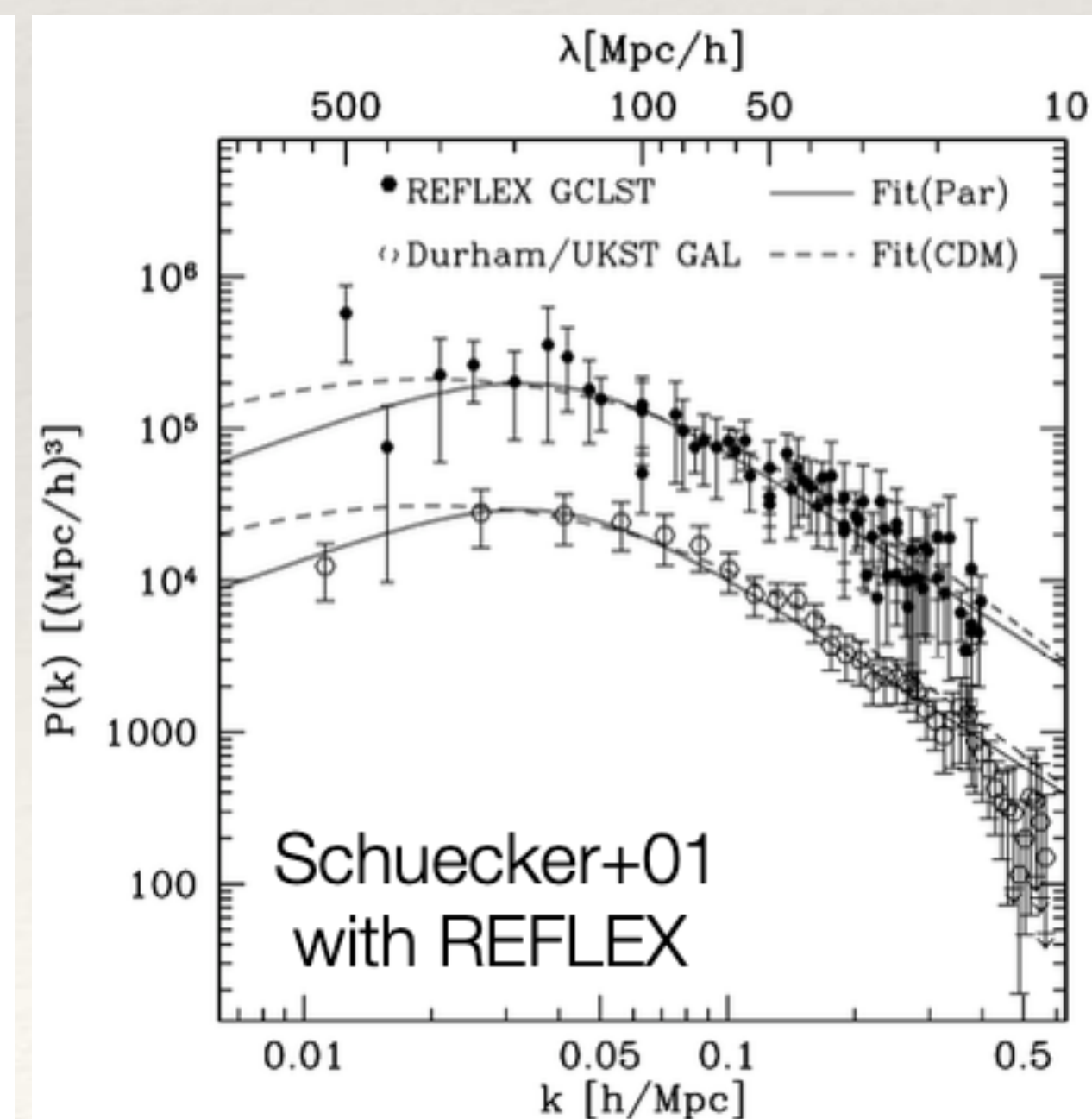
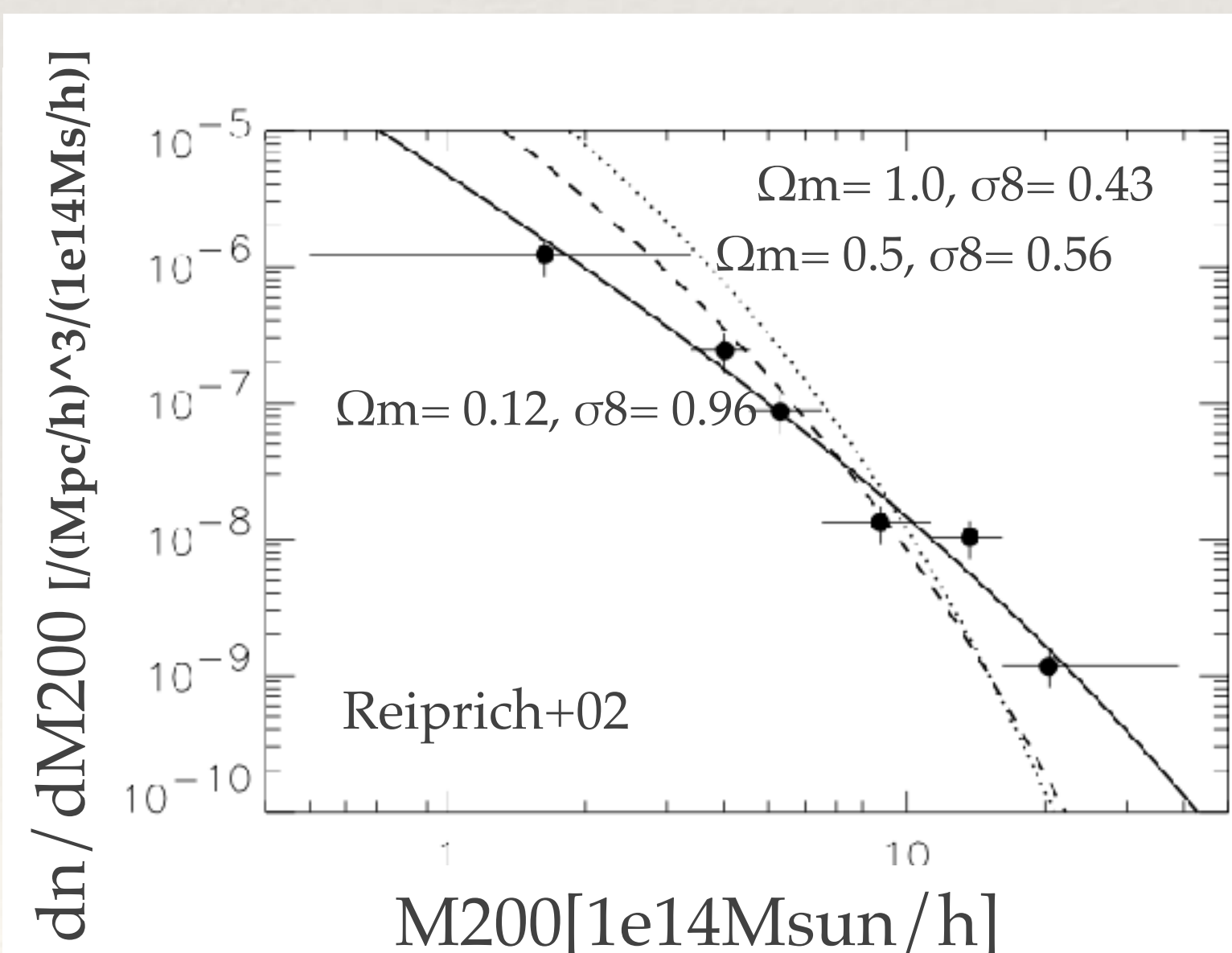
$$n(M, z) = \int_0^M f(\sigma) \frac{\bar{\rho}_m}{M'} \frac{d \ln \sigma^{-1}}{dM'} dM'$$

$$\sigma^2(M, z) = \frac{1}{2\pi^2} \int_0^\infty k^2 P(k, z) |W_M(k)|^2 dk$$

$$D(z) \equiv \frac{\delta(z)}{\delta(z_t)} \quad P(k, z) \propto k^{n_s} T^2(k, z_t) D(z)^2$$

$$\ddot{\delta} + 2 \frac{\dot{a}}{a} \dot{\delta} = 4\pi G \rho_m \delta$$

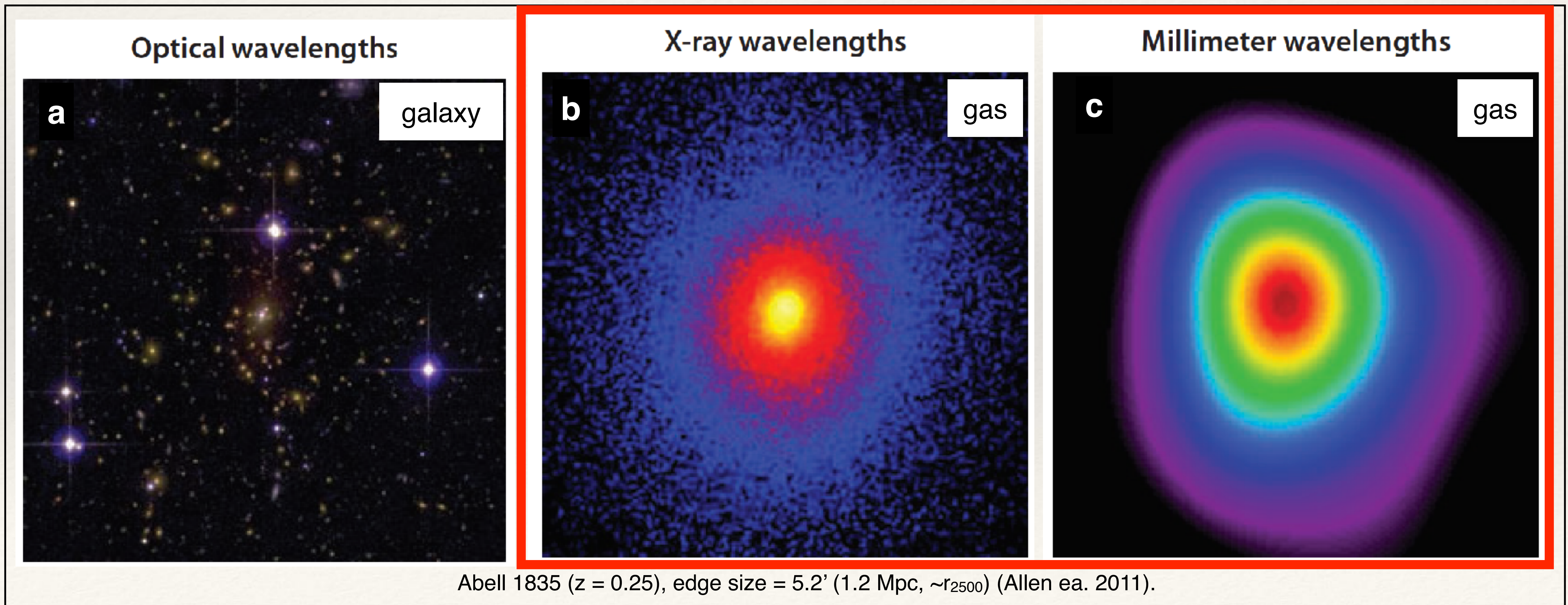
$$\frac{d \ln \delta}{d \ln a} = \Omega_m(a)^\gamma$$



Galaxy clusters

Galaxy clusters

- * galaxies (~ 100 - 1000 big ones), $\sim 5\%$,
- * Intra-cluster median (ICM, gas, $M_{\text{gas}} \sim 10^{13}$ - $10^{14} M_{\odot}$, $T_{\text{gas}} \sim 1$ - 10 keV), $\sim 15\%$,
- * dark matter, $\sim 80\%$.

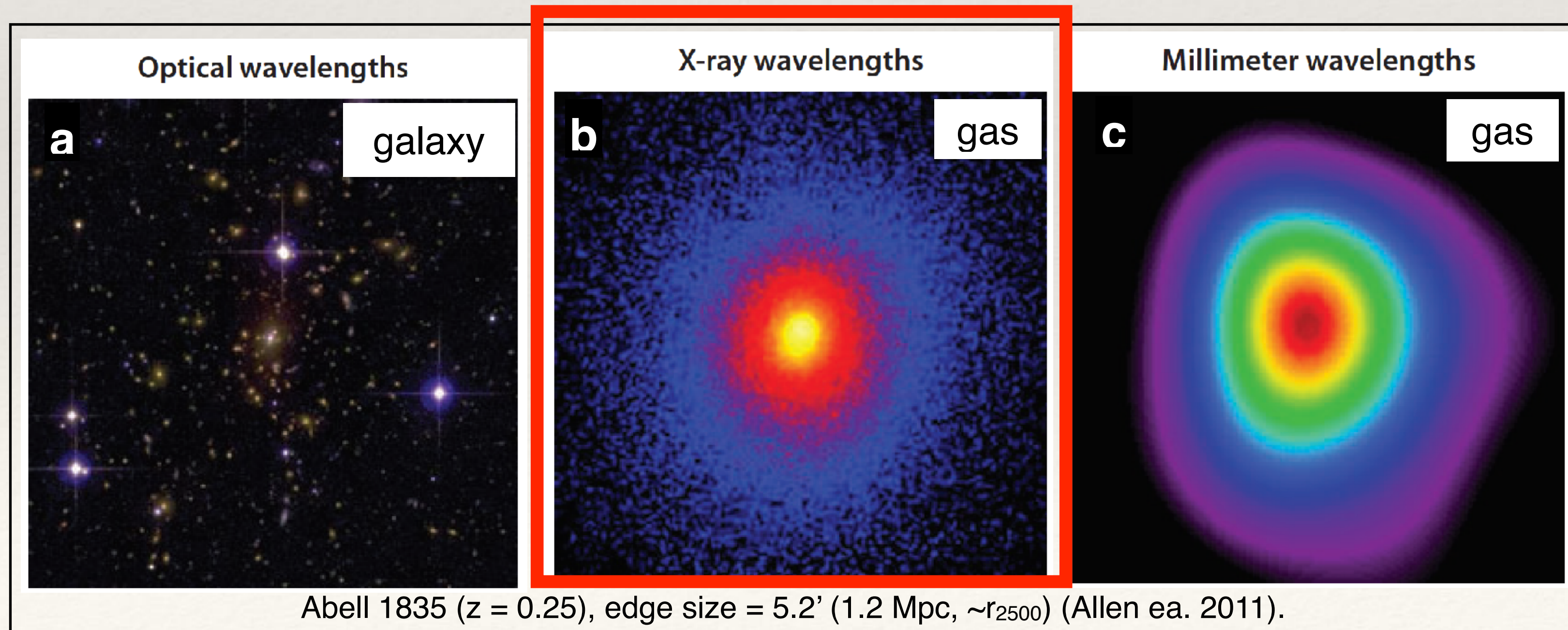


Galaxy clusters

- Optical/infrared band
 - galaxies (overdensity, color)
 - gravitational lensings

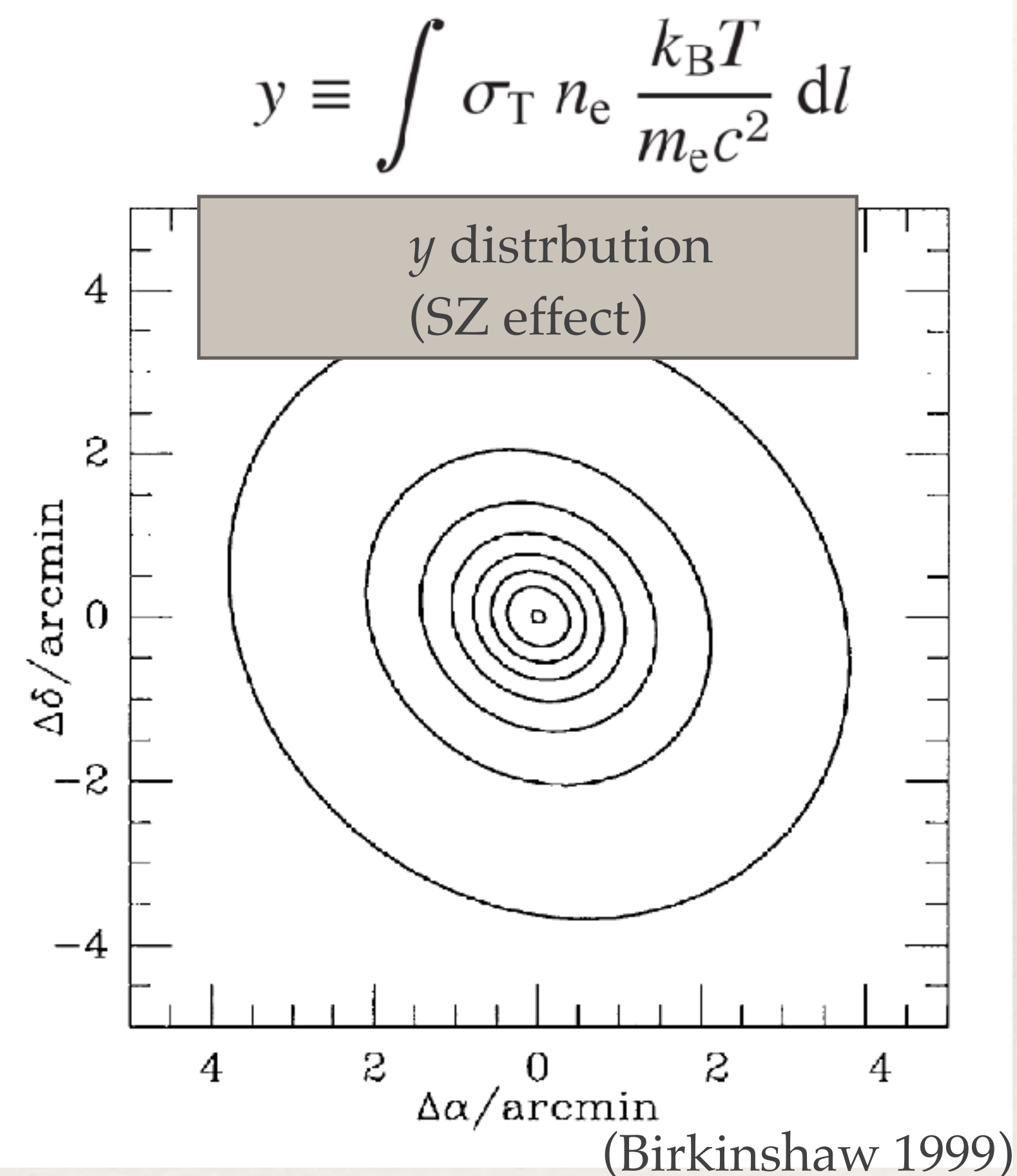
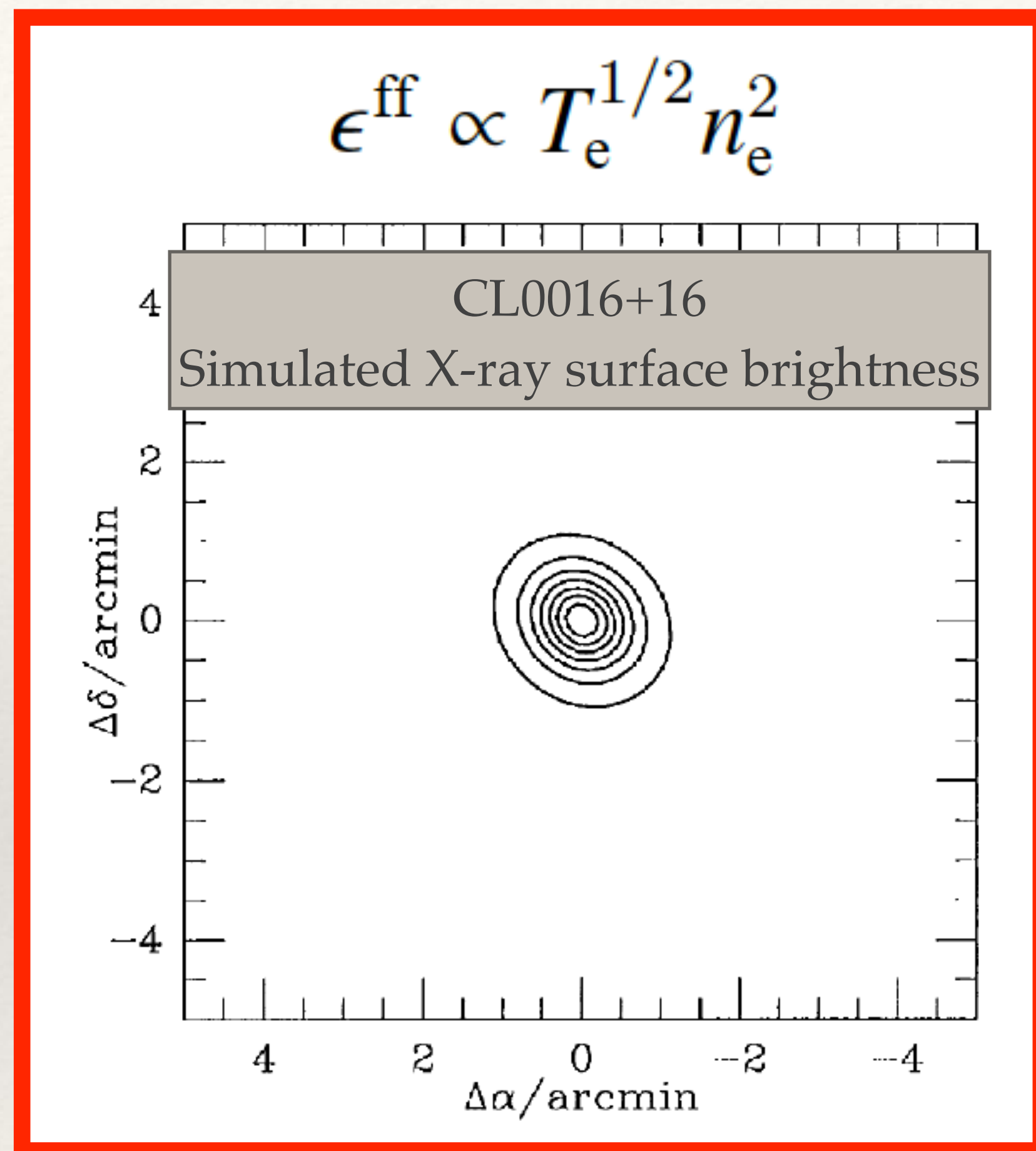
- X-ray band
 - thermal bremsstrahlung of ICM and line emission
 - less projection effects,
 - trace genuine gravitational potential wells,
 - L_x tightly related with M

- mm/sub-mm band
 - SZ effect



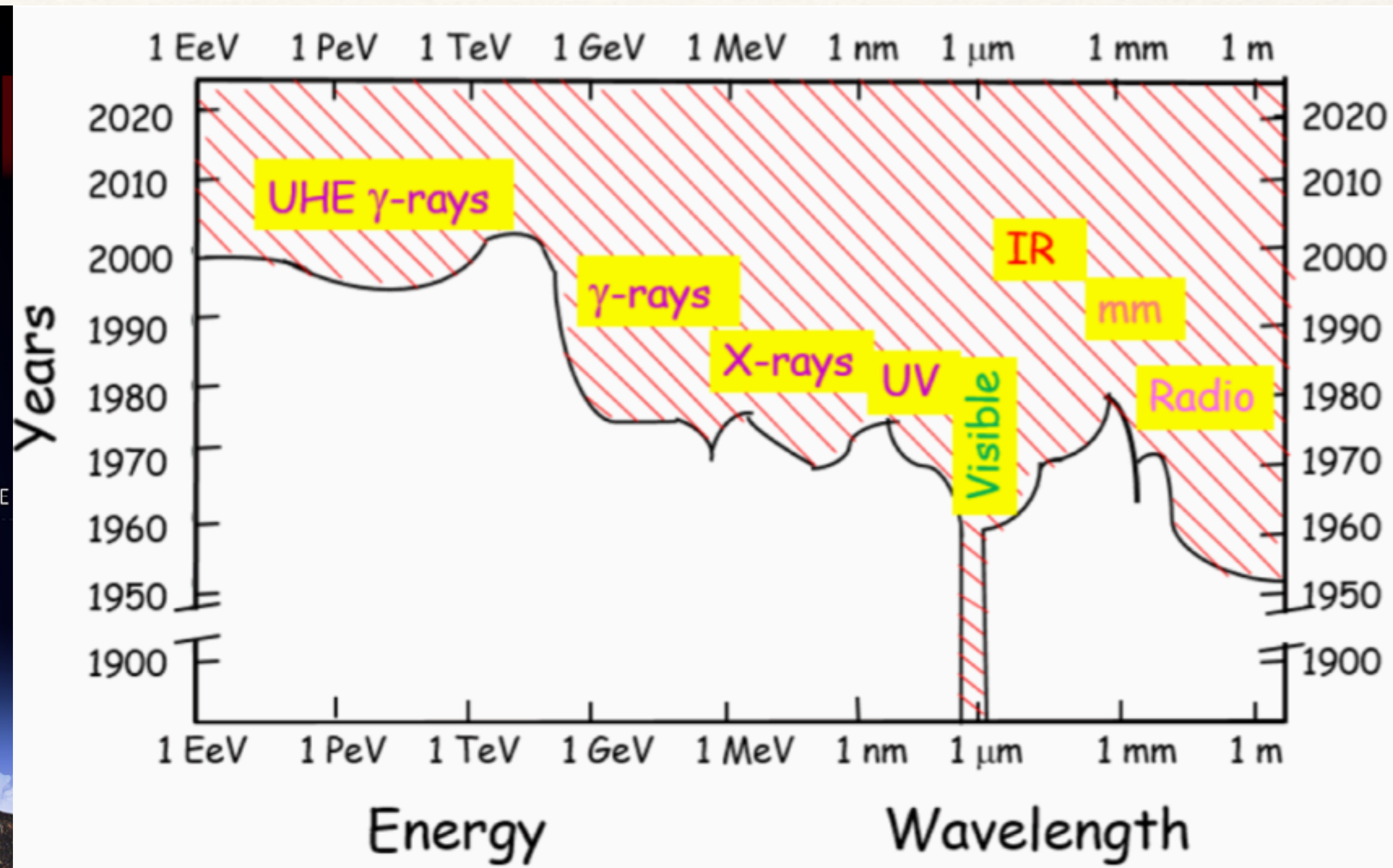
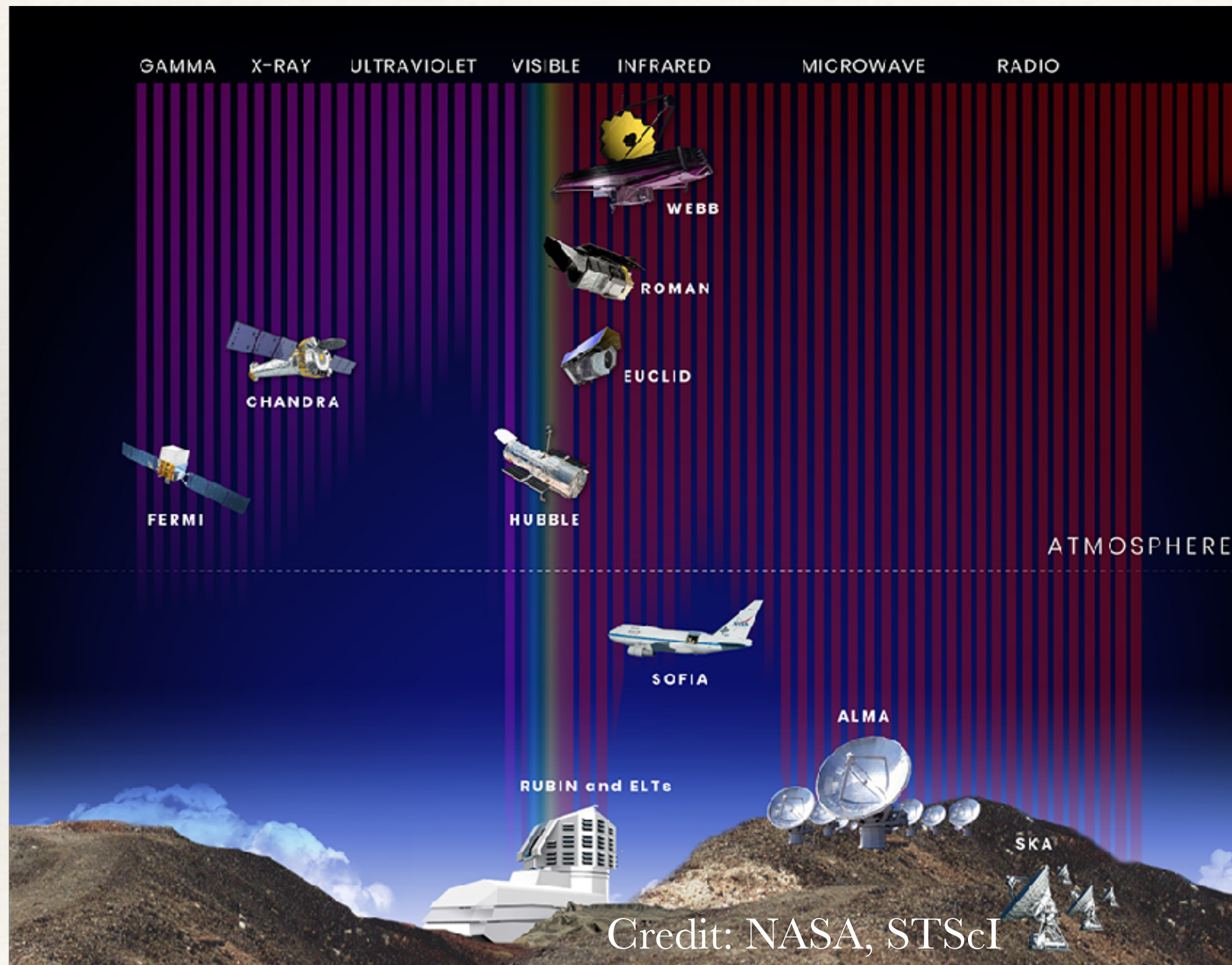
ICM observation

- X-ray surface brightness $\propto n_e^2$
- surface brightness with SZ effect $\propto n_e$
- X-ray emission is more compact than SZ effect



Contour level = 12.5% × Max.

Observations in multi-bands



First cosmic X-ray source

- ❖ 1962, with Geiger counters of an Aerobee rocket, the first X-ray source outside the solar system was detected, named as Sco X-1 (Tucker+85, Giacconi+62).

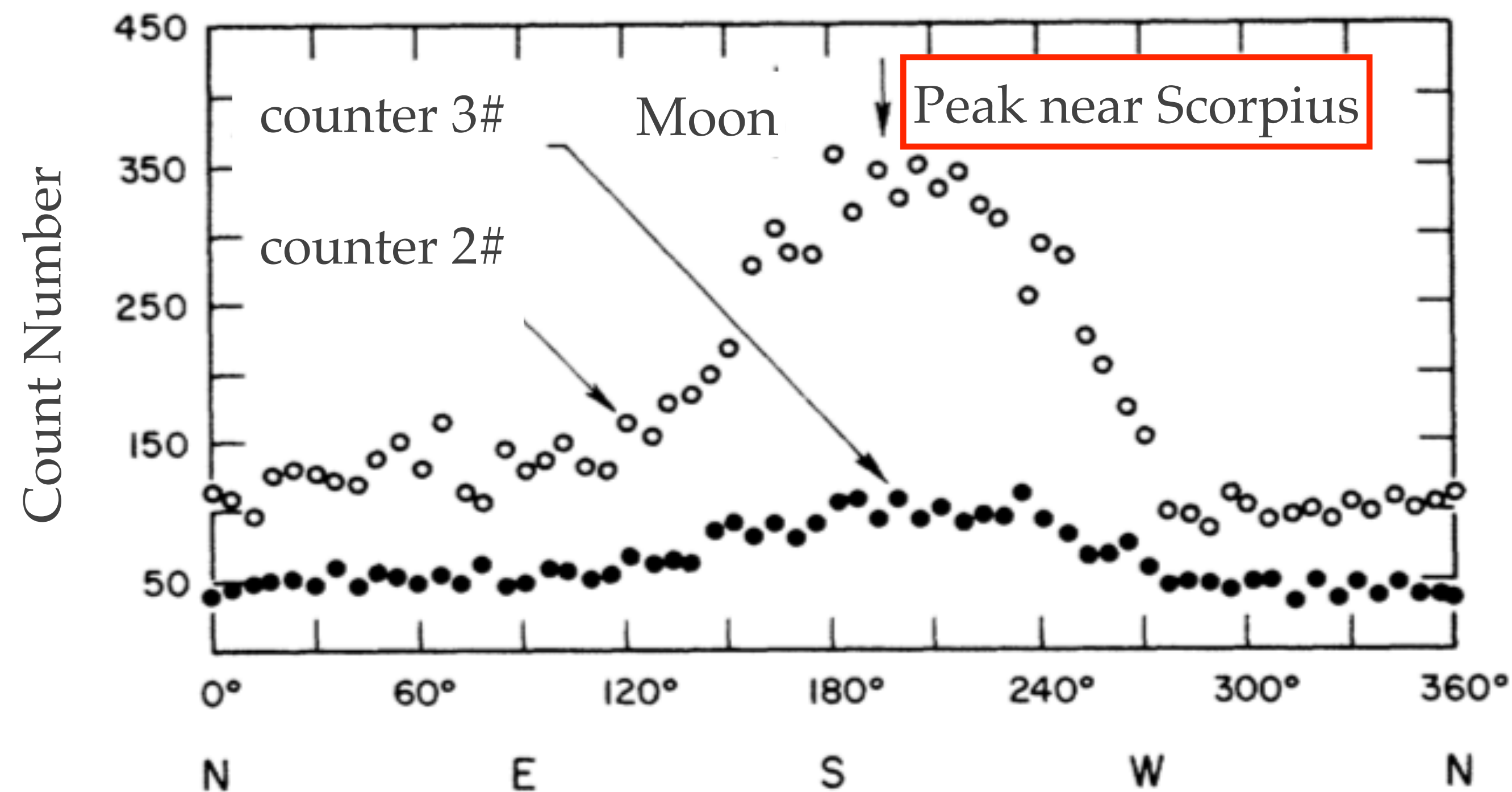


FIG. 1. Number of counts versus azimuth angle. The numbers represent counts accumulated in 350 seconds in each 6° angular interval.

X-ray sources

- Galactic sources: the Sun and its solar winds, comets, planets, stars, stellar winds, white dwarfs, cataclysmic variable stars, pulsars, neutron stars, black holes, binary systems, supernovae, supernova remnants, and the interstellar medium.
- Extragalactic sources: galaxies, AGN and galaxy groups and clusters.

Bands	sources
Gamma rays	nuclear reactions
X-rays	Gas in galaxy clusters, SNR, solar corona
Ultraviolet	SNR, very hot stars
Visible	Exterior of stars
Infrared	cool clouds of dust and gas; planets, satellites
Radio	dark dust clouds

First detection of X-ray emission from cluster

- ❖ The first detection of X-ray emission from the Perseus cluster occurred during an Aerobee rocket flight on March 1, 1970. The X-ray source may be associated with NGC 1275 (Per A, 3C 84), and was reported in 1971. If the source is NGC 1275, then L_x is about 4×10^{45} ergs/s (0.5-10 keV).

DISCOVERY OF AN X-RAY SOURCE IN PERSEUS

GILBERT FRITZ, ARTHUR DAVIDSEN, JOHN F. MEEKINS,
AND H. FRIEDMAN

E. O. Hulburt Center for Space Research, Naval Research Laboratory,
Washington, D.C. 20390

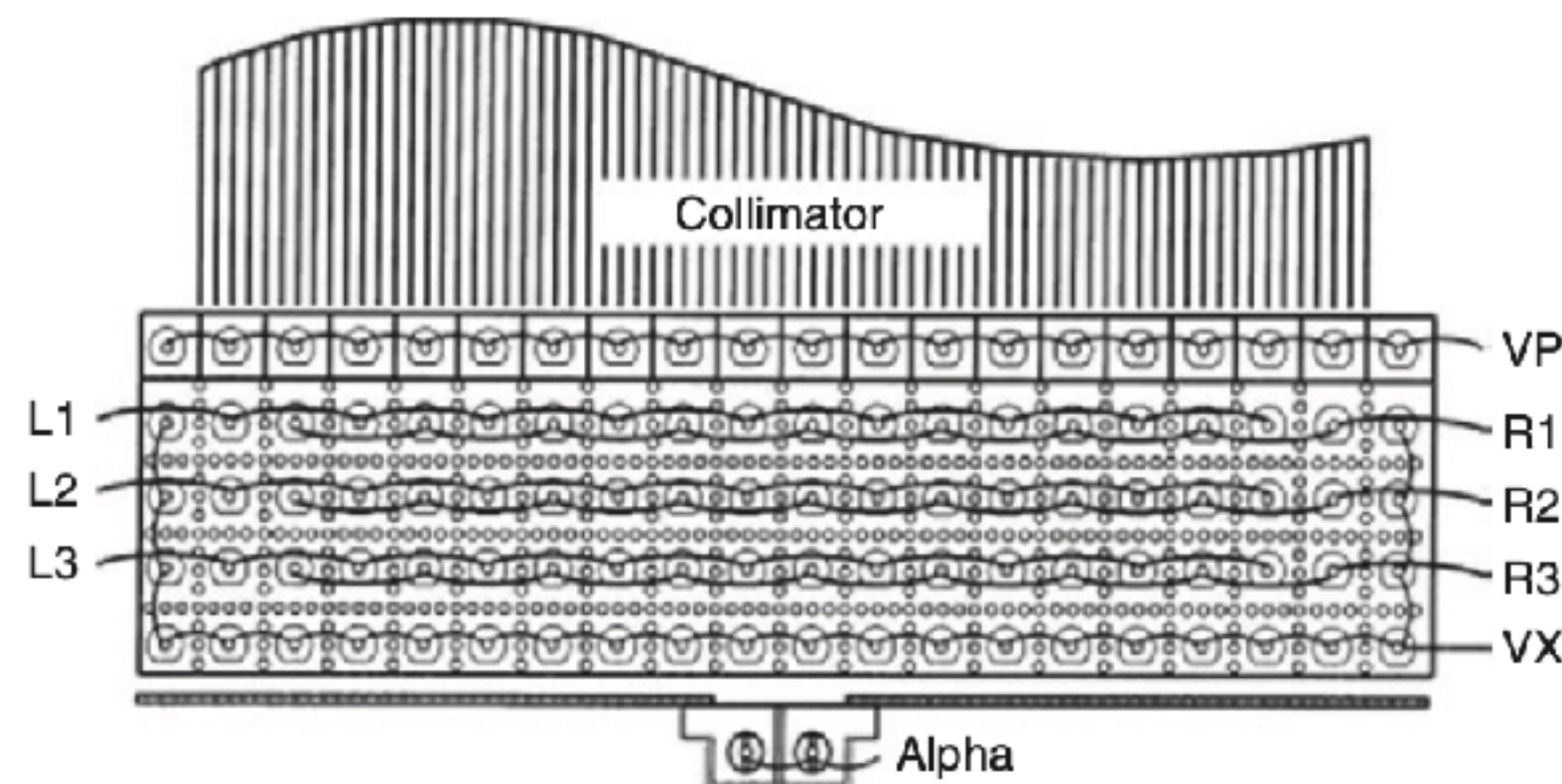
Received 1971 January 22

ABSTRACT

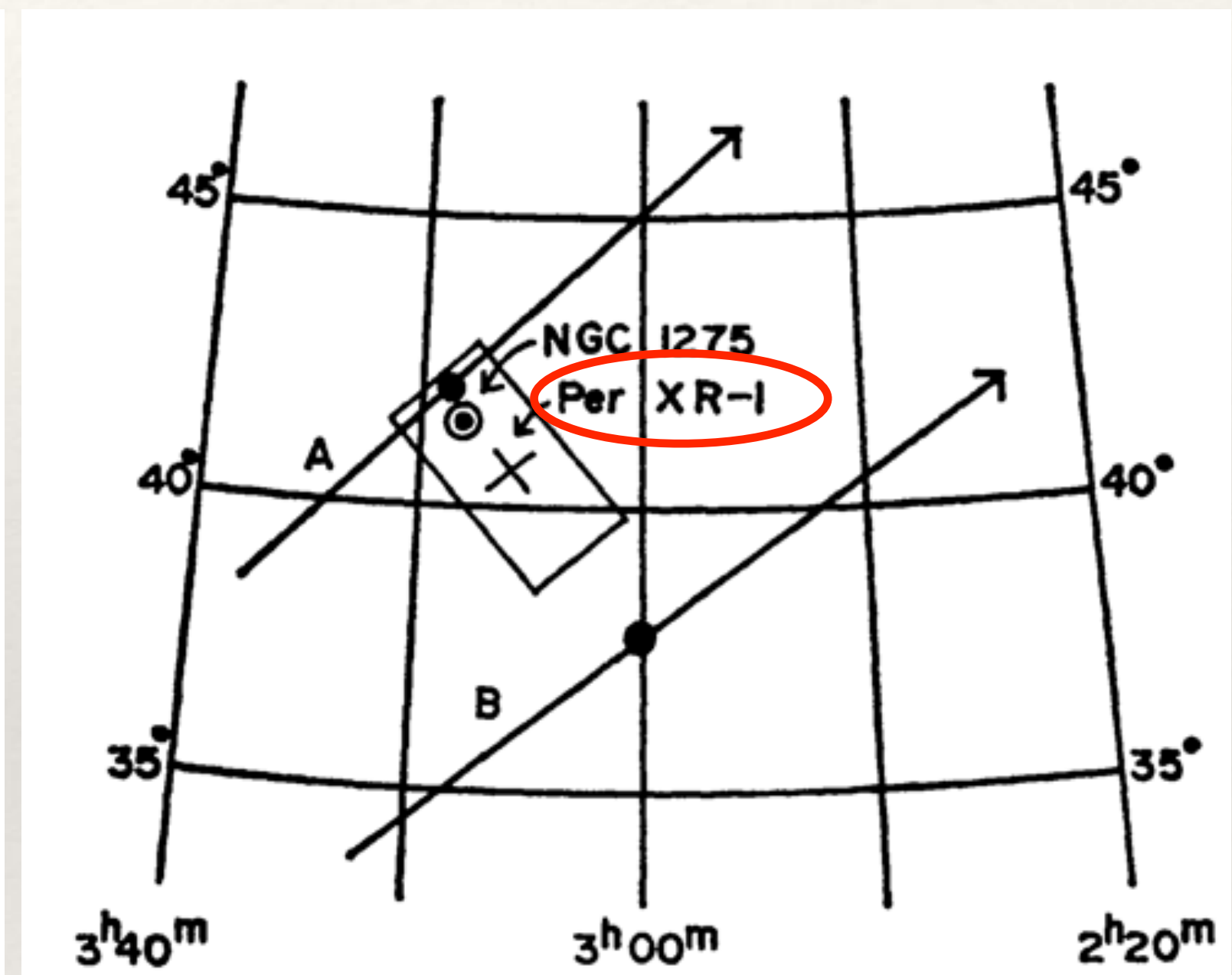
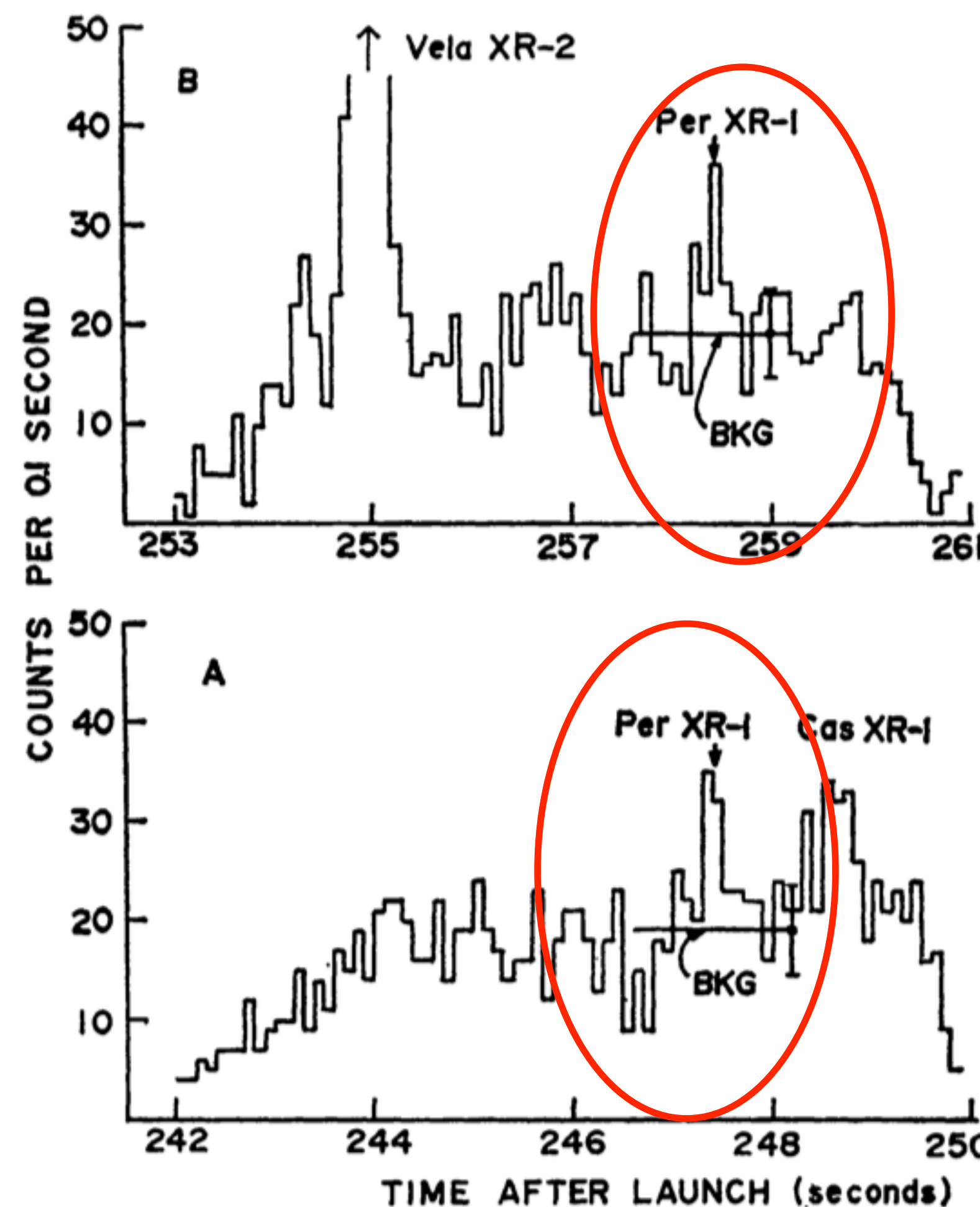
A new X-ray source, Per XR-1, has been observed. It may be associated with the Seyfert galaxy NGC 1275 (Per A, 3C 84). If the identification is correct, the X-ray power is 4×10^{45} ergs sec⁻¹ (0.5-10 keV).

I. INTRODUCTION

An Aerobee rocket carrying two X-ray proportional counters was launched at 0400 UT on 1970 March 1 from White Sands Missile Range. The detectors were sensitive in the energy range 0.5-10 keV and had a combined area of 550 cm². Each was collimated to provide a circular field of view 10° full width at half-maximum (FWHM). The rocket was allowed to roll and precess freely, producing nearly complete coverage of one hemisphere of the sky. Aspect was determined from two optical sensors. The observations reveal a new X-ray source in Perseus which may be associated with the Seyfert galaxy NGC 1275.



(Handbook of X-ray astronomy, Arnaud+11)



(A proportional counter can be flown without any focusing optic, but only a mechanical collimator)

(Fritz+71)

First confirmed X-ray cluster

- ❖ 1972, Uhuru confirmed the X-ray emission from Perseus cluster.

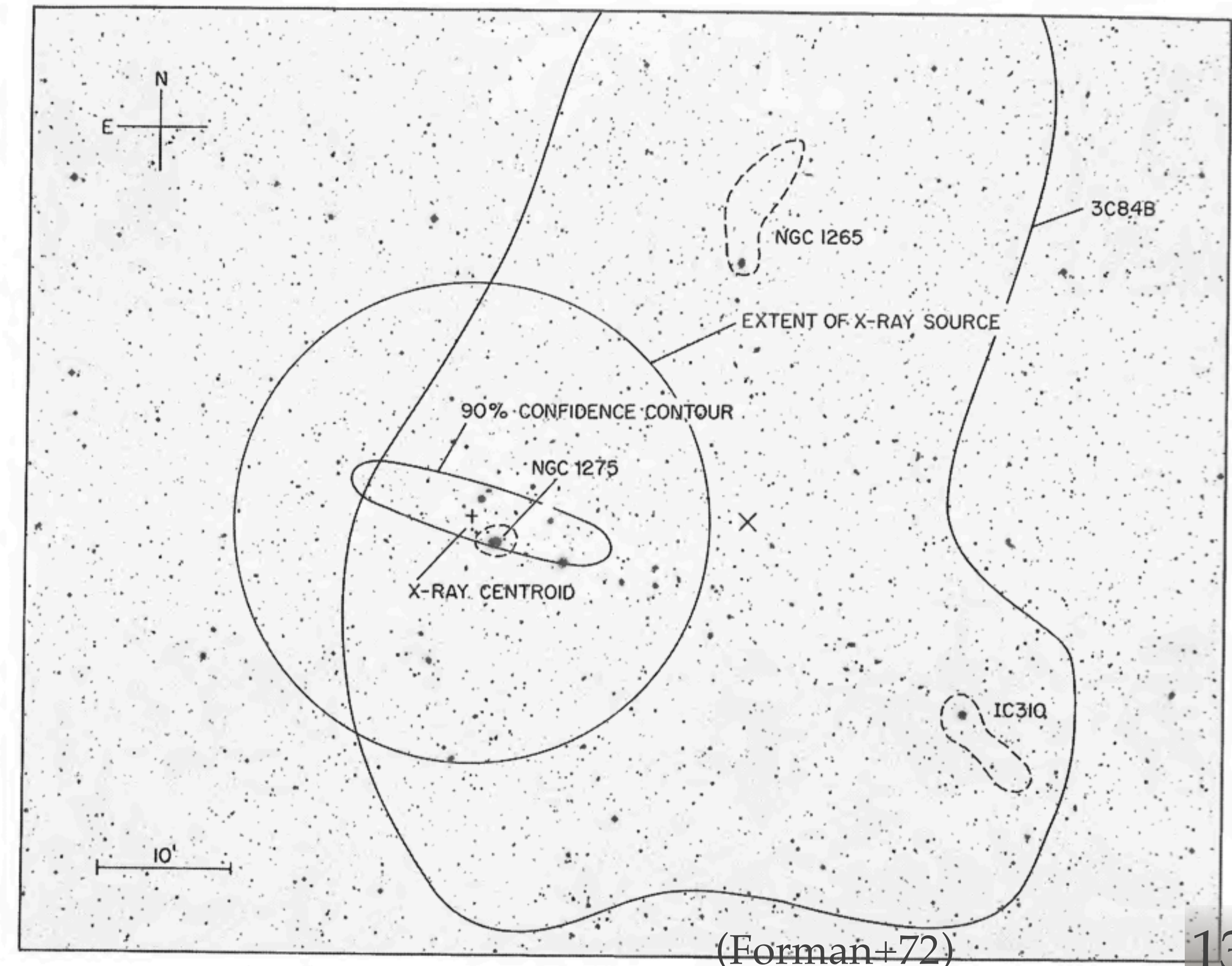
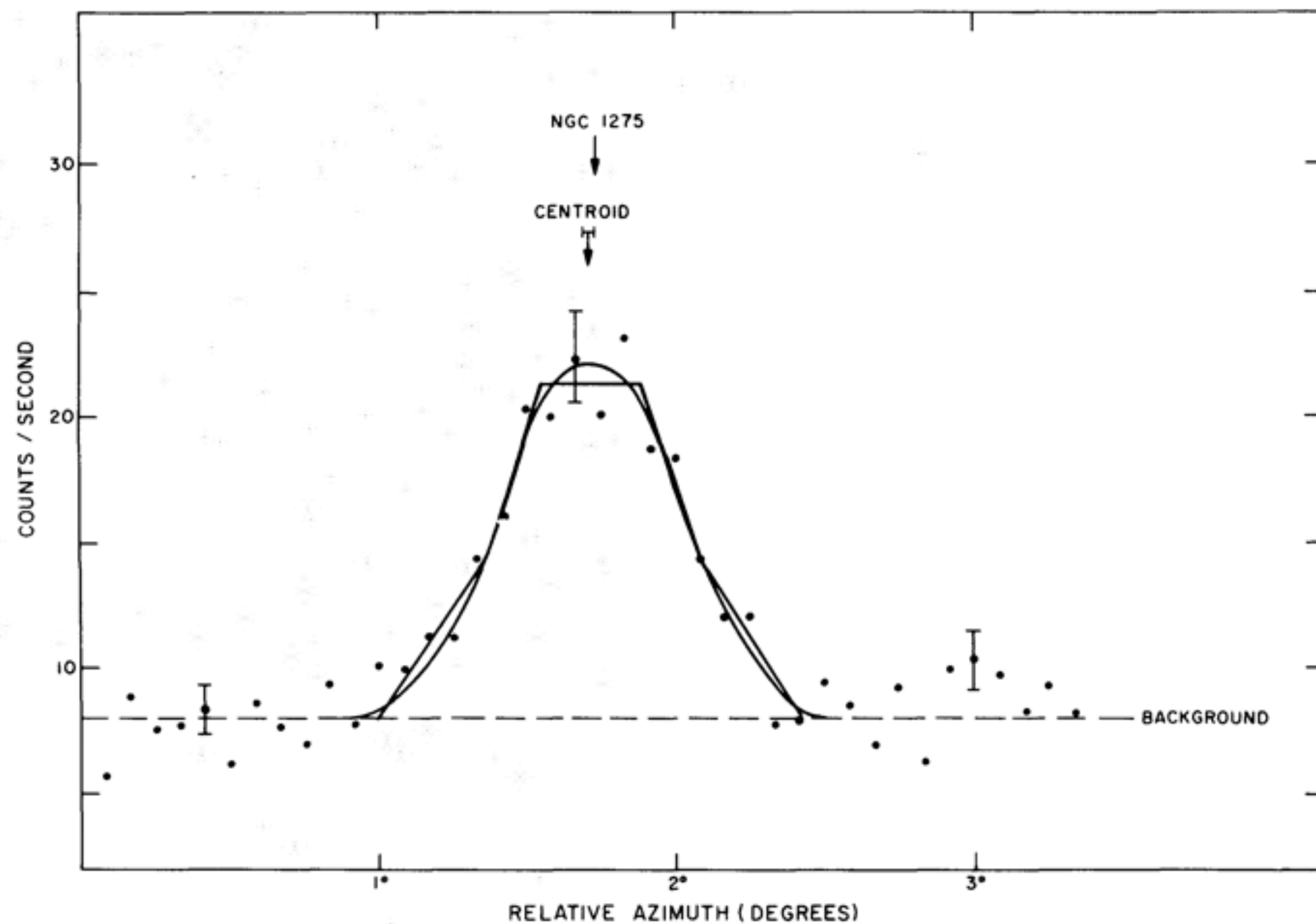
OBSERVATIONS OF THE EXTENDED X-RAY SOURCES IN THE PERSEUS AND COMA CLUSTERS FROM *UHURU*

W. FORMAN*

Harvard College Observatory, Cambridge, Massachusetts

AND

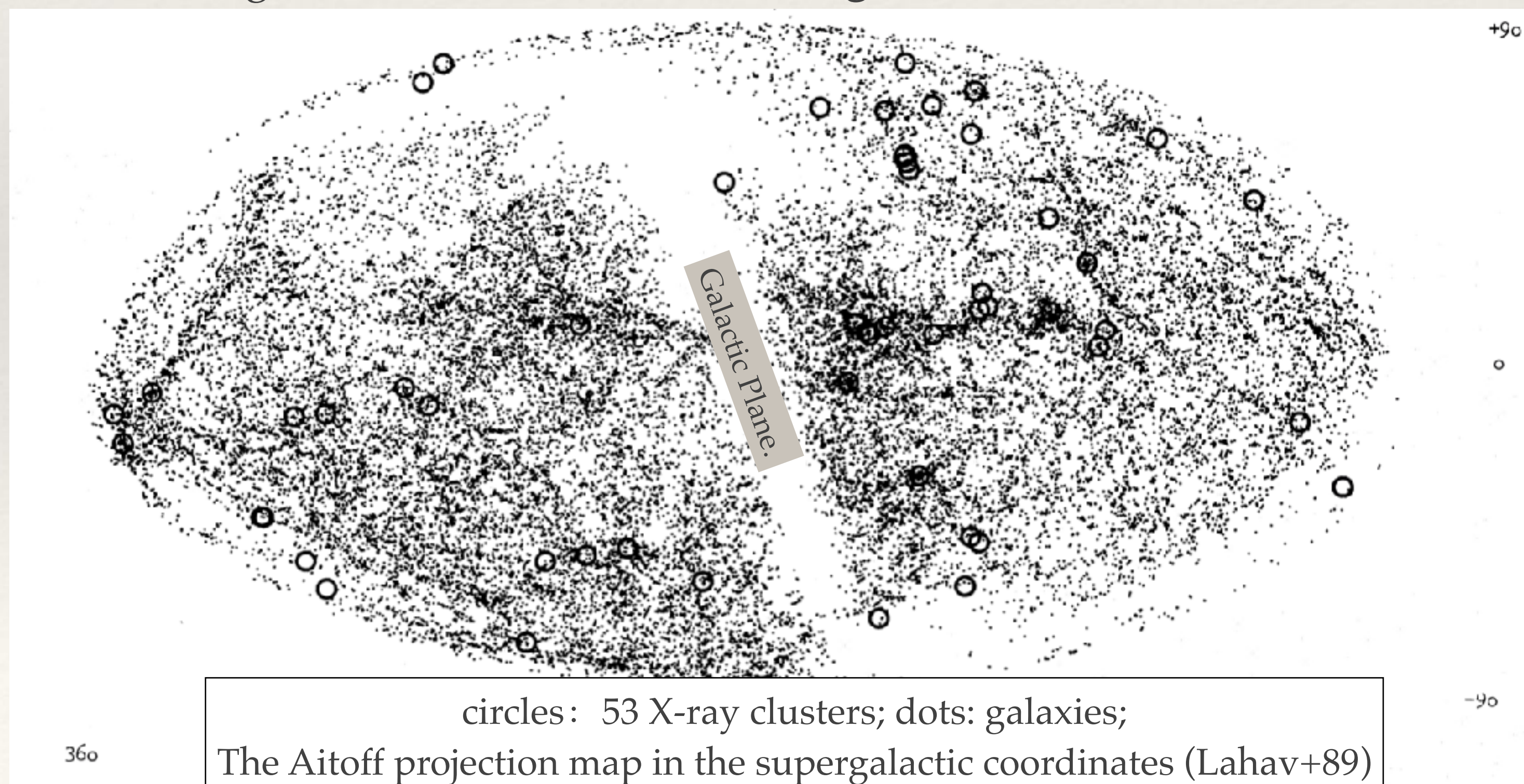
E. KELLOGG,† H. GURSKY,† H. TANANBAUM, AND R. GIACCONI†



(Forman+72)

Early cluster samples

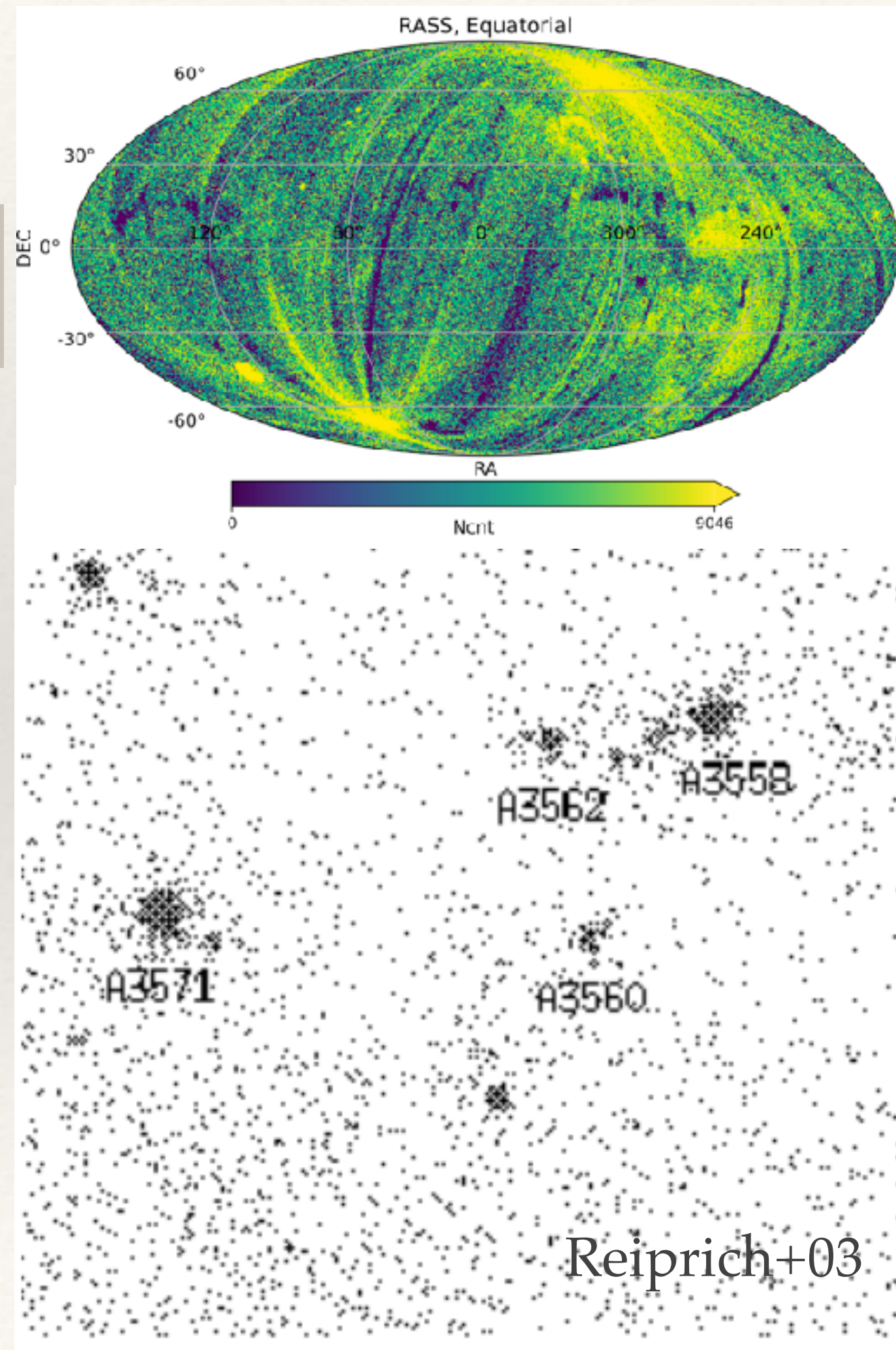
- ❖ The construction of large cluster samples begin with X-ray surveys covering the whole sky (**HEAO-1 and ARIEL V instruments**, Piccinotti et al. 1982; Kowalski et al. 1984). And the all-sky sample of the 53 X-ray brightest galaxy cluster (**EINSTEIN and EXOSAT telescopes**, Lahav et al. 1989; Edge et al. 1990).
- ❖ UHURU (Giacconi et al. 1972; Forman et al. 1978, $f_{\text{lim}} \sim 4 \times 10^{-11} \text{ erg/s/cm}^2$),
- ❖ Ariel-V (McHardy et al. 1981; Warwick et al. 1981, $f_{\text{lim}} \sim 3.5 \times 10^{-11} \text{ erg/s/cm}^2$)
- ❖ HEAO-1 (Piccinotti et al. 1982, $f_{\text{lim}} \sim 3.1 \times 10^{-11} \text{ erg/s/cm}^2$).
- ❖ EINSTEIN and EXOSAT (Edge et al. 1990, $f_{\text{lim}} \sim 1.7 \times 10^{-11} \text{ erg/s/cm}^2$).



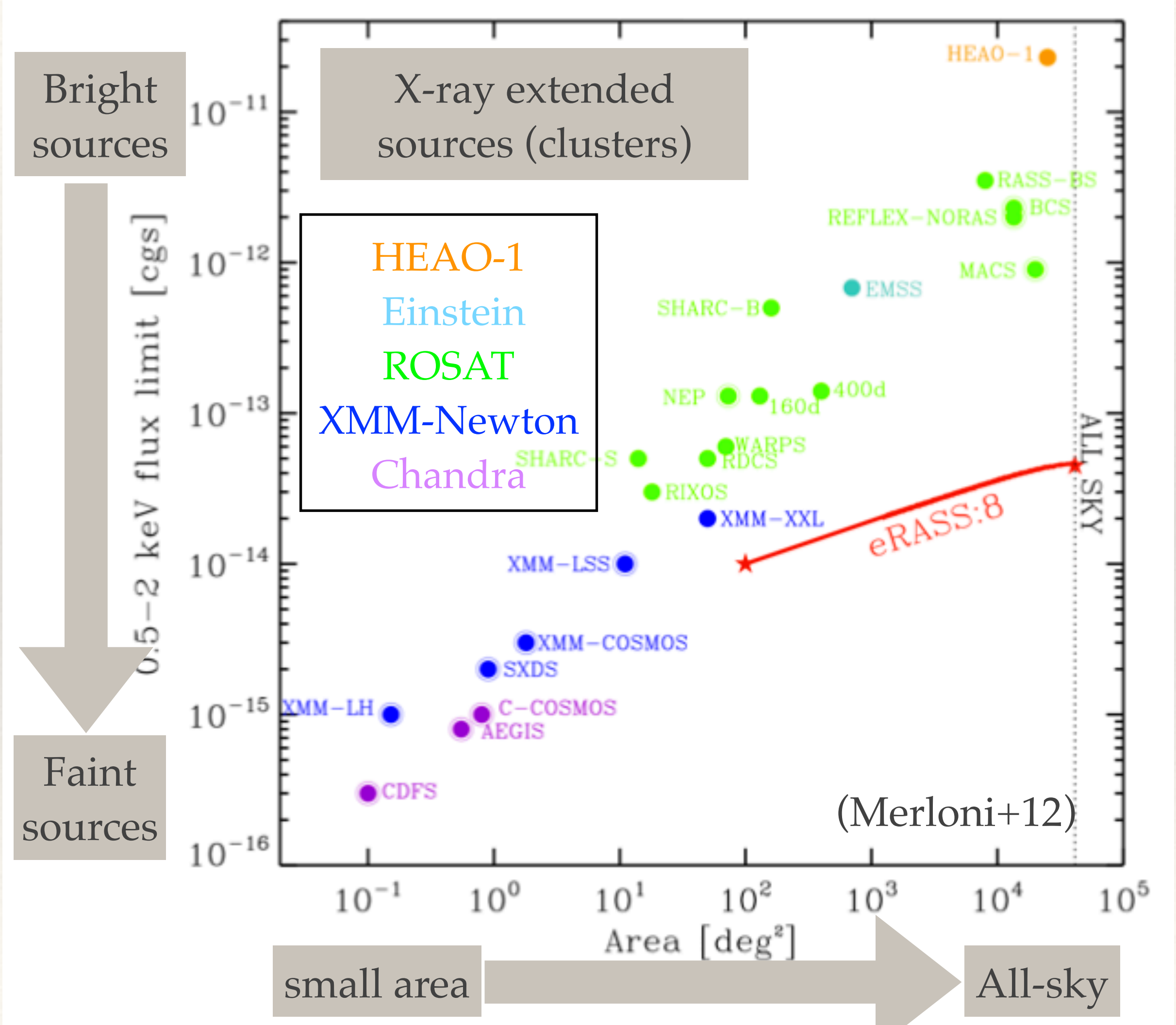
Main X-ray surveys

- ❖ X-ray surveys are hard to have large X-ray coverage and high sensitivity. y survey
- ❖ ROSAT, the first X-ray imaging telescope covering the whole sky.

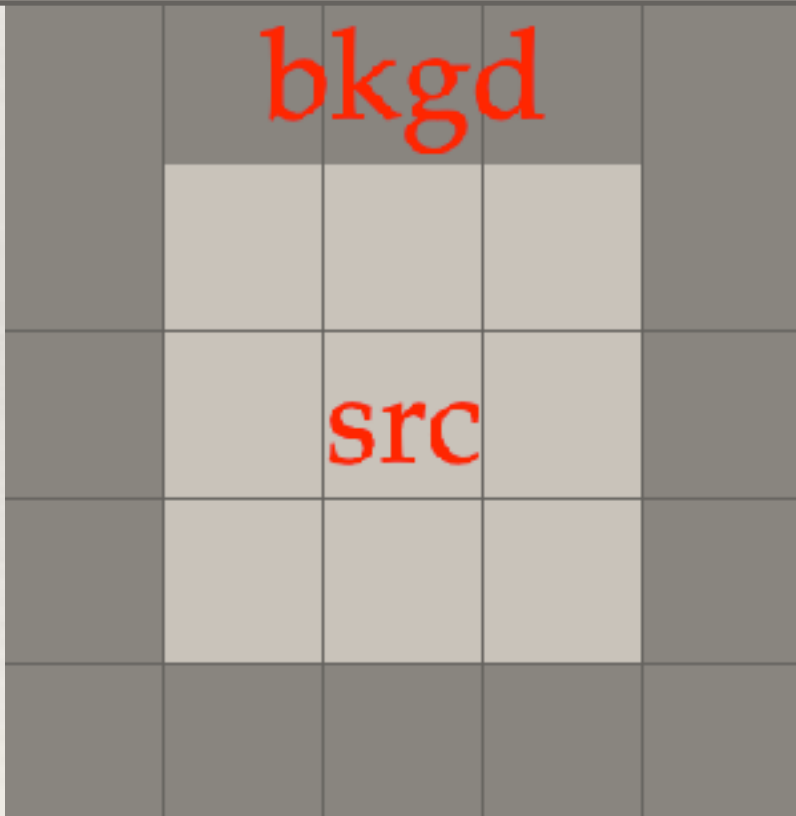
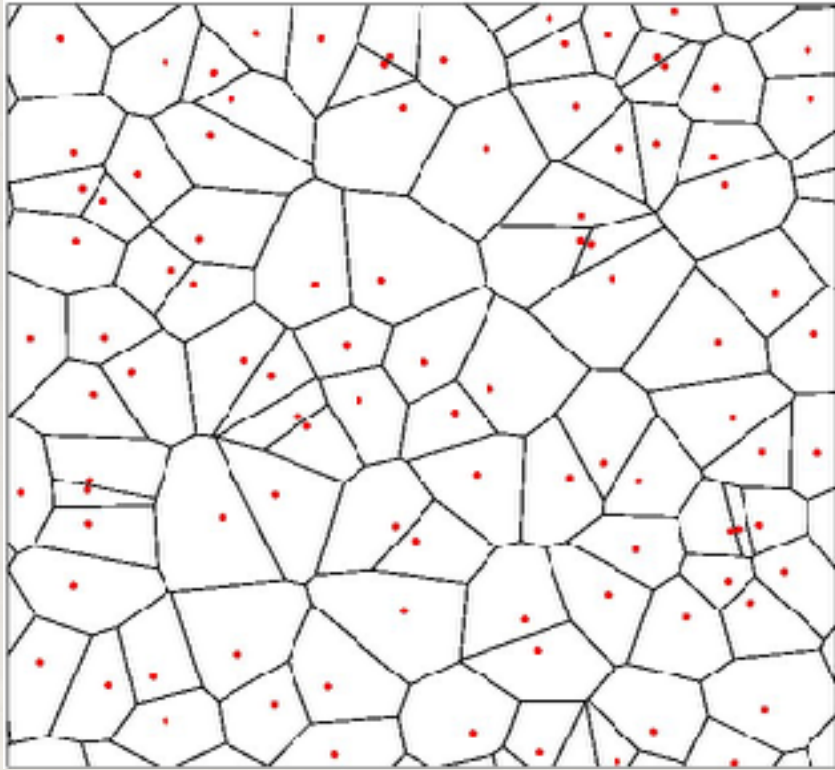
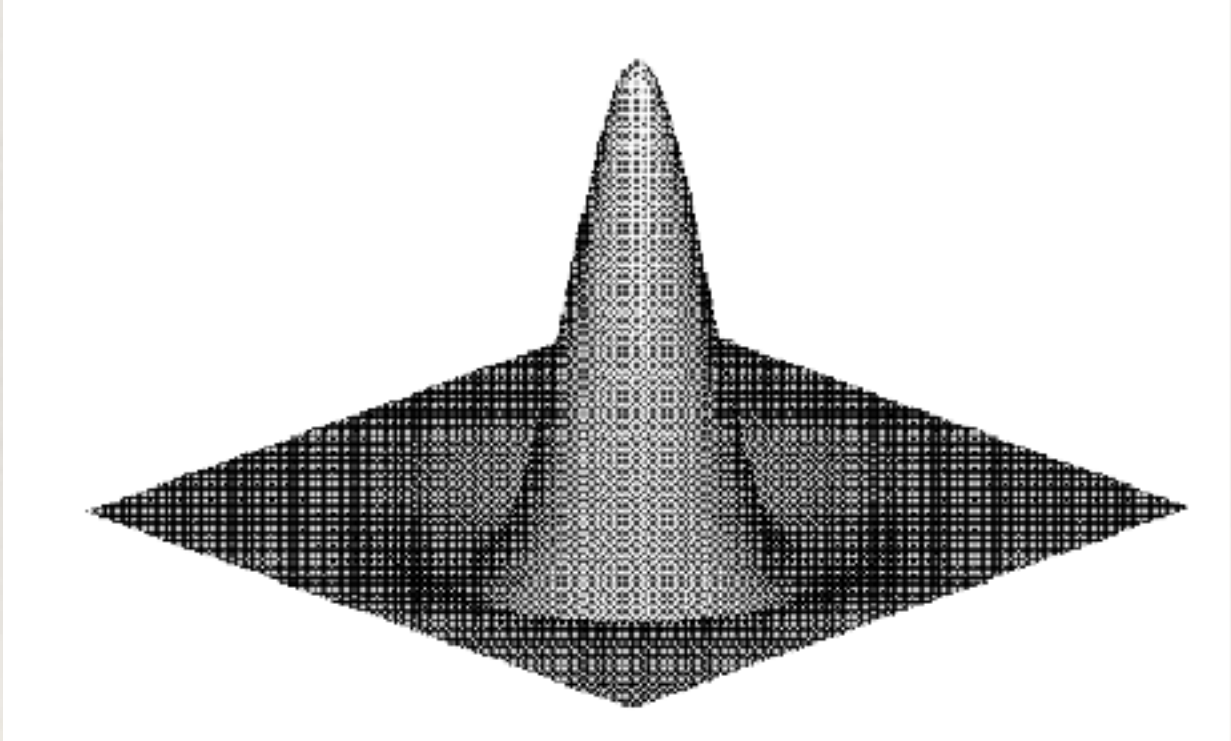
ROSAT All-Sky Survey
(RASS) photon map



RASS image
(7deg*7deg)



Cluster detection methods

Sliding box	Voronoi tessellation and percolation (VTP)	Wavelet transformation.
		

Sliding window method

1. The local-detect method (**EXSAS** command: *detect/local*): a sliding window technique.

- Window for source: 3×3 pixels, for bgd: 16 pixels surrounding.
- For extended sources, $A_{\text{bgd}} / A_{\text{src}} = 16 / 9$.

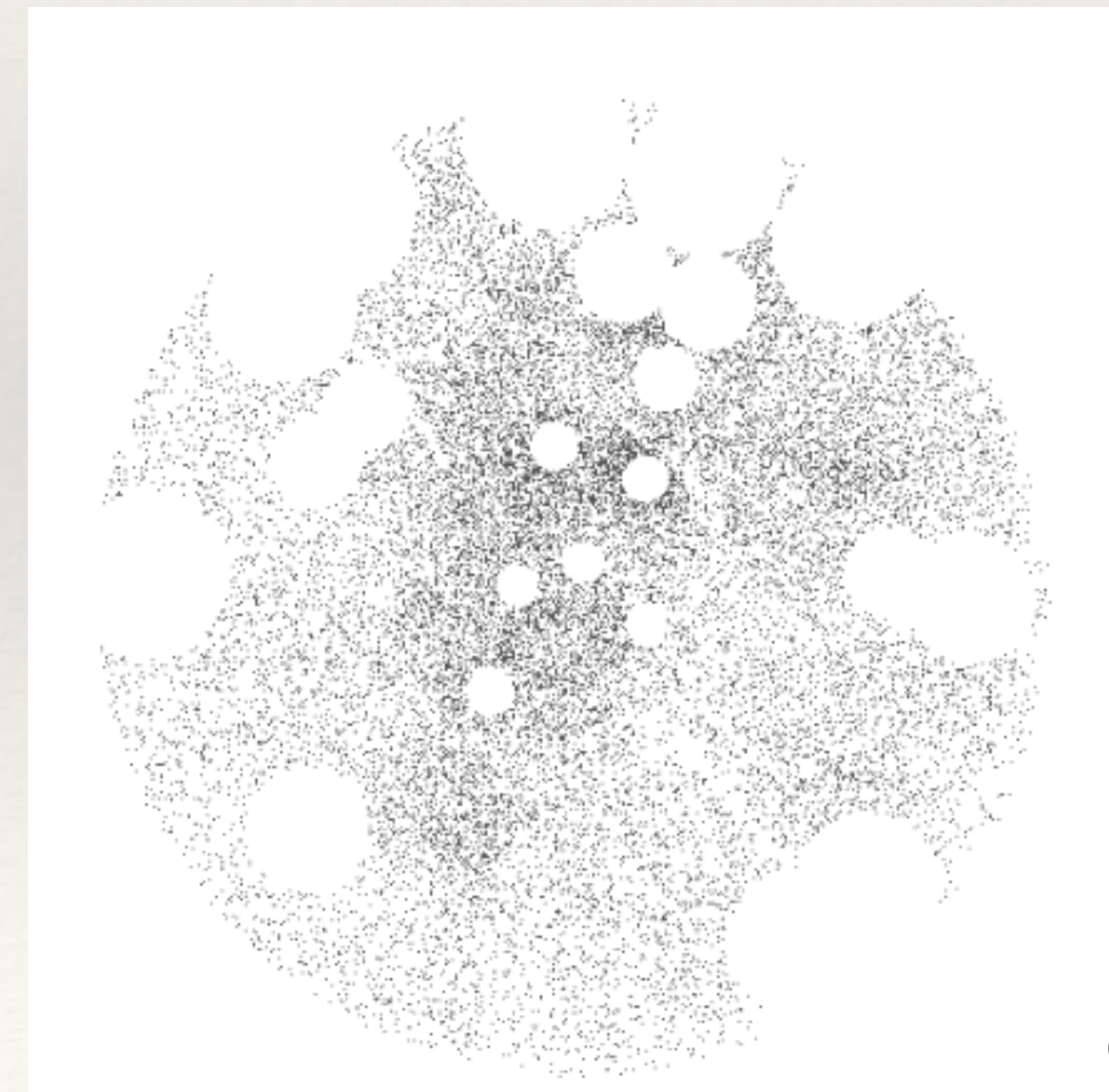
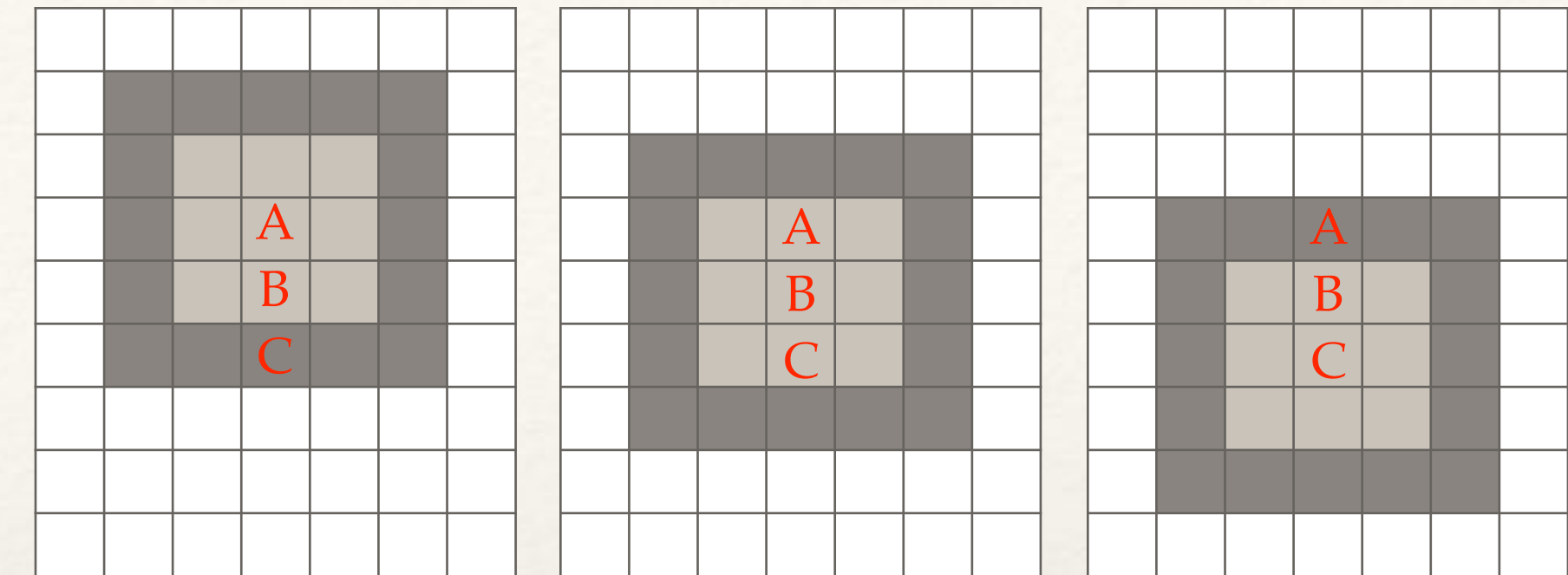
2. The background map (*create/bg_image*).

- Remove sources with circles.
- Fill the holes with a two-dimensional spline function, generate background maps.

3. The map-detect algorithm (*detect/map*).

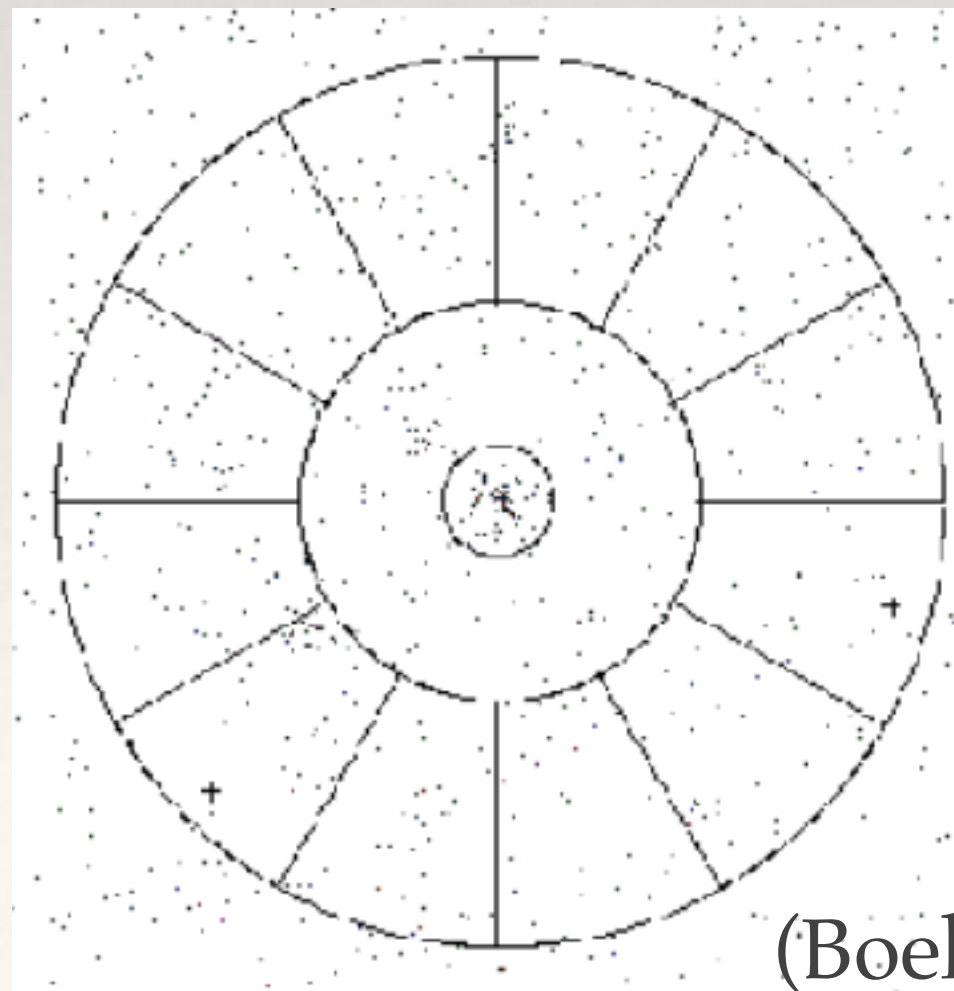
- Repeat step 1 with the background map.

4. Merging of source lists (*merge/source_tables*).

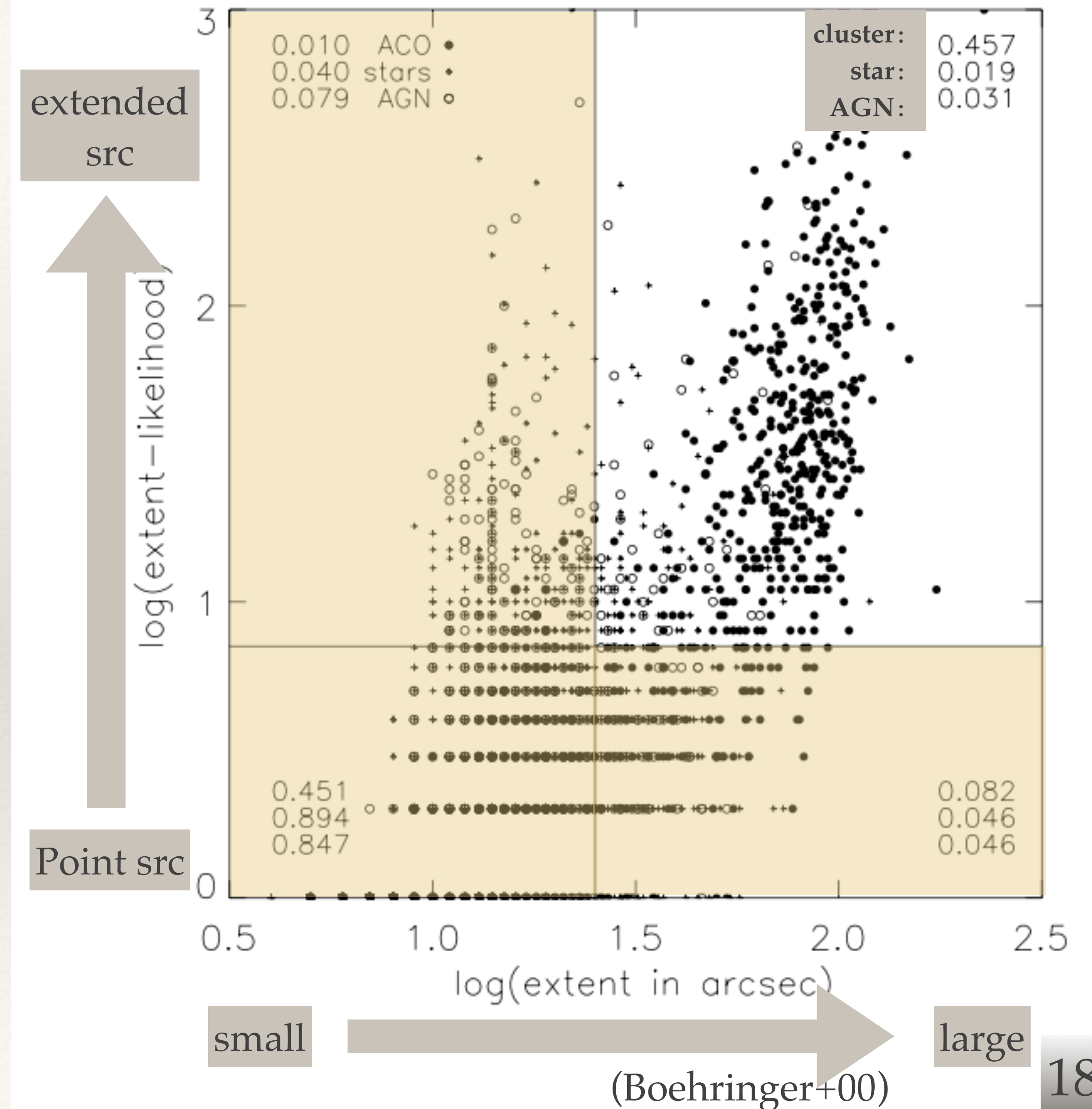
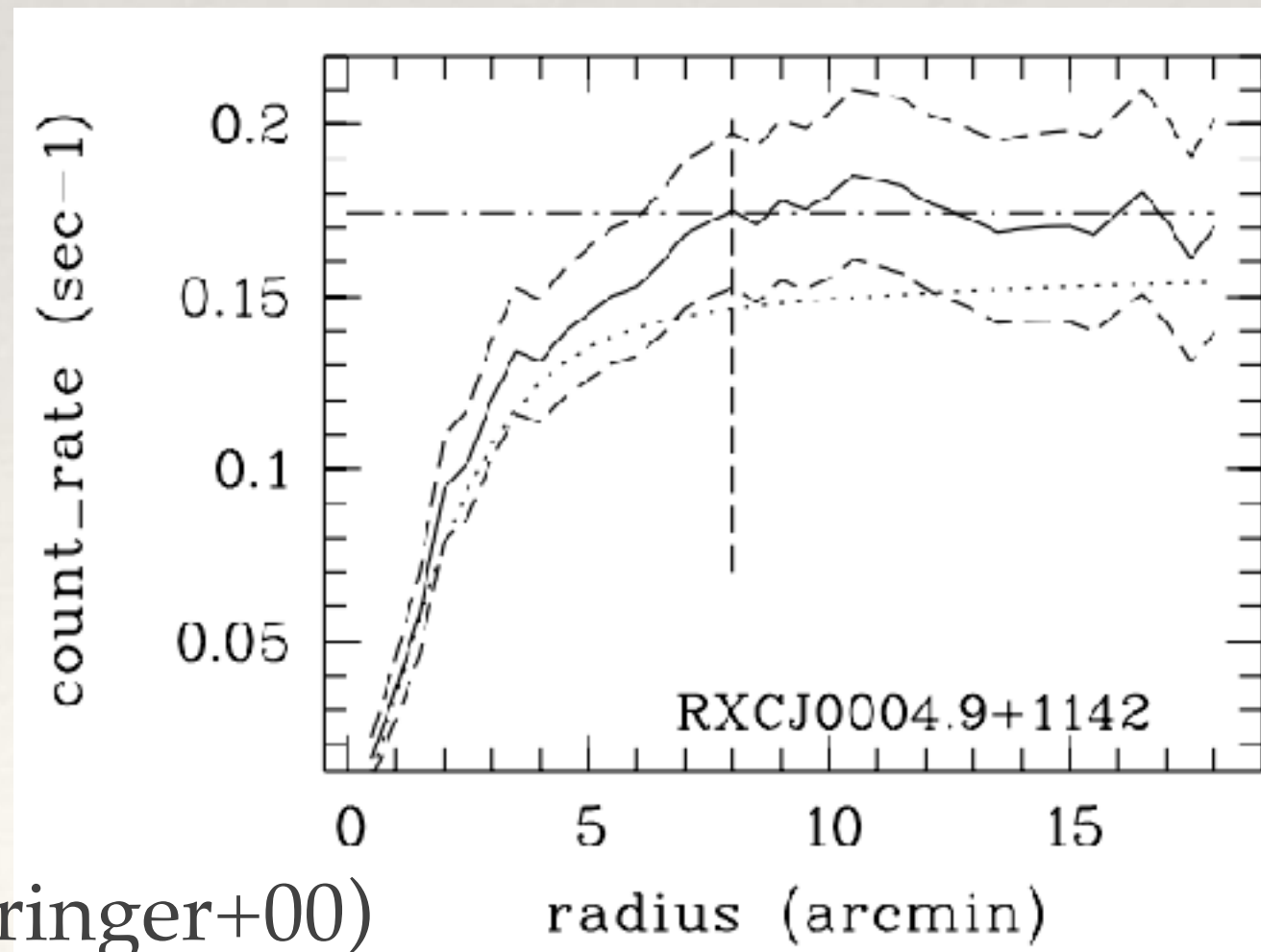


Sliding window for cluster detection

- ❖ 5. Growth curve analysis for source properties, size, count rate.
- ❖ 6. Sliding window to evaluate of the source detection significance and extension, and select extended sources.
 - $L_{\text{det}} = -\ln P > 10$, where P is the probability for a spurious source detection.
 - $L_{\text{ext}} = -\ln P > 7$, P is the probability for a spurious extent detection.
 - Extent radius $> 25''$.



(Boehringer+00)



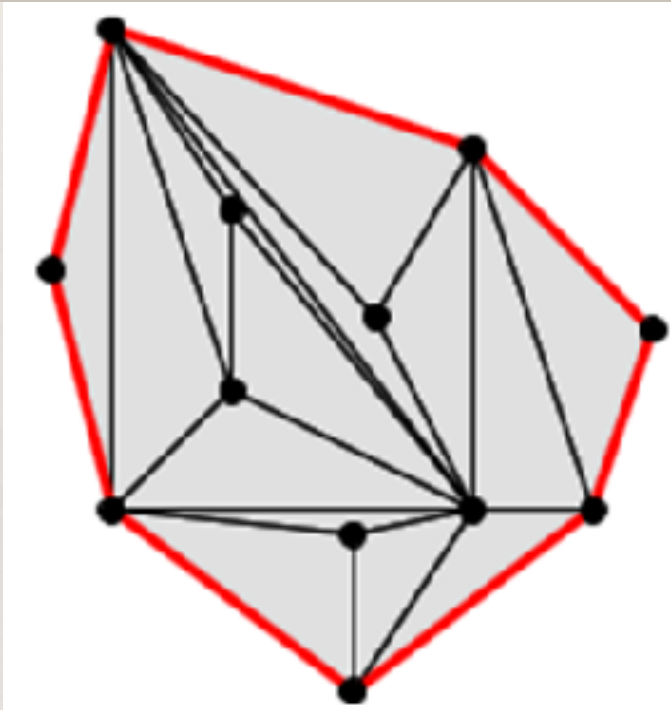
Sliding window method - catalogs

- ❖ The northern ROSAT all-sky (*NORAS*) galaxy cluster survey (Boehringer et al. 2000);
- ❖ The ROSAT-ESO flux limited X-ray (*REFLEX*) galaxy cluster survey (Boehringer et al. 2001, 2004);
- ❖ The ROSAT all-sky survey bright source catalogue (RASS-BCS, Voges et al. 1999)
- ❖ The extended ROSAT-ESO flux limited X-ray galaxy cluster survey (*REFLEX II*, Boehringer et al. 2013)
- ❖ A Catalog of Clusters of Galaxies in a Region of 1 Steradian around the South Galactic Pole (*SGP*, Cruddace et al. 2002)
- ❖ The ROSAT North Ecliptic Pole survey (*NEP*, Henry et al. 2006).
- ❖ **eROSITA Final Equatorial-Depth Survey (eFEDS) clusters and groups (Liu+21)**
- ❖ **The SRG/eROSITA All-Sky Survey (eRASS) clusters and groups (Bulbul+24)**

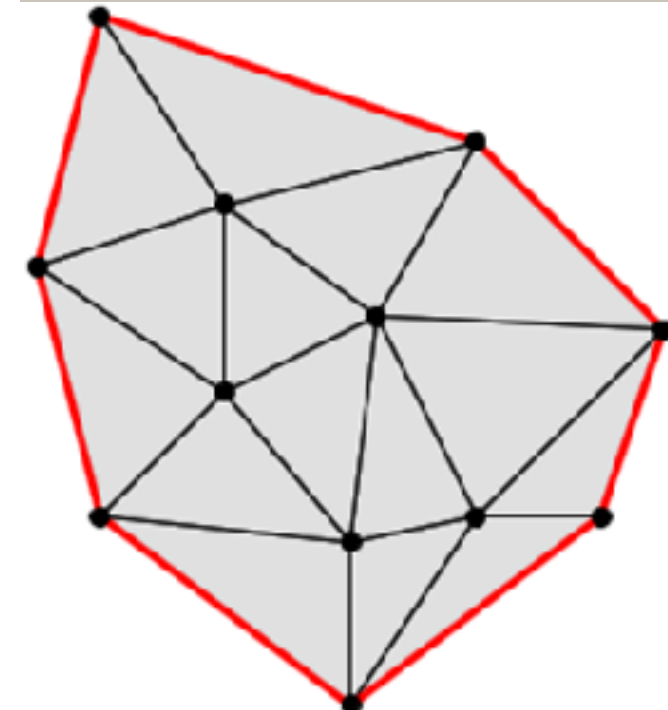
Voronoi tessellation and percolation (VTP)

- ❖ Delaunay triangulation (Delaunay, 1934):
 - its open circumdisk is *empty*— i.e. contains no point as vertices.
- ❖ Voronoi edges are constructed by creating the perpendicular bisector of the line between two points respectively and blending them.

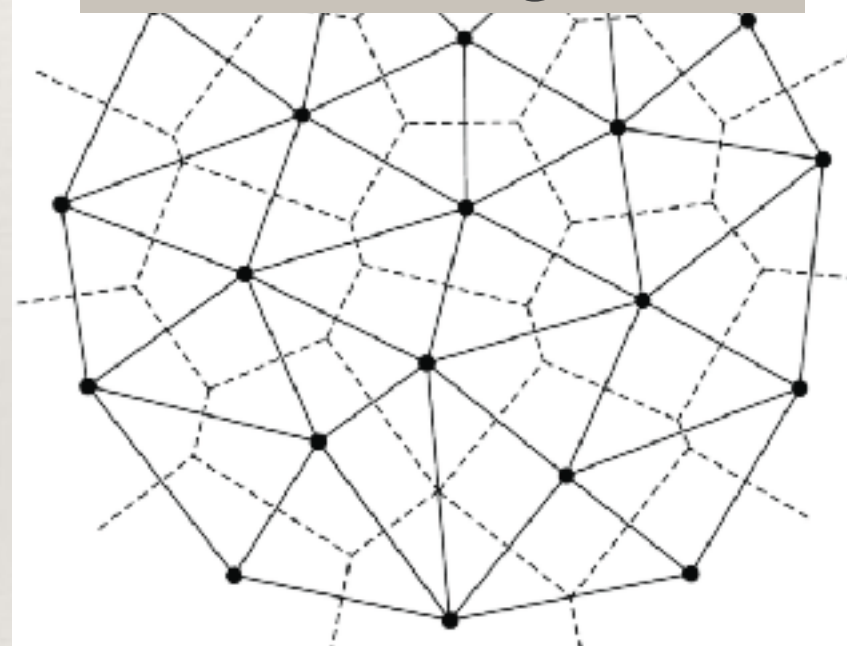
Random triangles



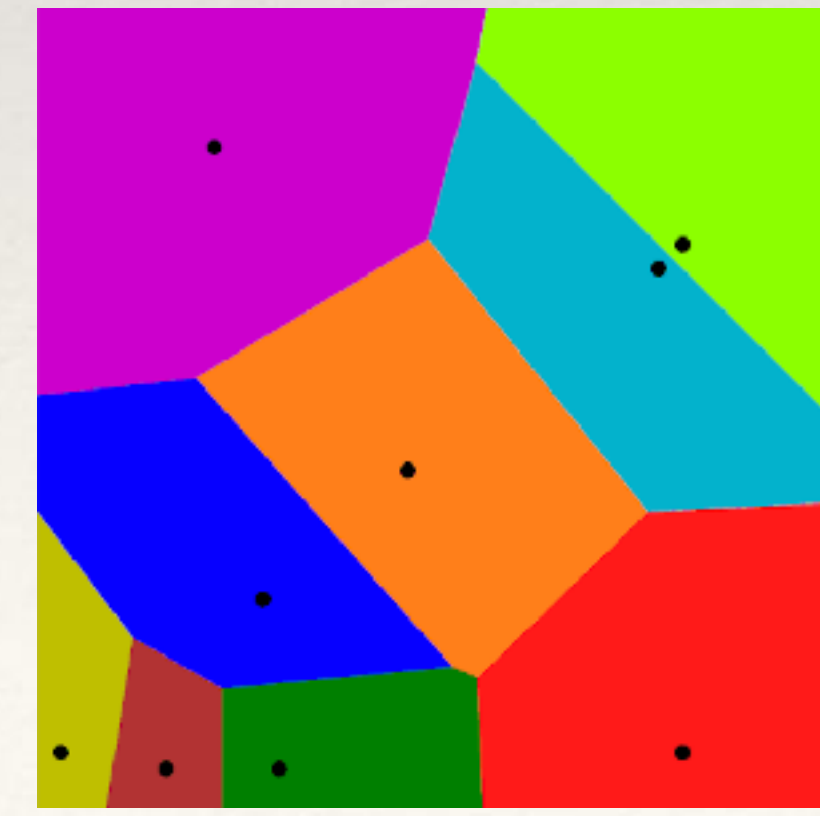
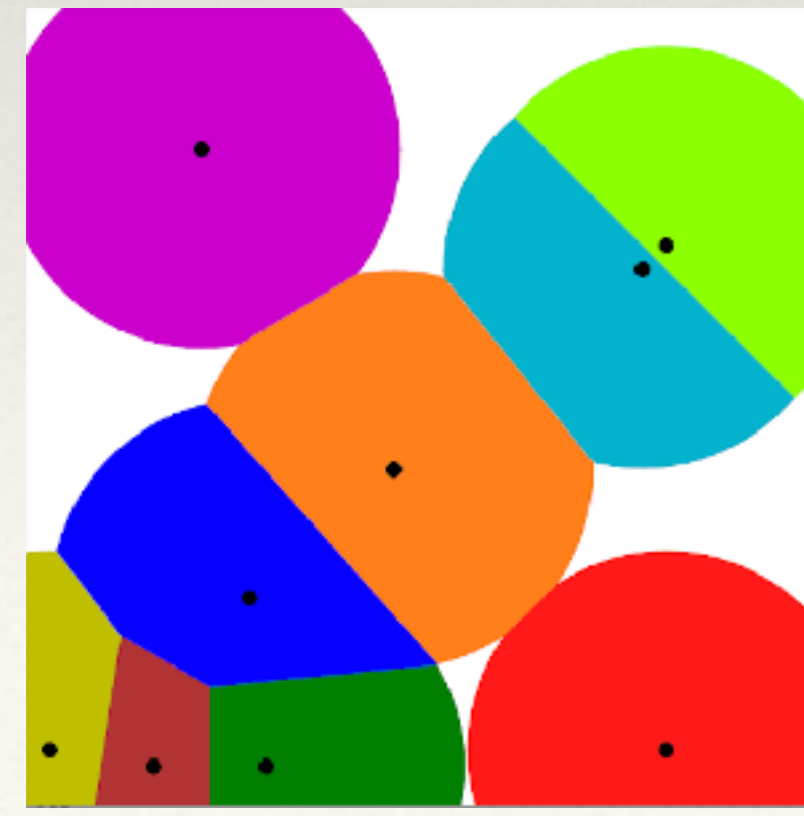
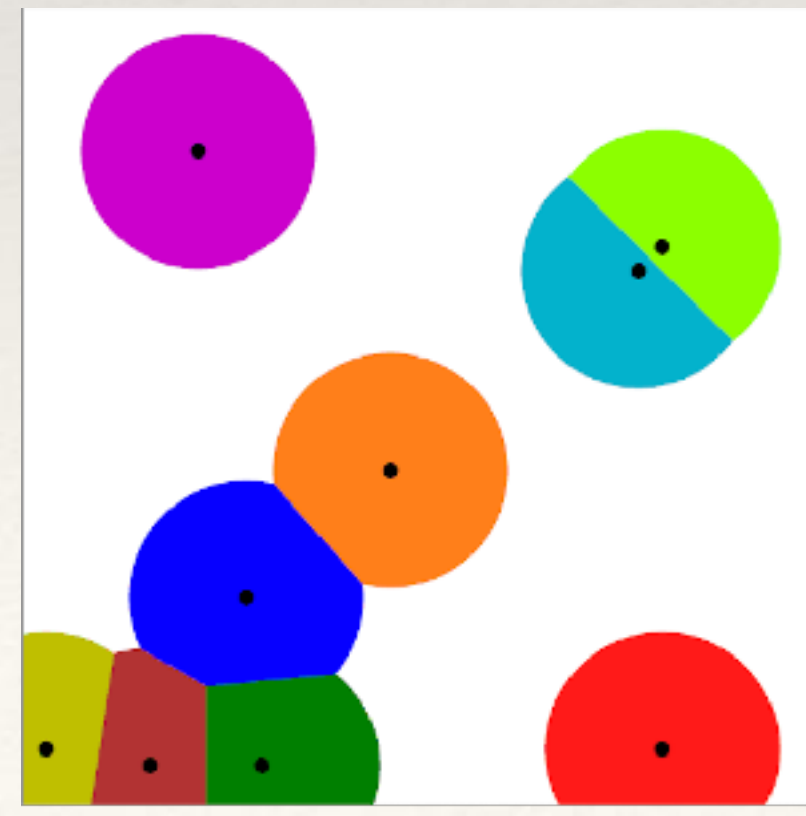
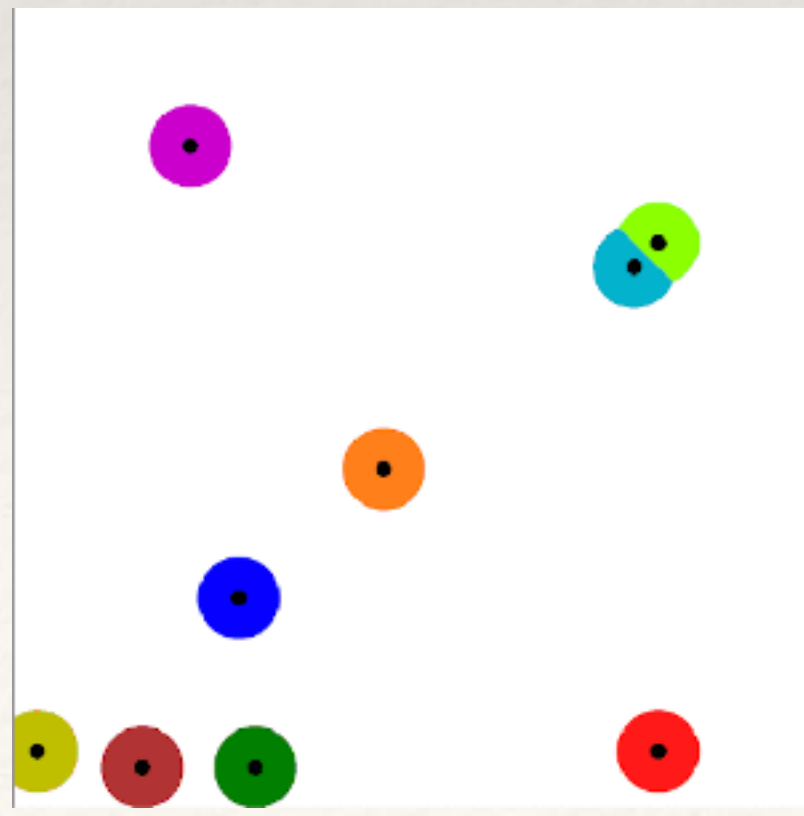
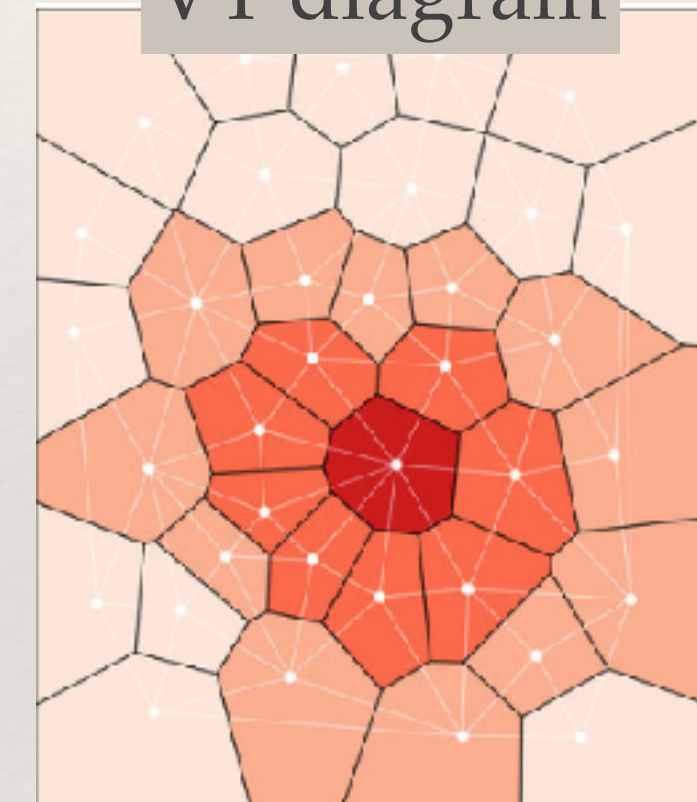
Delaunay triangles



Delaunay triangle
& VT diagram

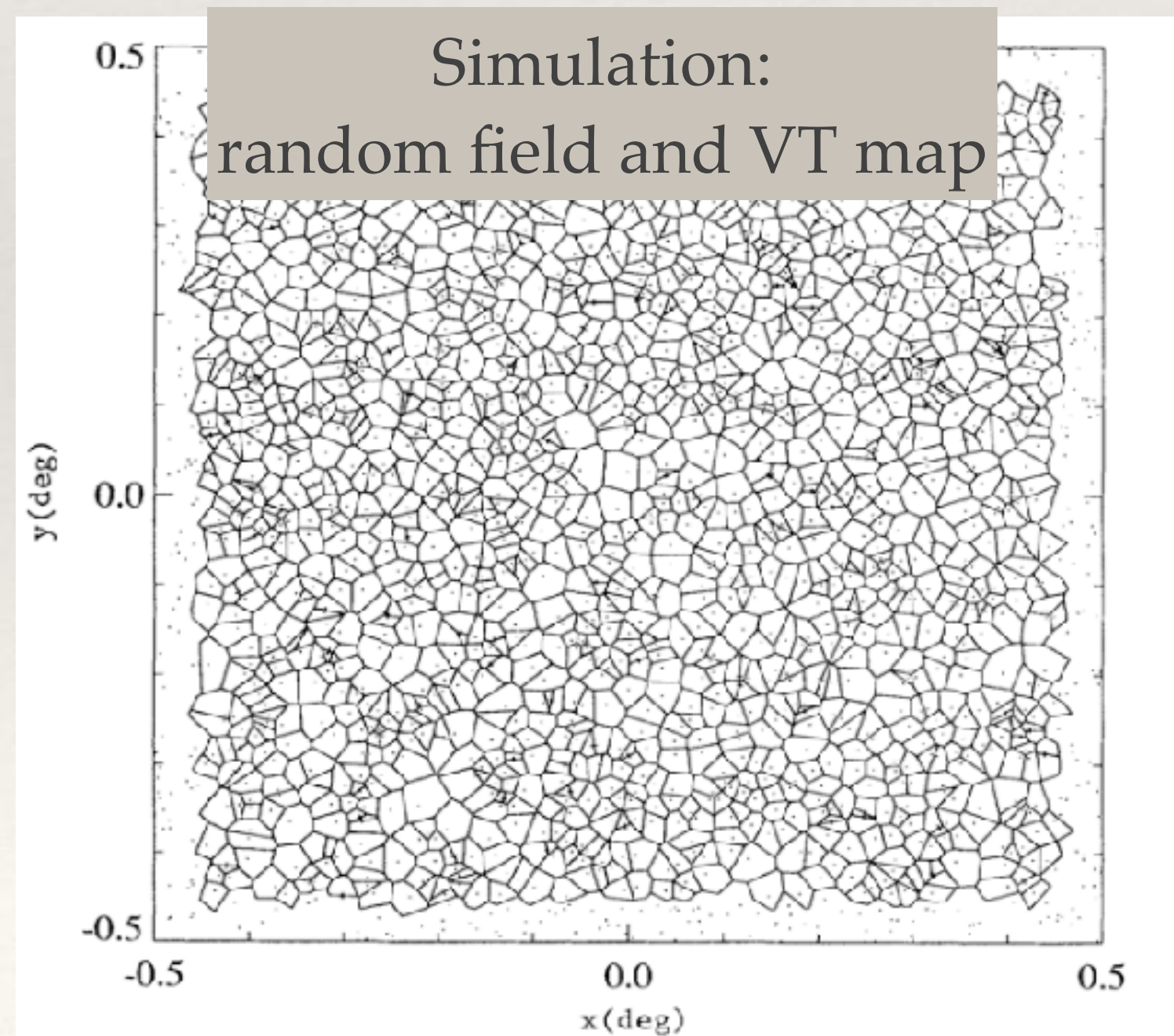
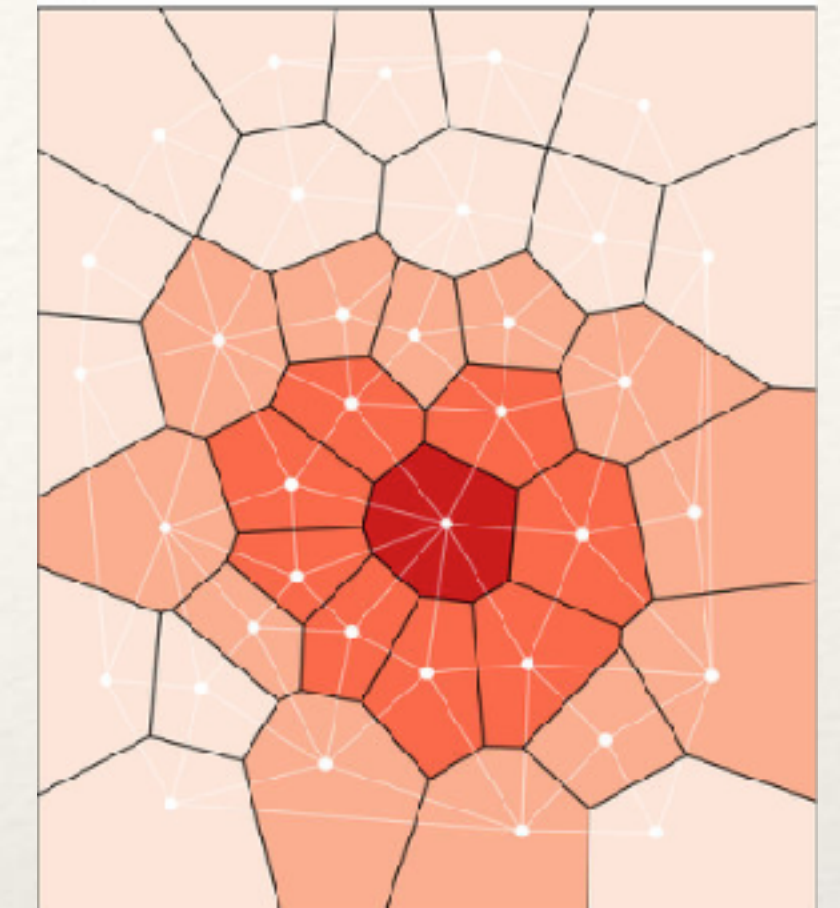


VT diagram

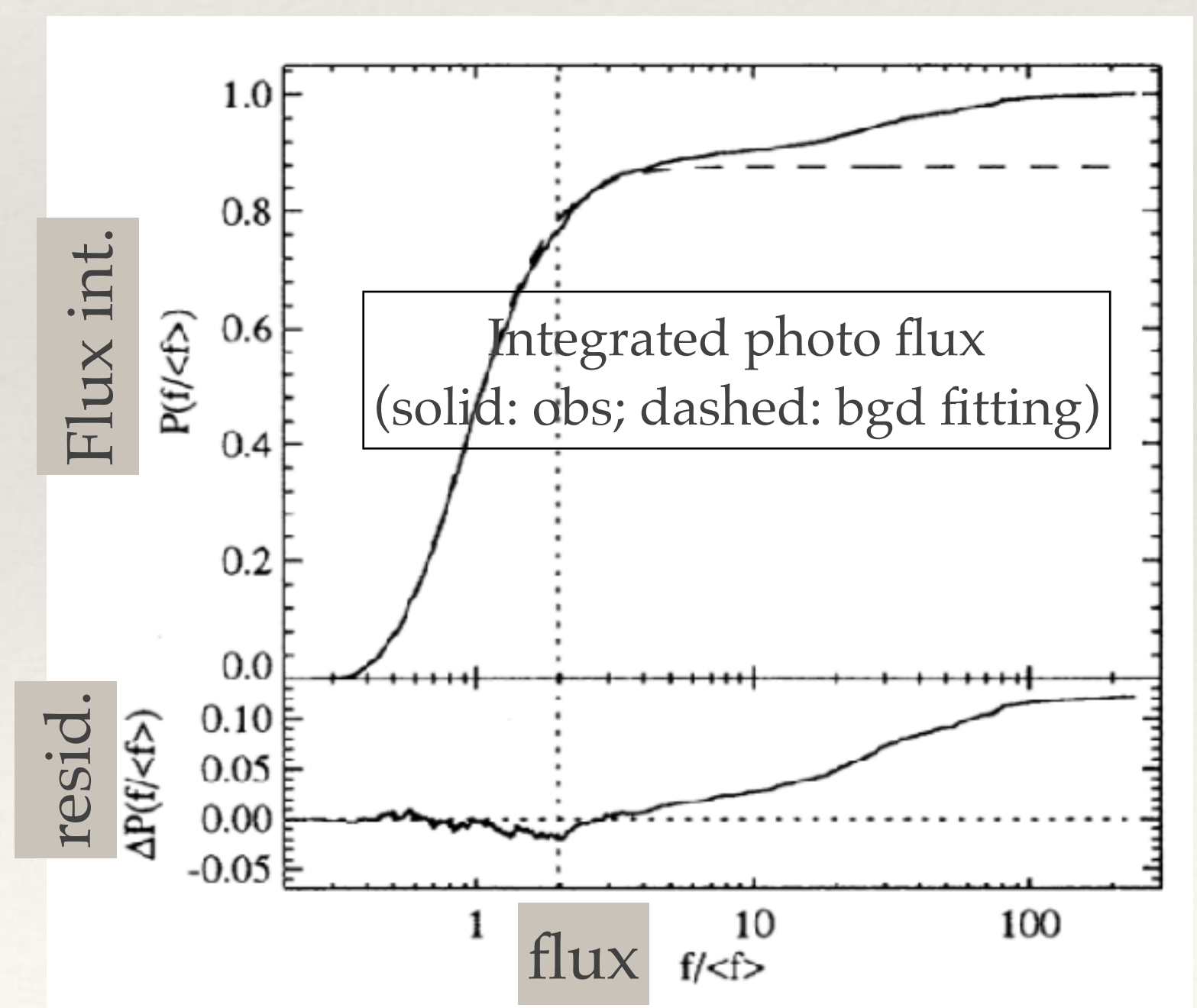
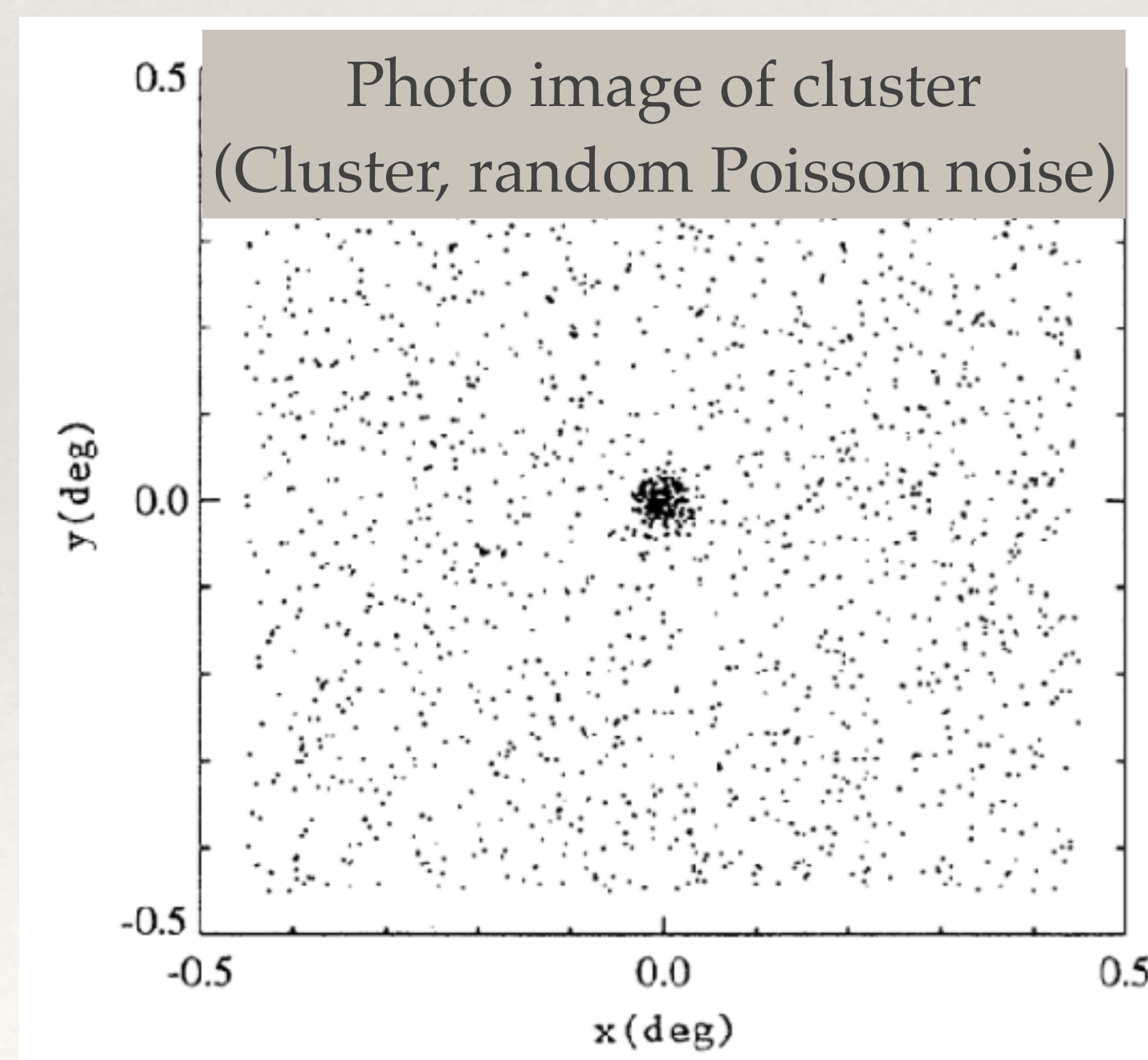


Main steps of VTP

1. Compute the VT diagram with the photon distribution.
2. Compute the cumulative distribution of the inverse of cell areas, compare with random Poisson field, and estimate the background.
3. Run a spatial percolation algorithm on cells, and group nearby cells.
4. Select detections with high SNR.



(Ebeling+03)



(Ebeling+93)

Advantages and parameters from VTP

- ❖ VTP does not introduce any artificial bias (BCS+eBCS, Ebeling et al. 1998, 2000, Ebeling & Wiedenmann 1993; Scharf et al. 1997; Perlman et al. 2002)
 - makes full use of the unbinned two-dimensional event distribution,
 - cells with high SNR directly to the source list, be free of any assumptions about the source geometry,
 - yields individual densities, or fluxes automatically and straightforward, without any model-dependent profile-fitting,
 - works well in crowded area.
- ❖ Parameters:
 - ❖ **POS**, the source position (determined as a weighted sum over photons),
 - ❖ **CR_src**, the detected source count rate (corrected for the background count rate),
 - ❖ **A_src**, the detected source area,
 - ❖ **CNT_bgd**, an estimate of the background count,
 - ❖ **SNR**, signal-to-noise ratio,
 - ❖ **Photons_mem**, the full set of photons associated with each source is stored

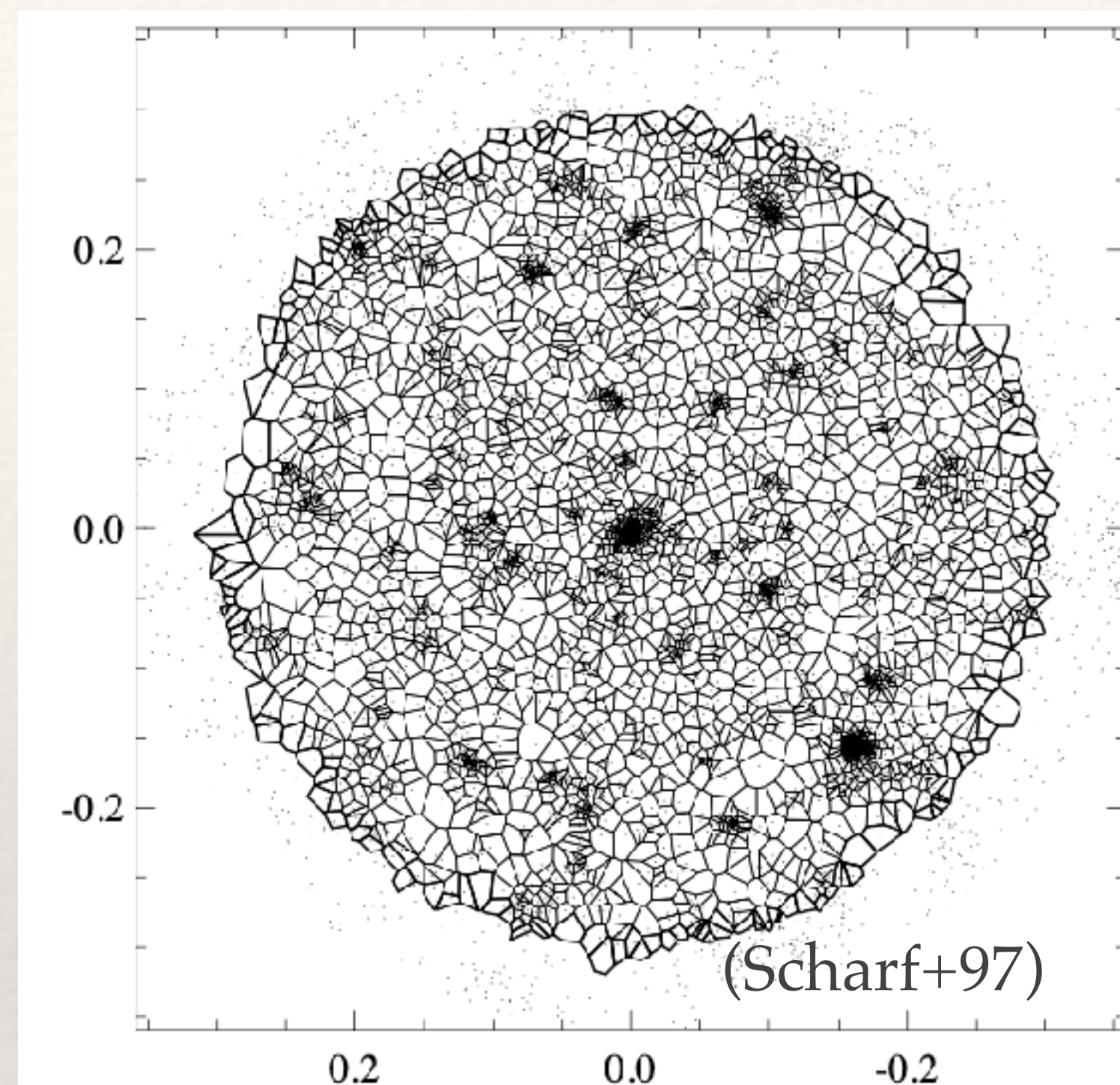
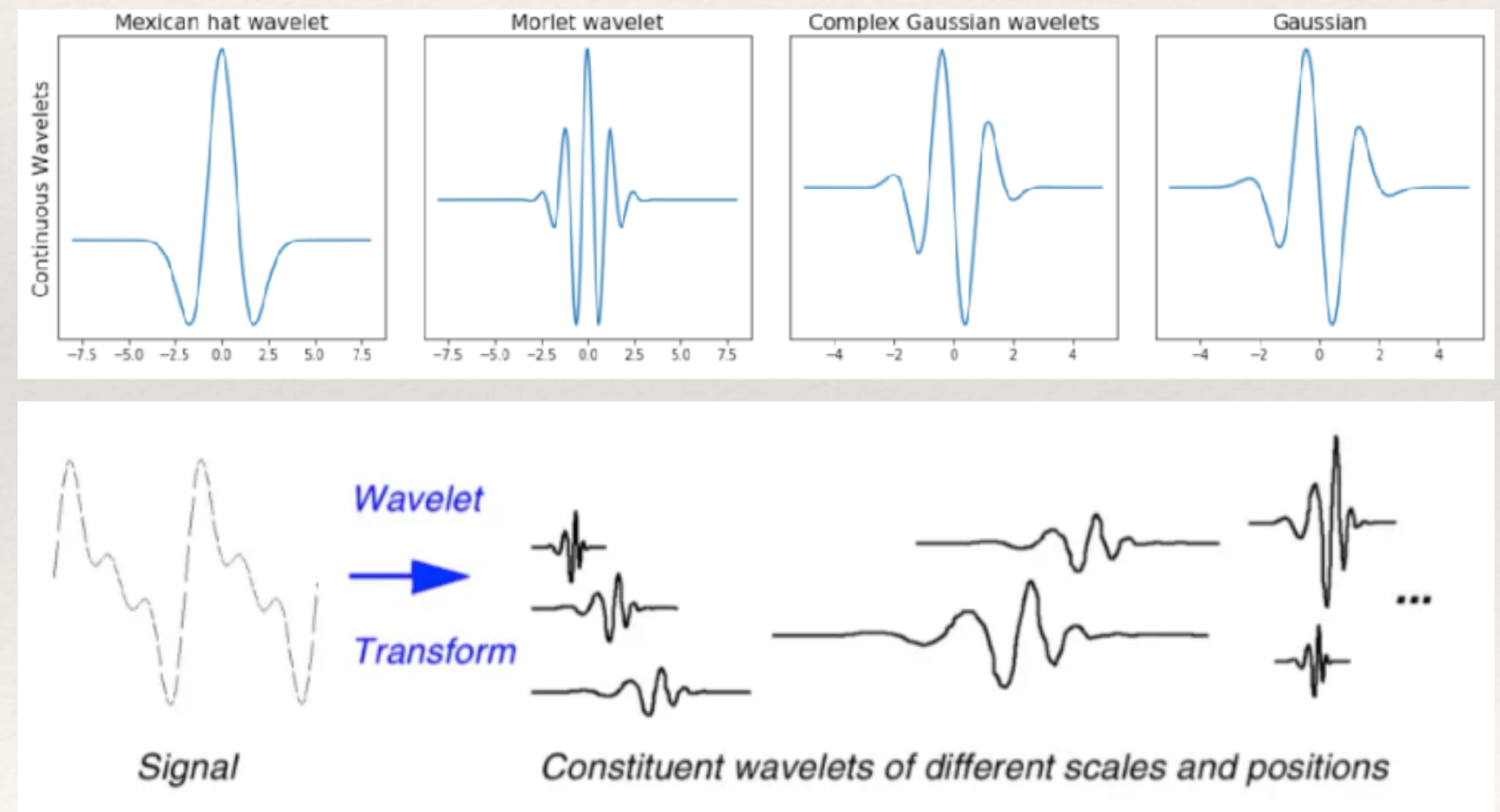
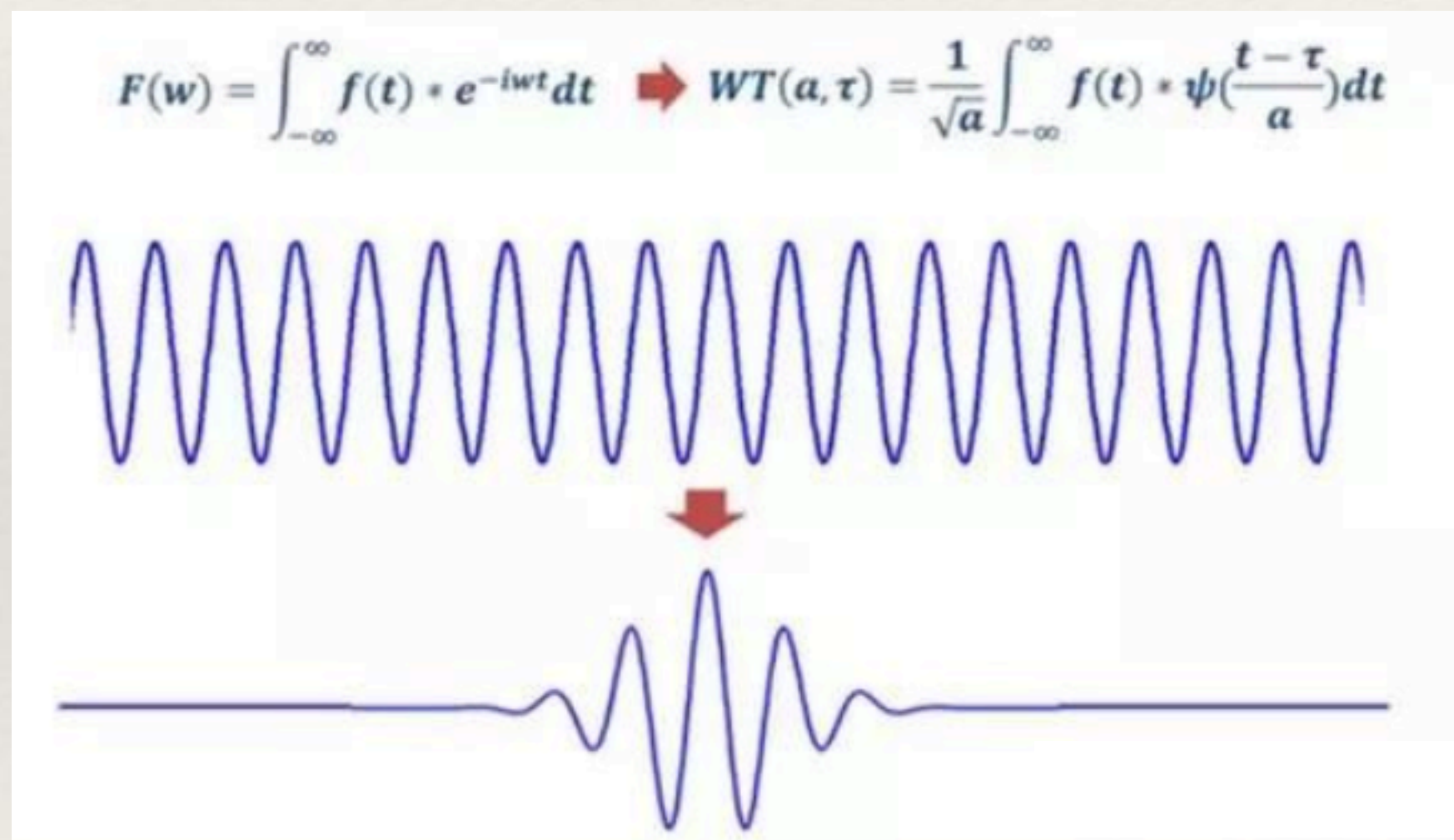


FIG. 13.—The raw PSPC photons and Voronoi cells for field 600520

Wavelet-based algorithm

- ❖ Wavelet methods successfully applied to ROSAT, Chandra, XMM-Newton data (Rosati et al. 1995; Vikhlinin et al. 1998; Valtchanov et al. 2001, Pacaud et al. 2006; Mullis et al. 2003; Lloyd-Davies et al. 2011; Xu et al. 2018). It has potential to detect (very) extended sources.
- ❖ Wavelet transform, provides both position and frequency of signals.



Wavelet-based algorithm

- ❖ Two-dimensional Gaussian function use to create a mother wavelet :

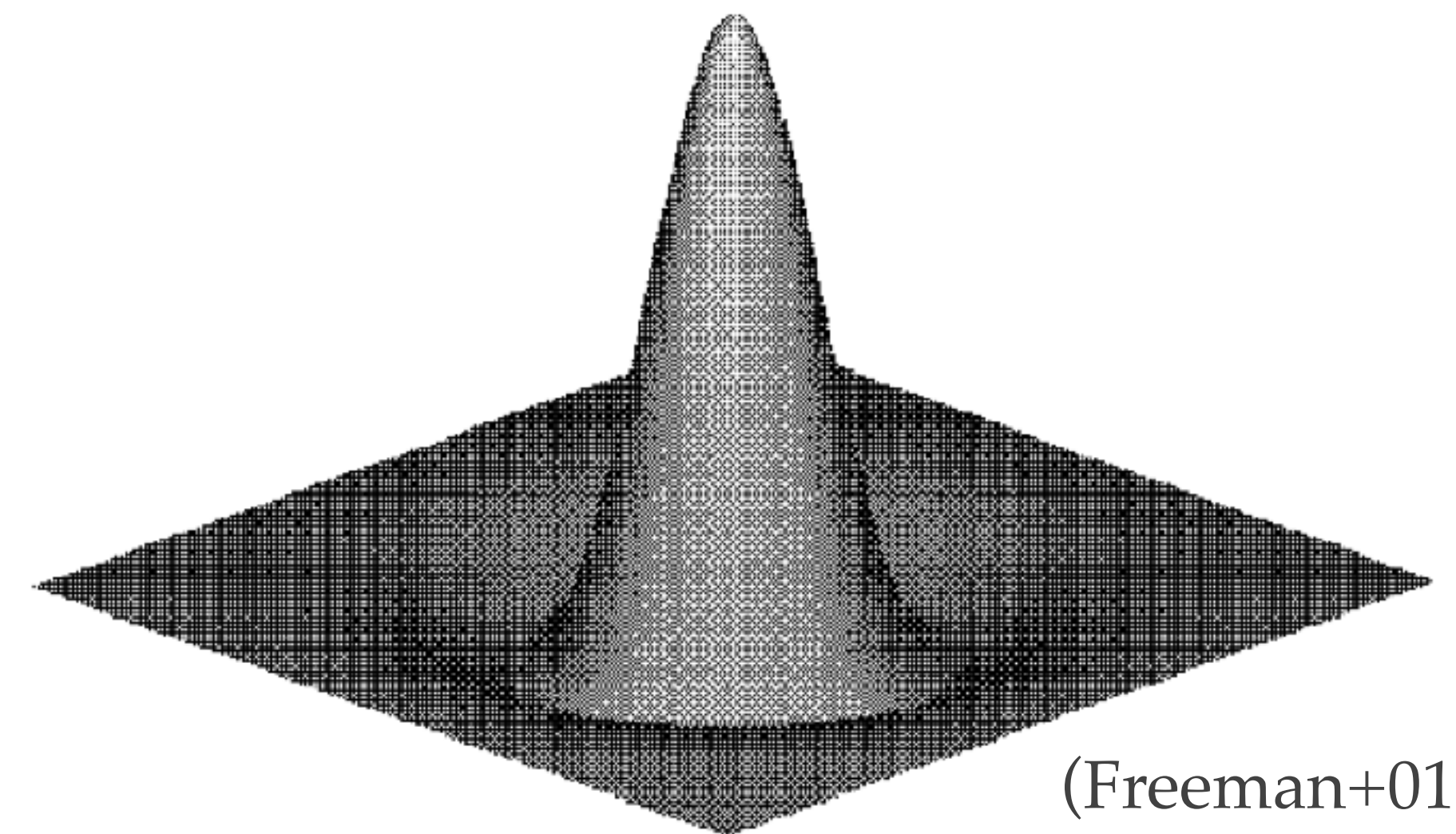
$$\phi\left(\frac{x}{\sigma_x}, \frac{y}{\sigma_y}\right) = \frac{1}{2\pi\sigma_x\sigma_y} \exp\left(-\frac{x^2}{2\sigma_x^2} - \frac{y^2}{2\sigma_y^2}\right),$$

- ❖ The Marr, or “Mexican Hat” (MH), wavelet function:

$$\begin{aligned} W'_m\left(\frac{x}{\sigma_x}, \frac{y}{\sigma_y}\right) &= \frac{1}{2\pi\sigma_x\sigma_y} \left[2 - \frac{x^2}{\sigma_x^2} - \frac{y^2}{\sigma_y^2}\right] e^{-\frac{x^2}{2\sigma_x^2} - \frac{y^2}{2\sigma_y^2}} \\ &= \frac{1}{2\pi\sigma_x\sigma_y} W_m\left(\frac{x}{\sigma_x}, \frac{y}{\sigma_y}\right). \end{aligned}$$

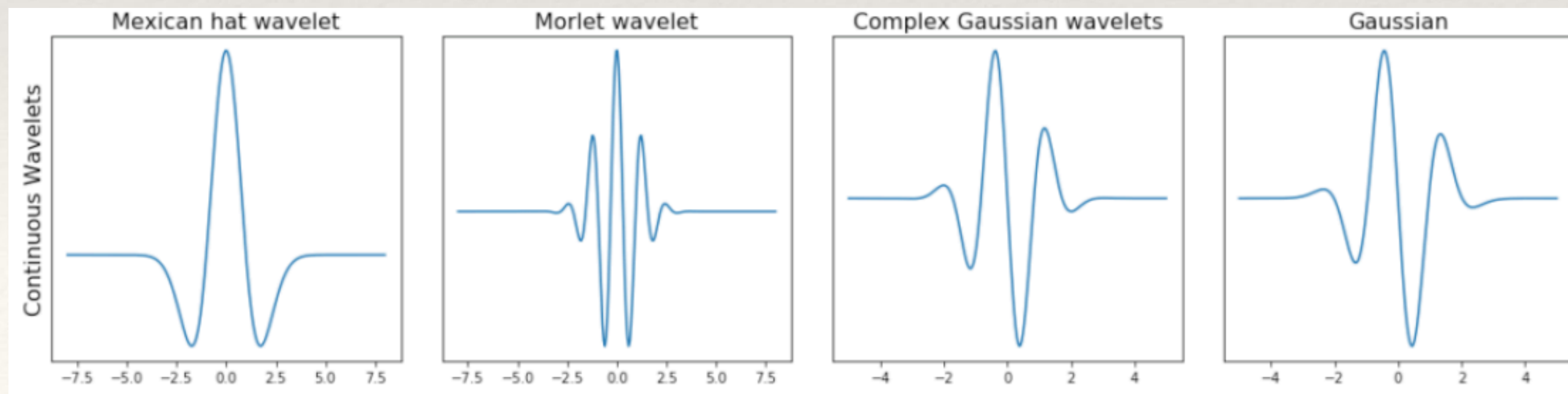
- ❖ The MH function has a positive kernel with shape a canonical PSF (PW), surrounded by a negative annulus (NW).

- ❖ Examples of popular wavelet functions:

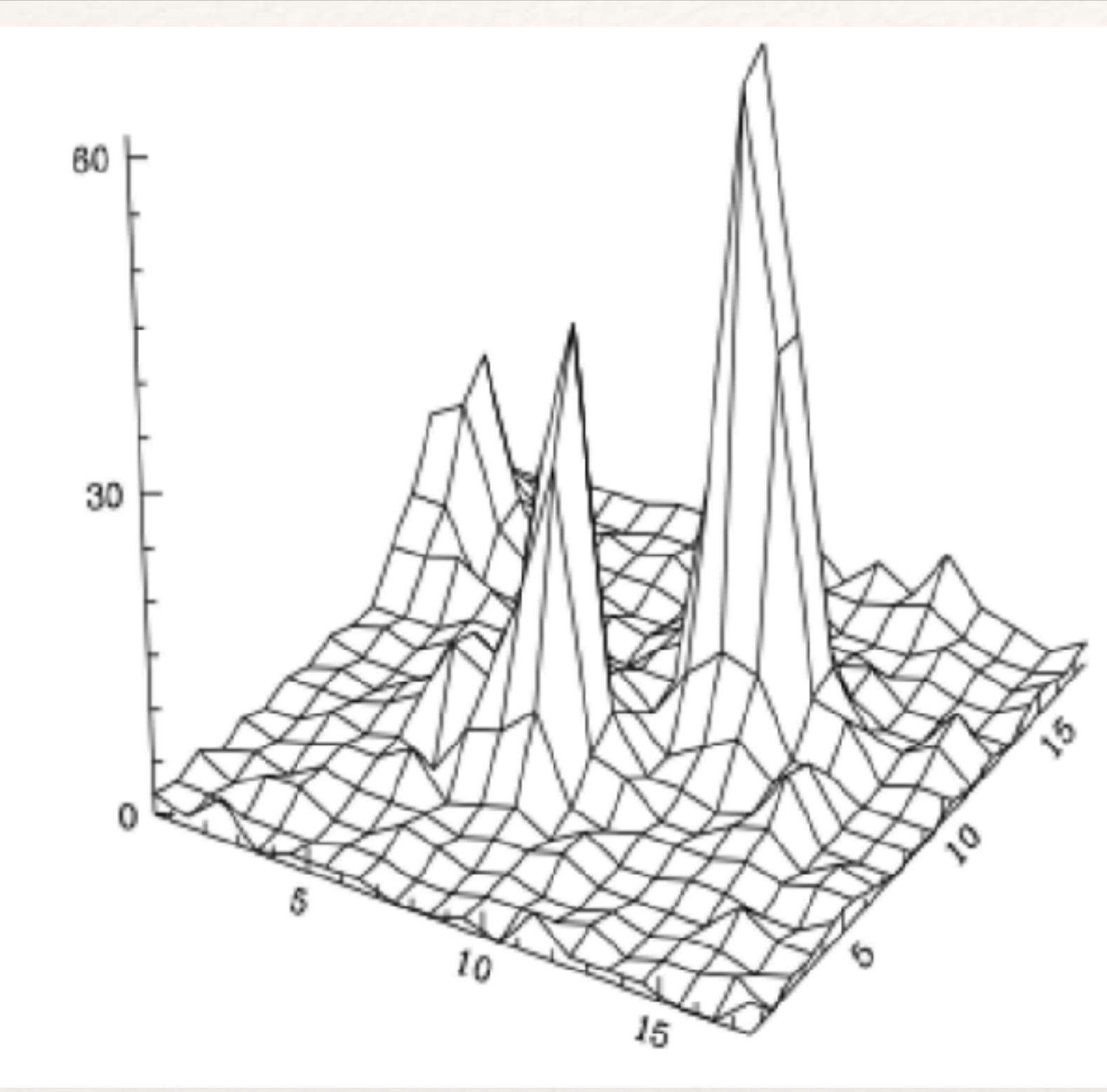
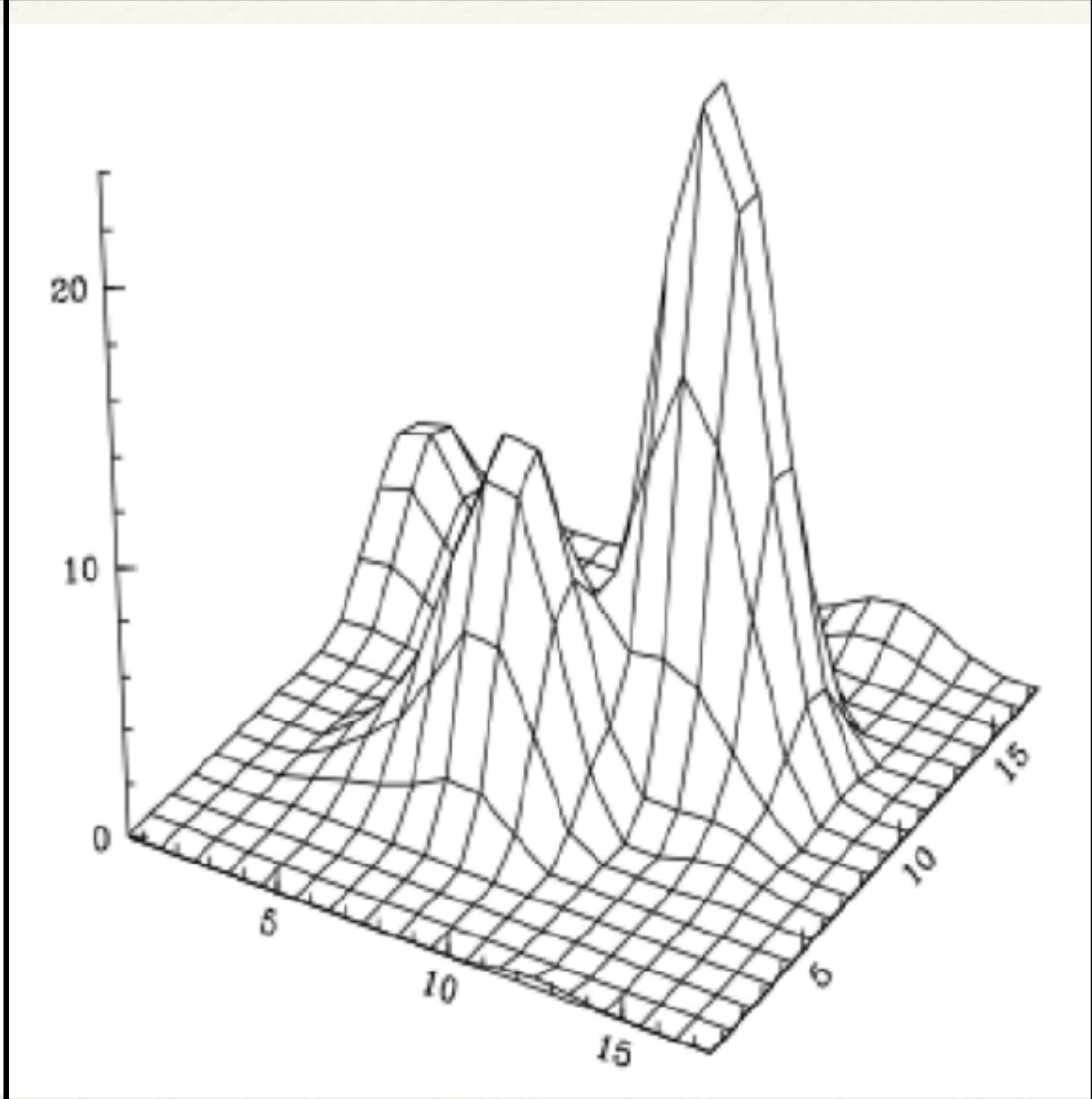
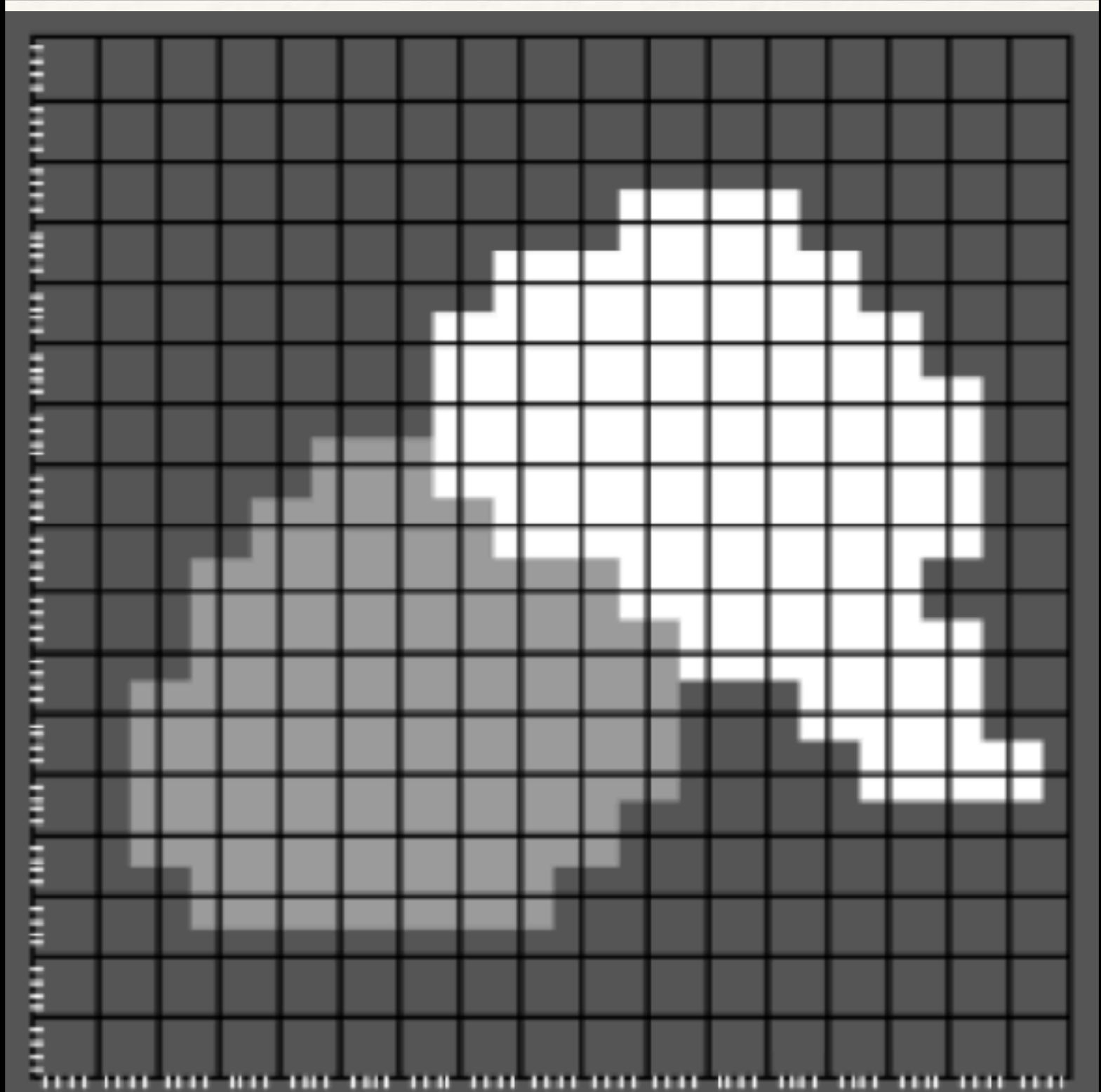


(Freeman+01)

2-dimensional Marr, or Mexican Hat, wavelet function.

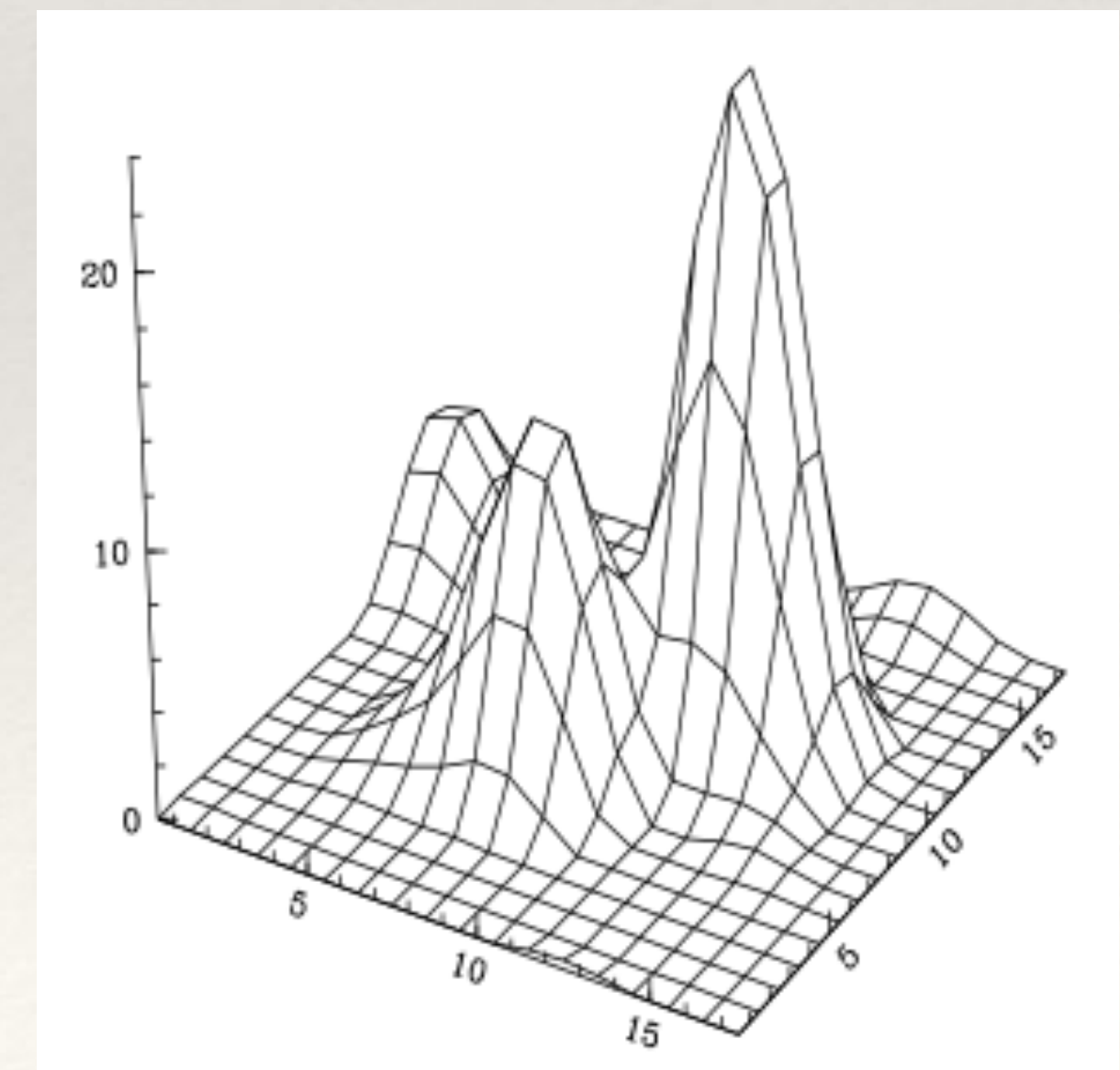
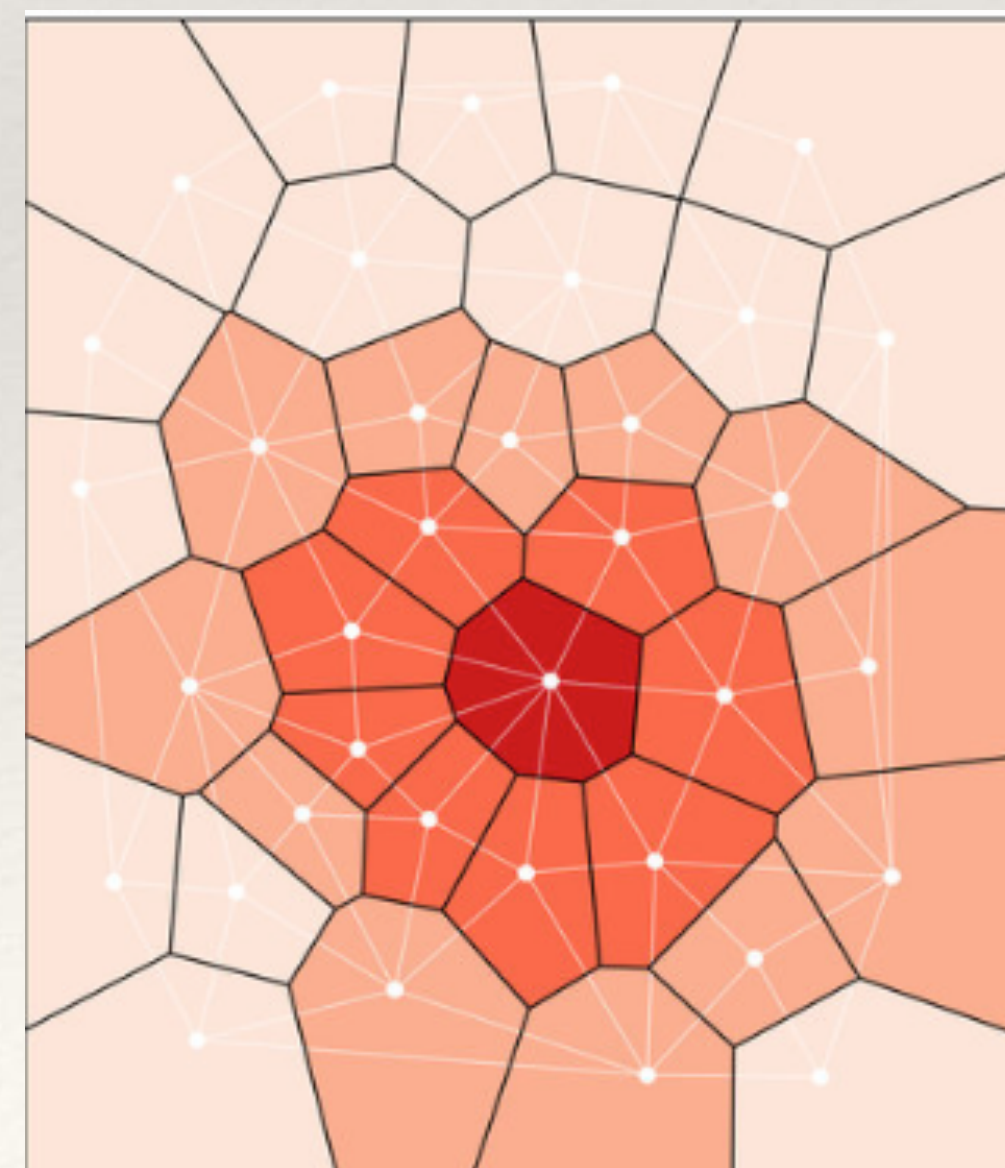
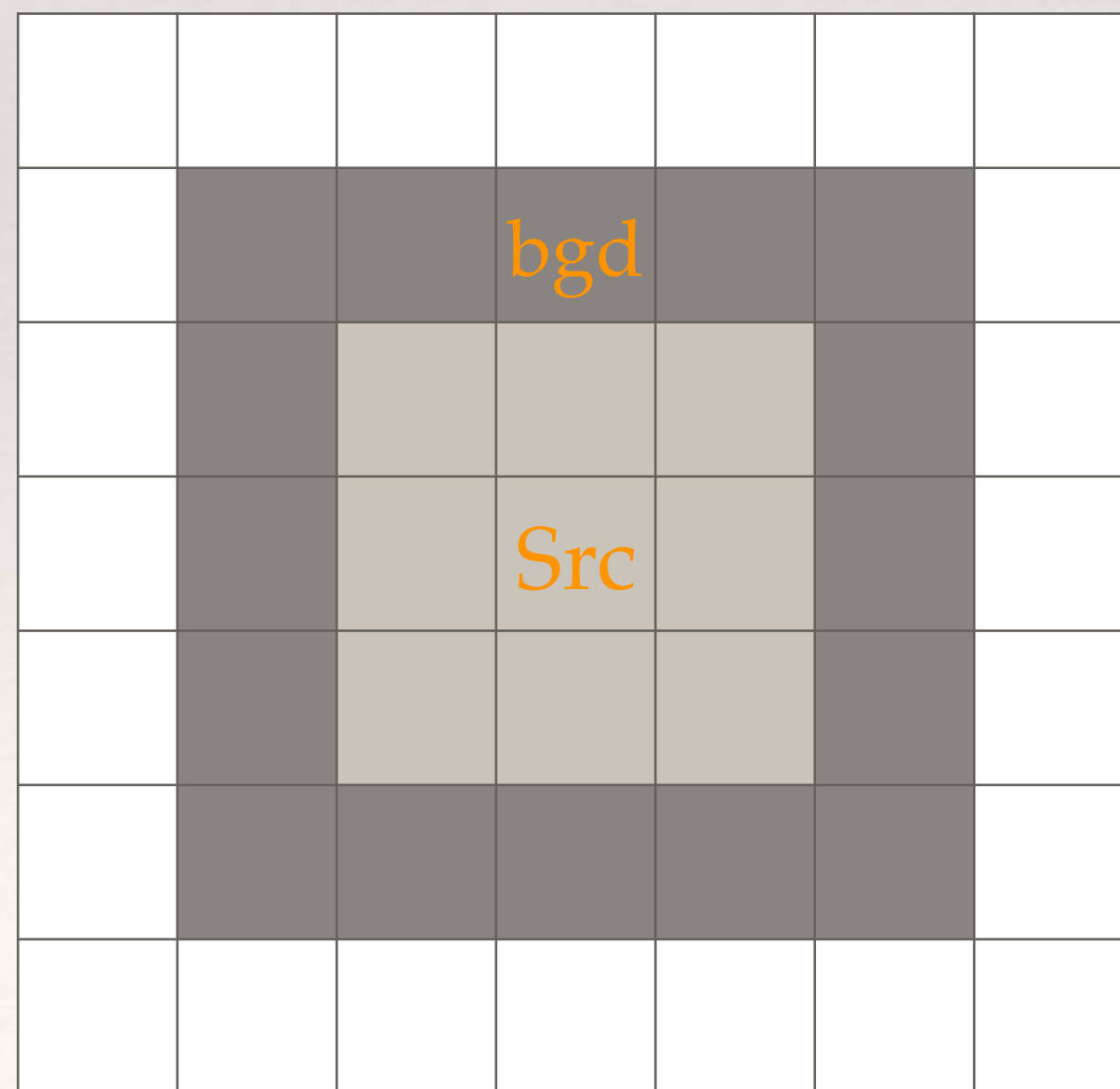


Wavelet-based algorithm - example

Obs.	Reconstructed image after wavelet filtering	Pixel map of each sources
		
Counts data of an isolated Cluster observed by ROSAT PSPC.	Reconstructed image, with background removed.	Pixels for each detections.

Summary of main cluster detection methods

- ❖ Sliding box is widely used in popular X-ray surveys, have high detection efficiency especially for compact objects,
- ❖ Voronoi tessellation and percolation (VTP) tends to detect in crowded region,
- ❖ Wavelet-based detections select out signals in specific scale. It has potential to detect (very) extended sources.

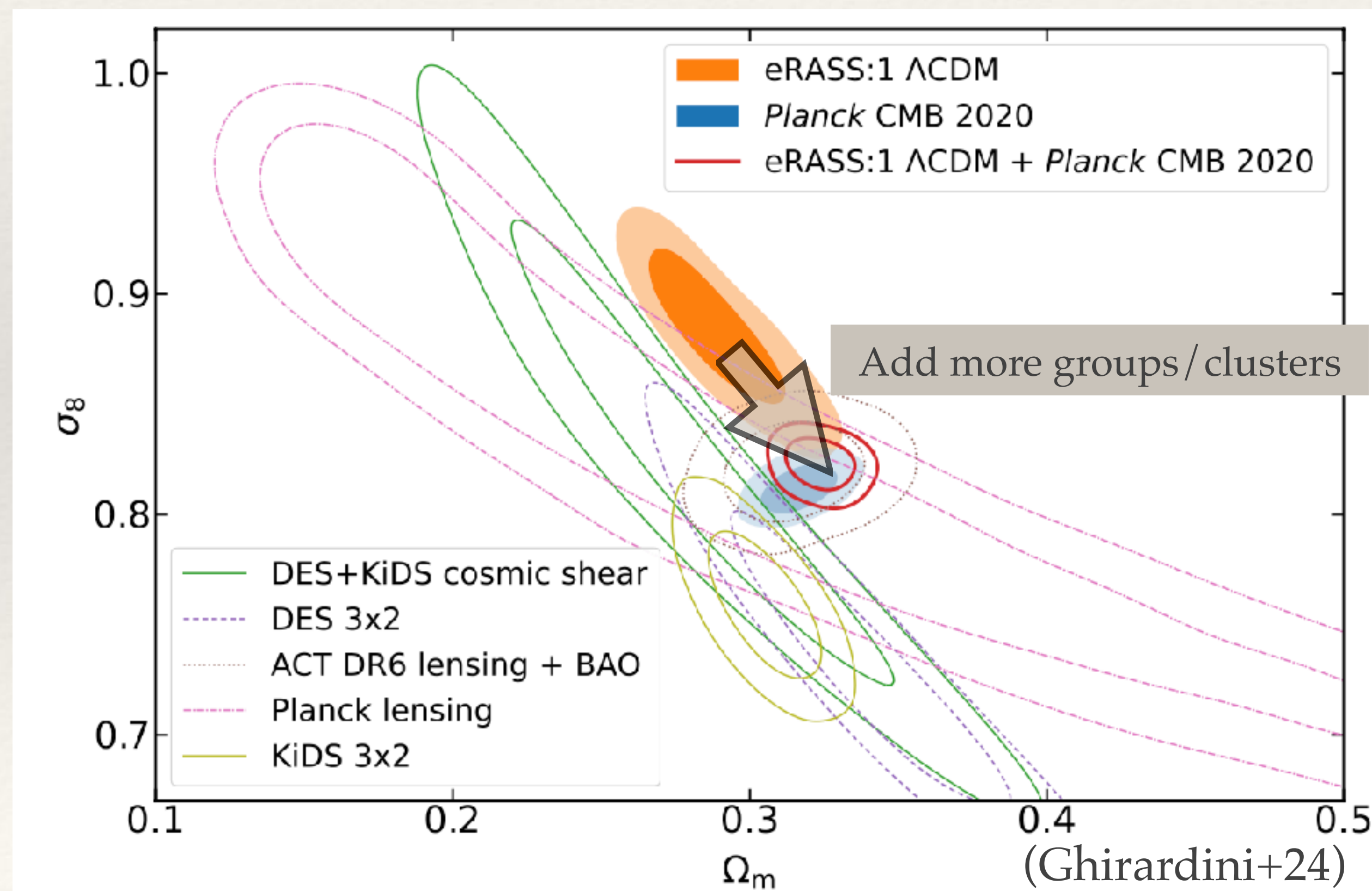


2. The detection of X-ray extended clusters

RXGCC (RASS-based extended X-ray Galaxy Cluster Catalog), arxiv:2110.14886, A&A
XVXGC (XMM-SERVS X-ray eXtended Galaxy Cluster catalog), arxiv:2406.06701, A&A

The problem of incompleteness

- Question: tension between cosmological parameters derived from cluster counts and the ones from primary CMB (Planck collaboration+14,15,20)
- One explanation: clusters samples might be incomplete.
- Our project: to search for very extended X-ray clusters that might be missed in previous ICM-based works.



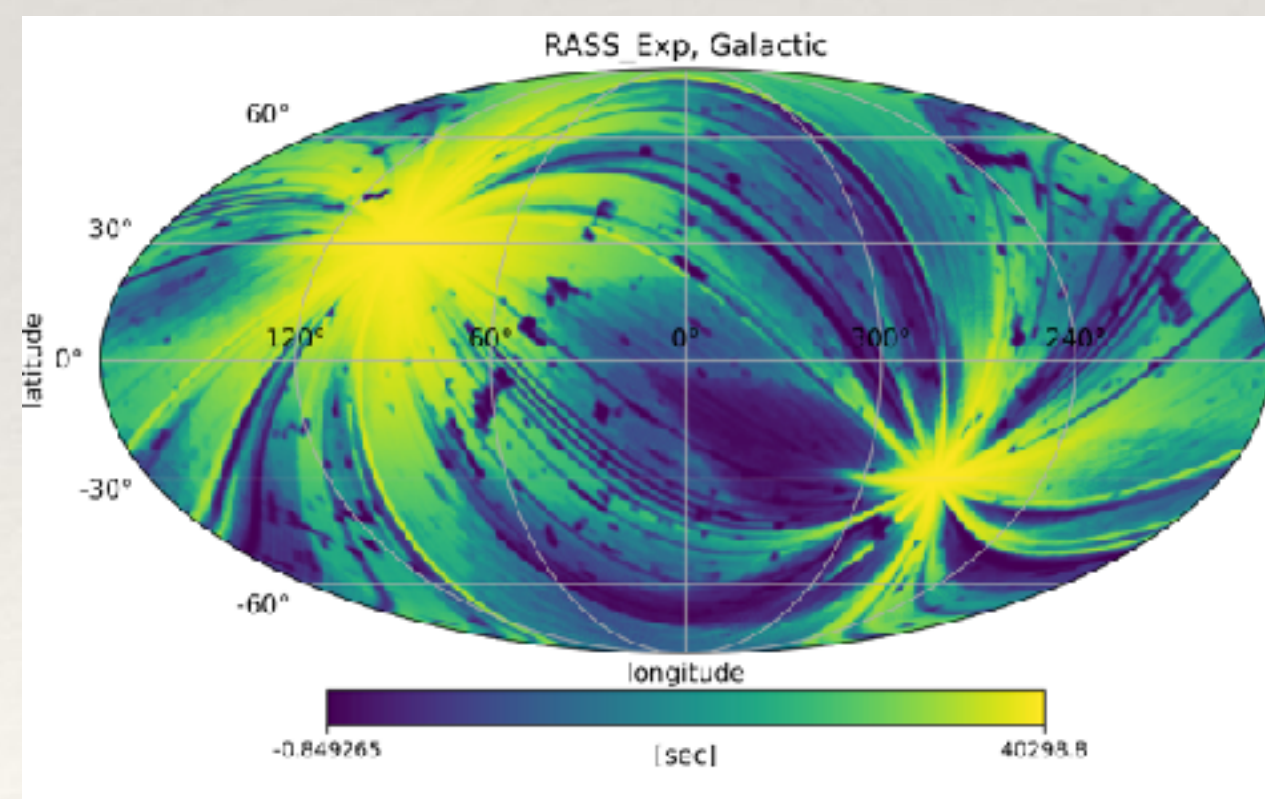
All-sky X-ray surveys

ROSAT (Voges et al. 1999)

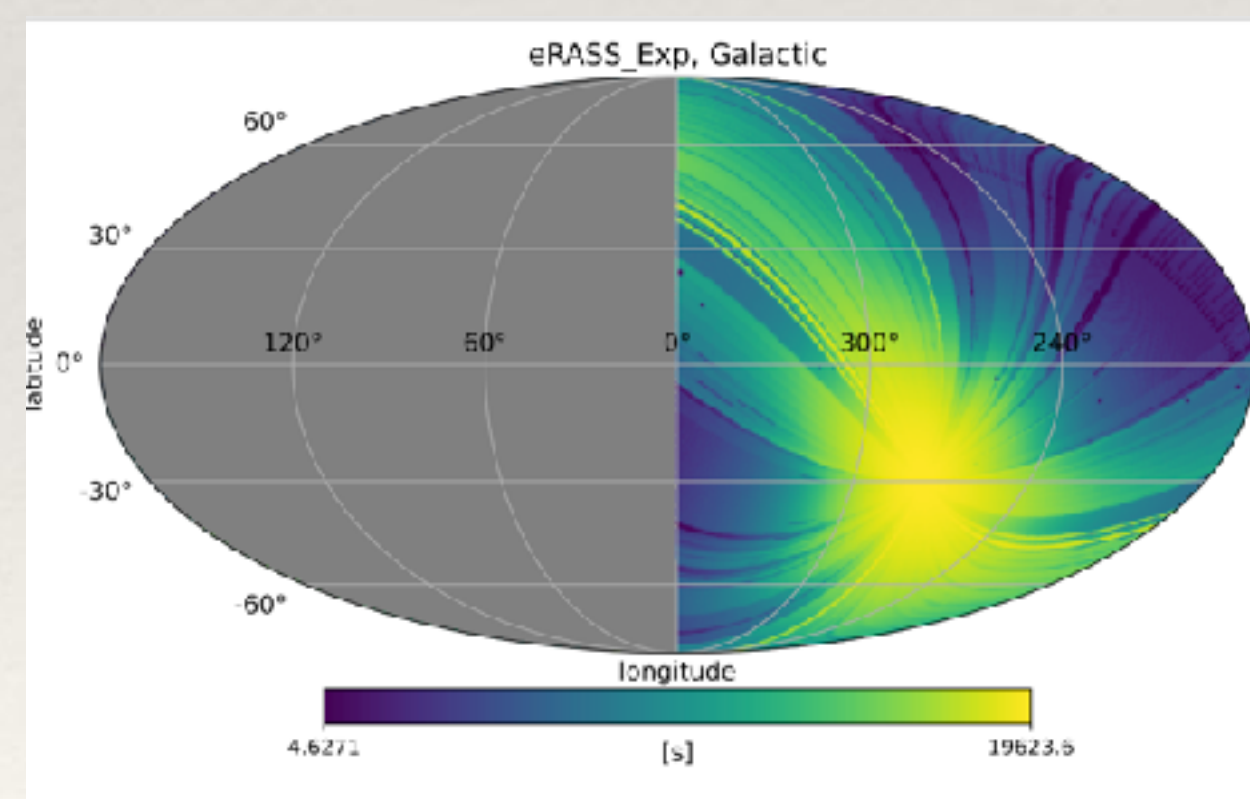
- 1990-1999, 0.1-2.4 keV
- ROSAT All-sky Survey (RASS): main source of cluster catalogs used for cosmological research.

eROSITA (Predehl et al. 2021)

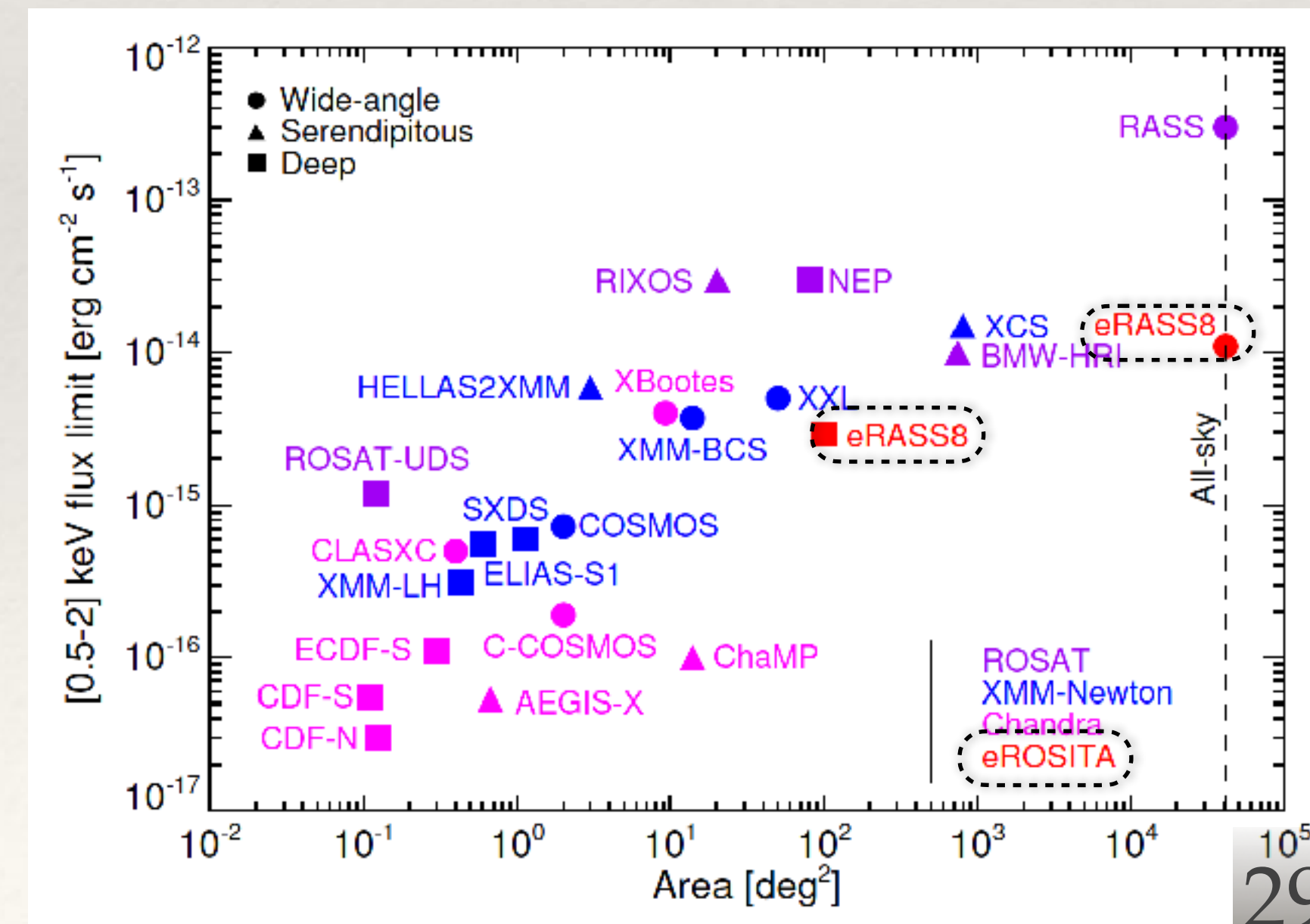
- 2019-?, 0.1-10keV, sensitivity 30 times better than the one of ROSAT.
- eROSITA all- sky survey (eRASS), to detect the hot ICM of 50-100 thousand GGs and GCs.



RASS exposure map

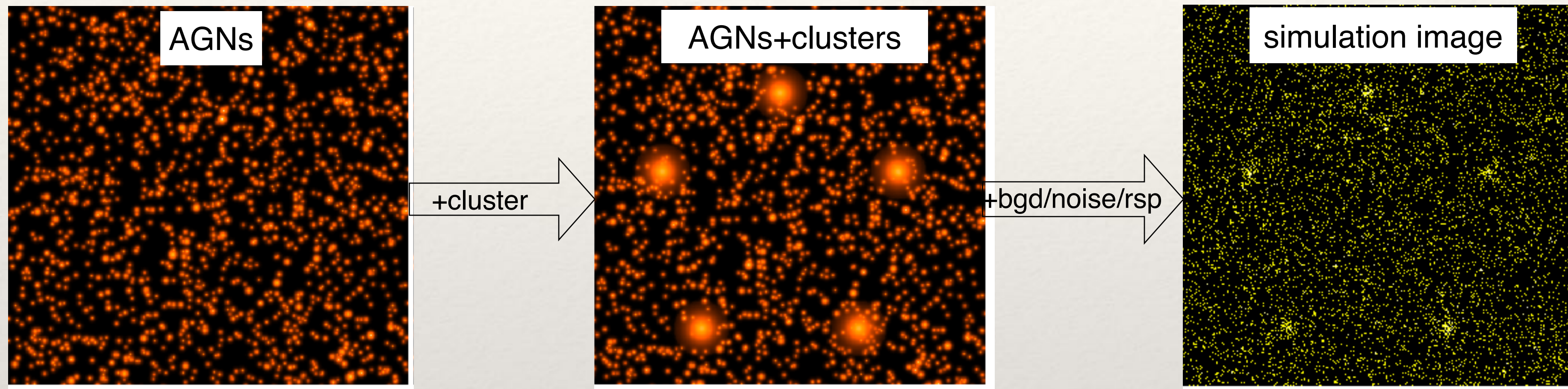


eRASS-DE exposure map



Simulation

1. **AGNs:** brightness distribution from Moretti ea. (2003), and randomly distributed.
2. **Clusters:** spherically symmetric β -model of the surface brightness of galaxy clusters (Cavaliere ea. 1976).

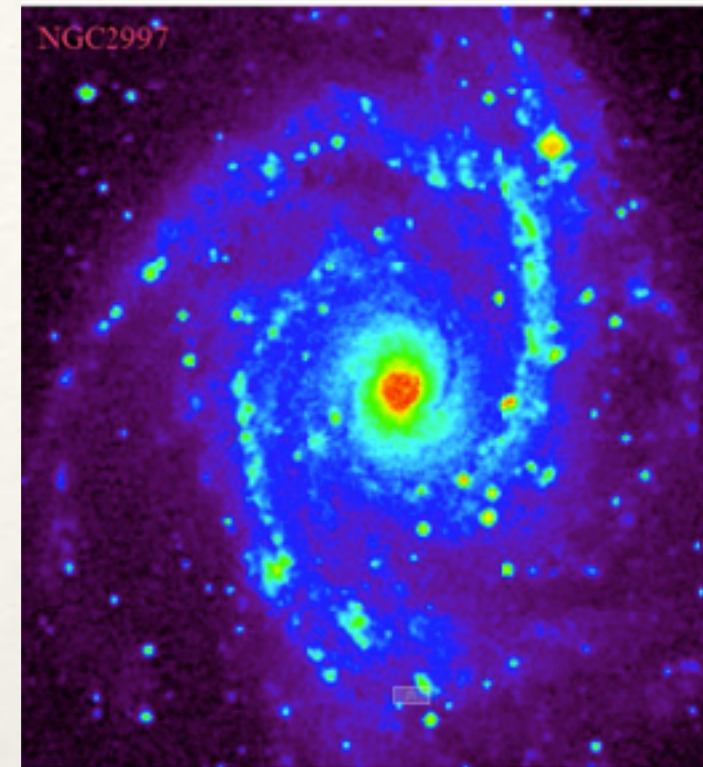


ICM profile of density, of X-ray surface brightness (β -model),

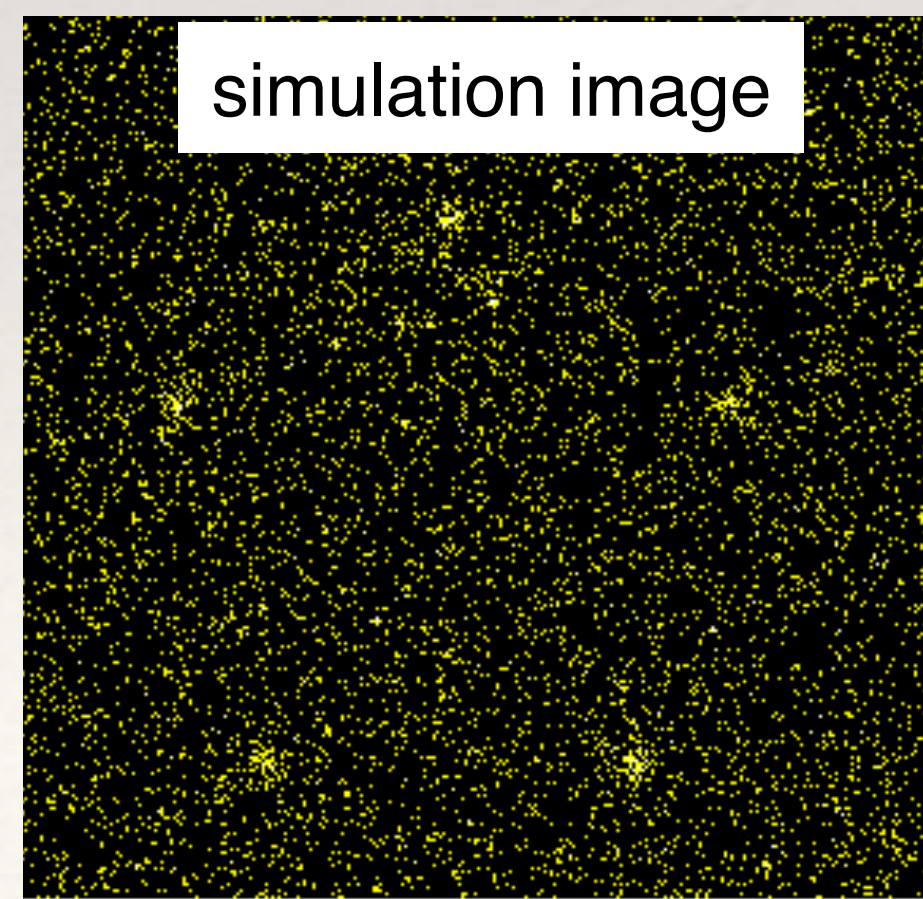
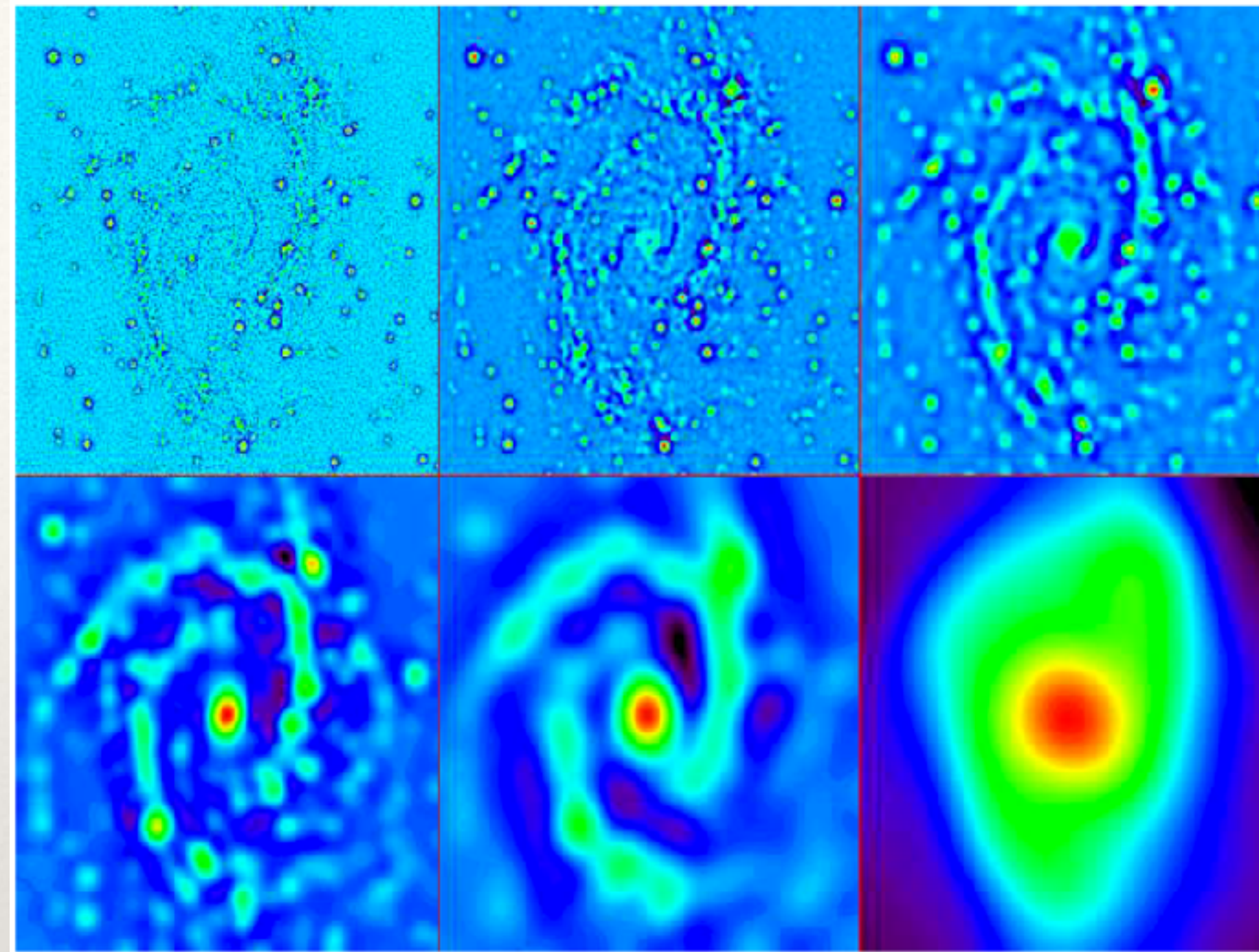
$$\rho_{\text{gas}}(r) = \rho_{\text{gas}}(0) \left(1 + \frac{r^2}{r_c^2} \right)^{-\frac{3}{2}\beta}.$$

$$S_X(R) = S_X(0) \left(1 + \frac{R^2}{r_c^2} \right)^{-3\beta + \frac{1}{2}},$$

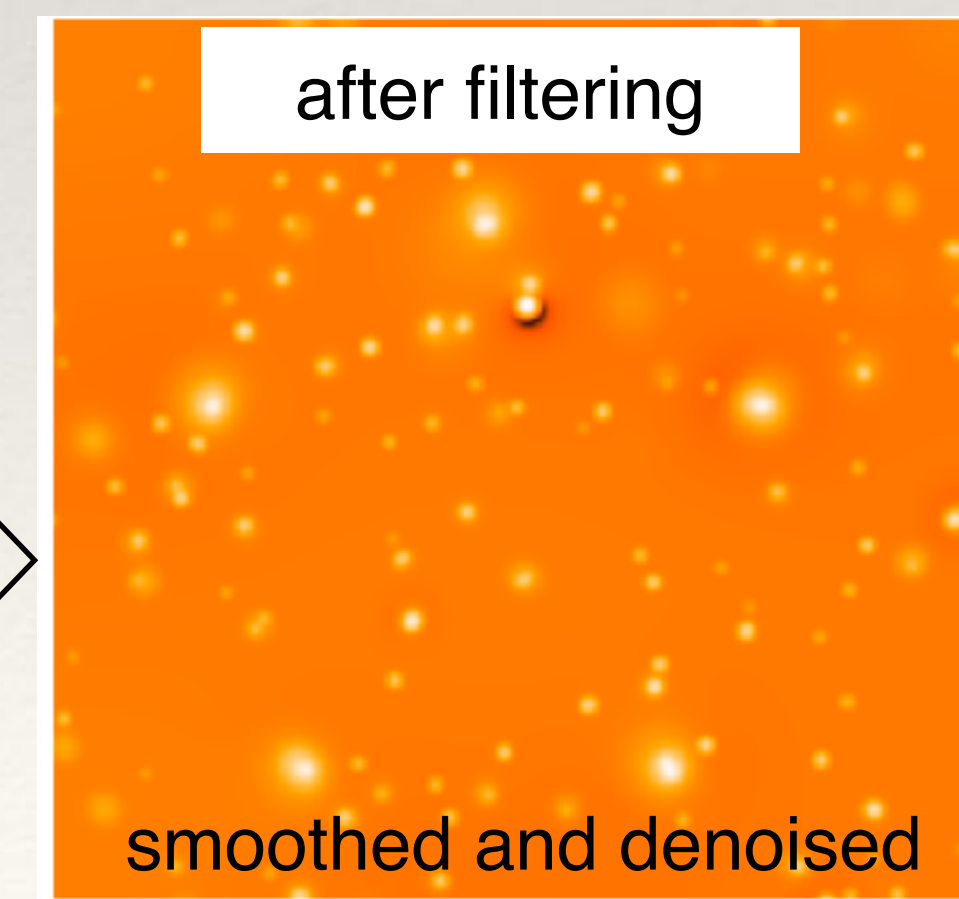
Step 1 of detection: wavelet



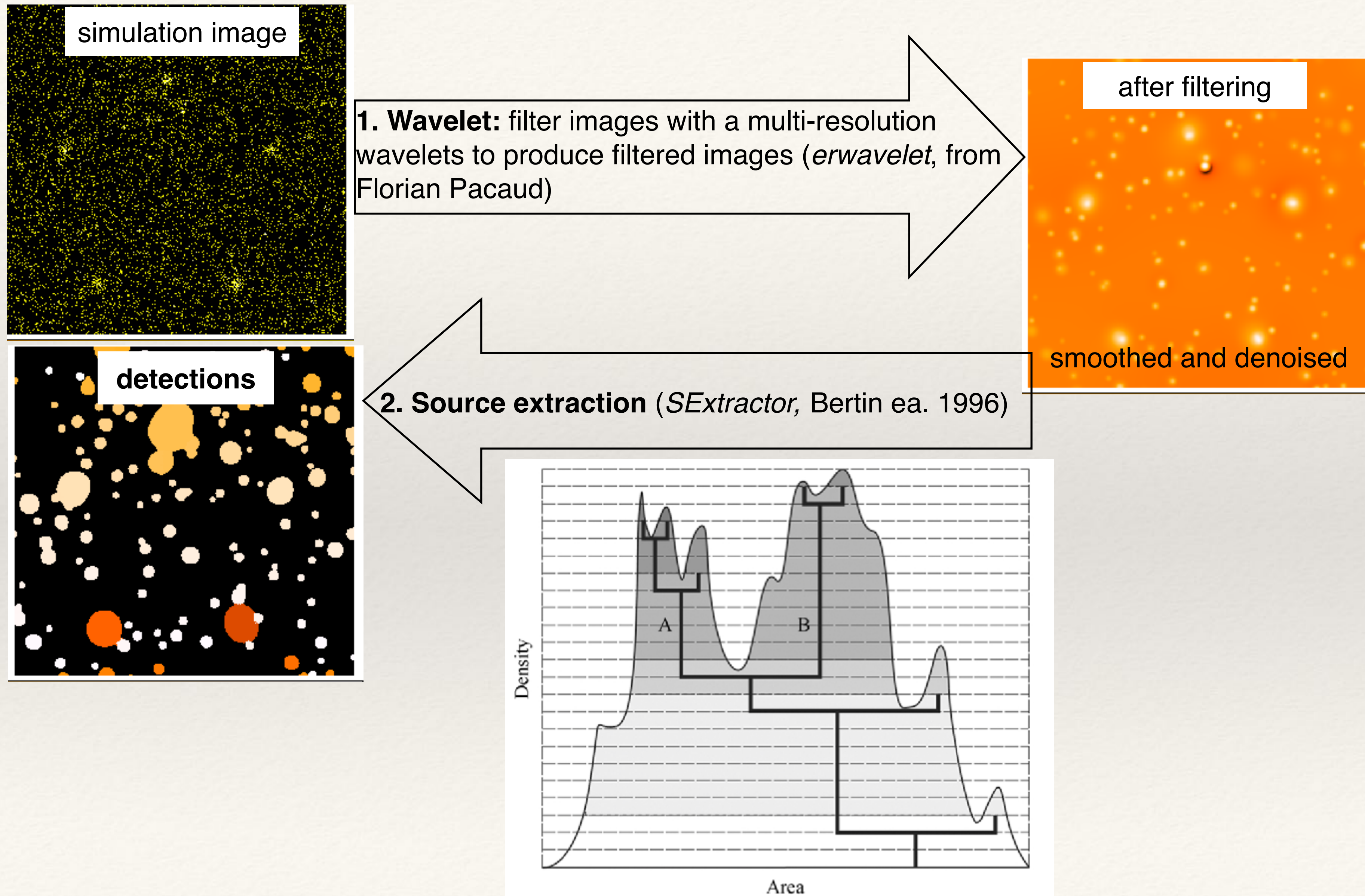
Example: Wavelet transform of NGC 2997 by the *à trous* algorithm (Starck & Murtagh).



1. Wavelet: filter images with a multi-resolution wavelets to produce filtered images (*erwavelet*, from Florian Pacaud)



Step2 of detection: source extraction



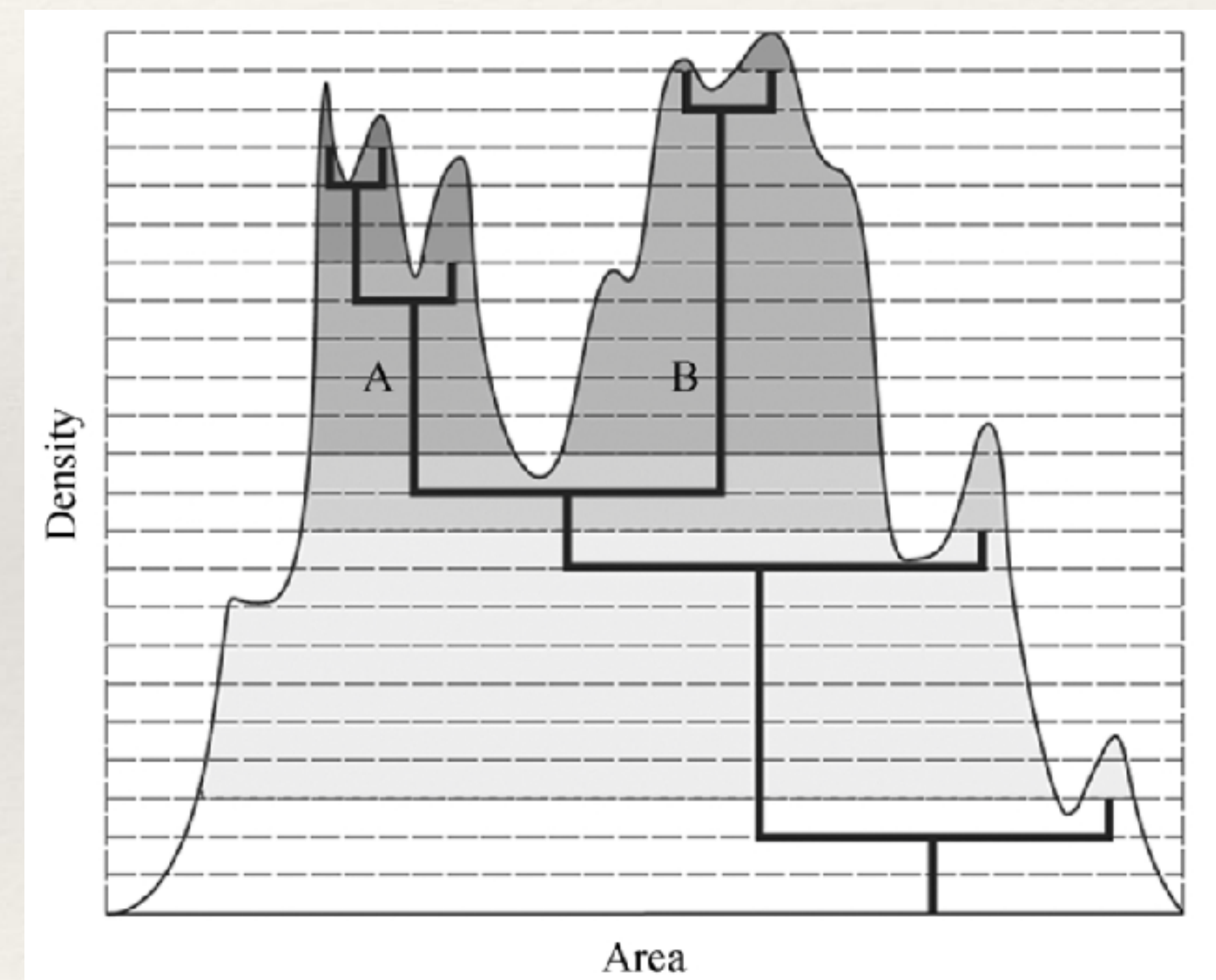
Parameter setting of SExtractor

1. Detect.

- ❖ *DETECT_THRESH*, the minimum signal-to-noise ratio above the local background. **Bright source.**
 - Example: 3.0.
- ❖ *DETECT_MINAREA*, the minimum number of pixels to trigger a detection. **Big source.**
 - Example: 5.

2. Deblend.

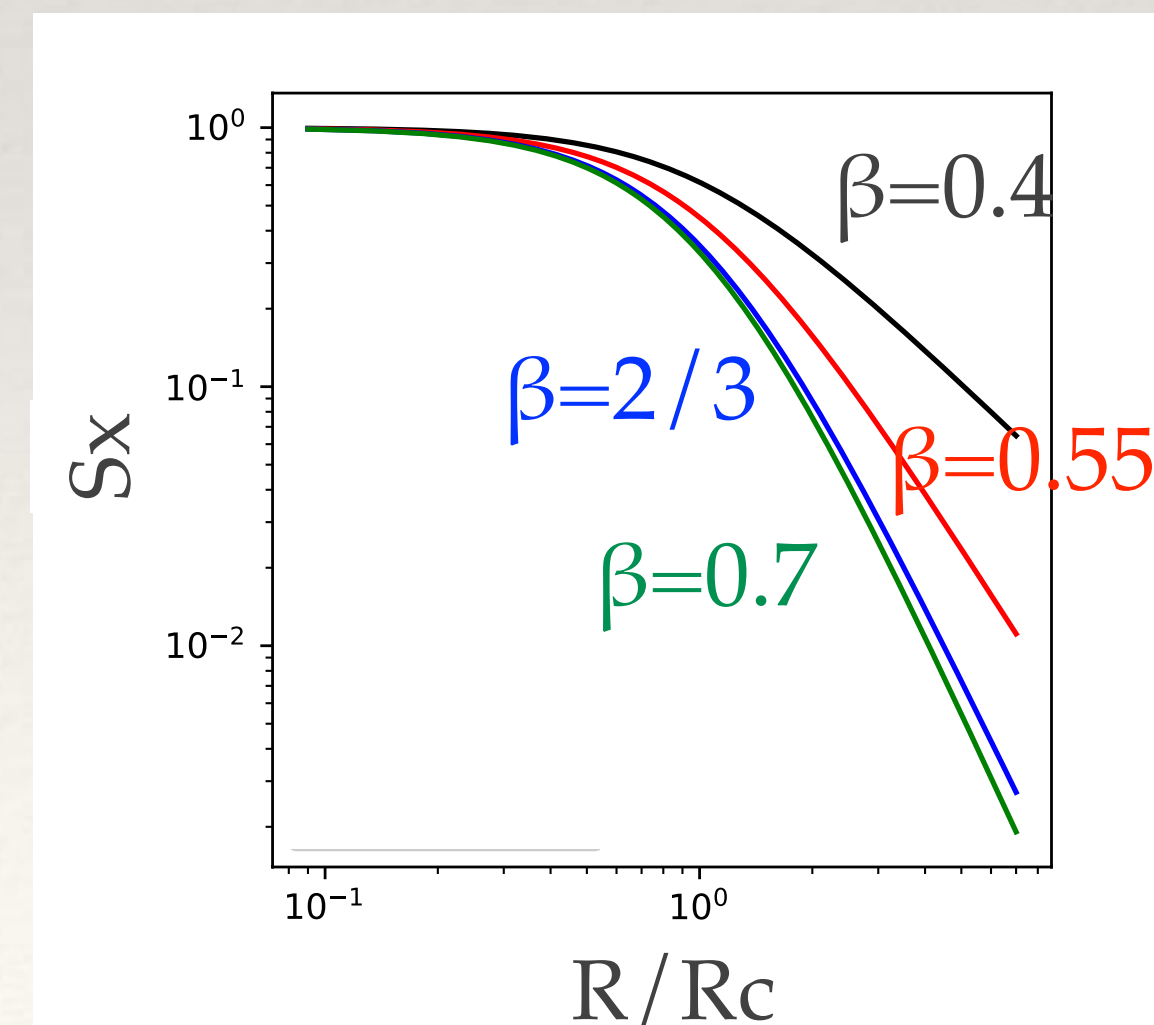
- ❖ *DEBLEND_NTHRESH*, the number of deblending sub-thresholds. **Big substructure.**
 - Example: 32.
- ❖ *DEBLEND_MINCONT*, the minimum contrast of local peaks to be considered as separate objects. **Bright substructure.**
 - Range: 0 to 1. Example: 0.01.



Step3 of detection: Maximum likelihood fitting

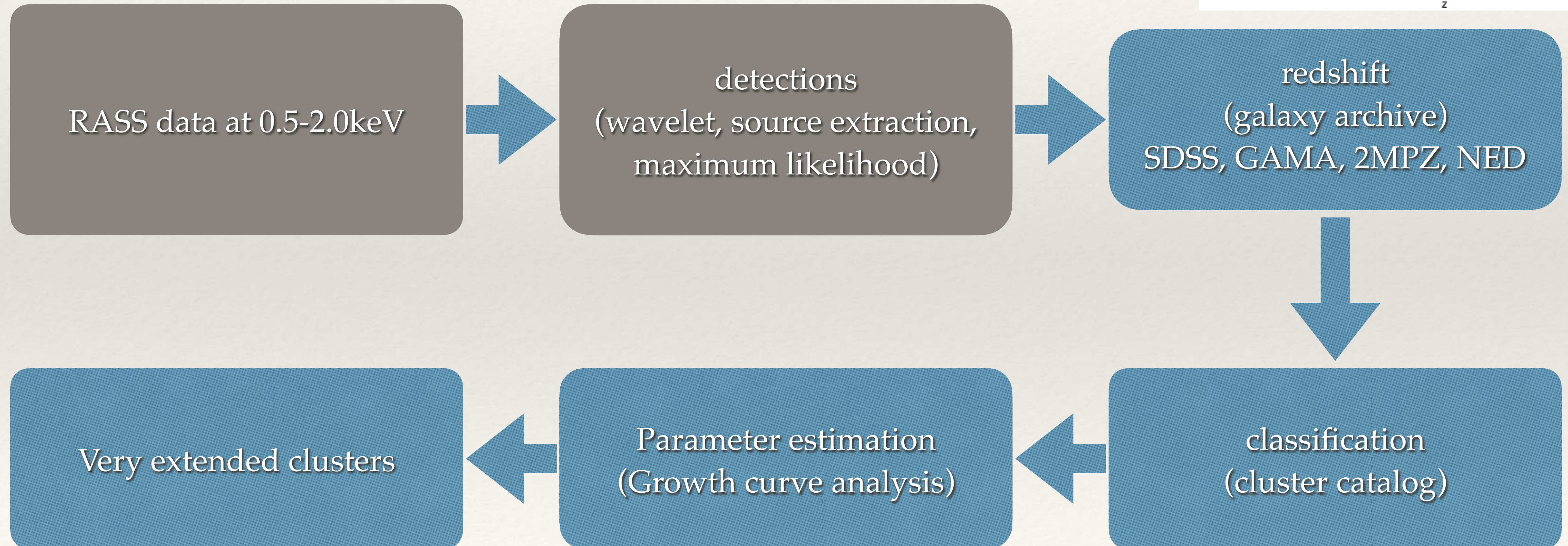
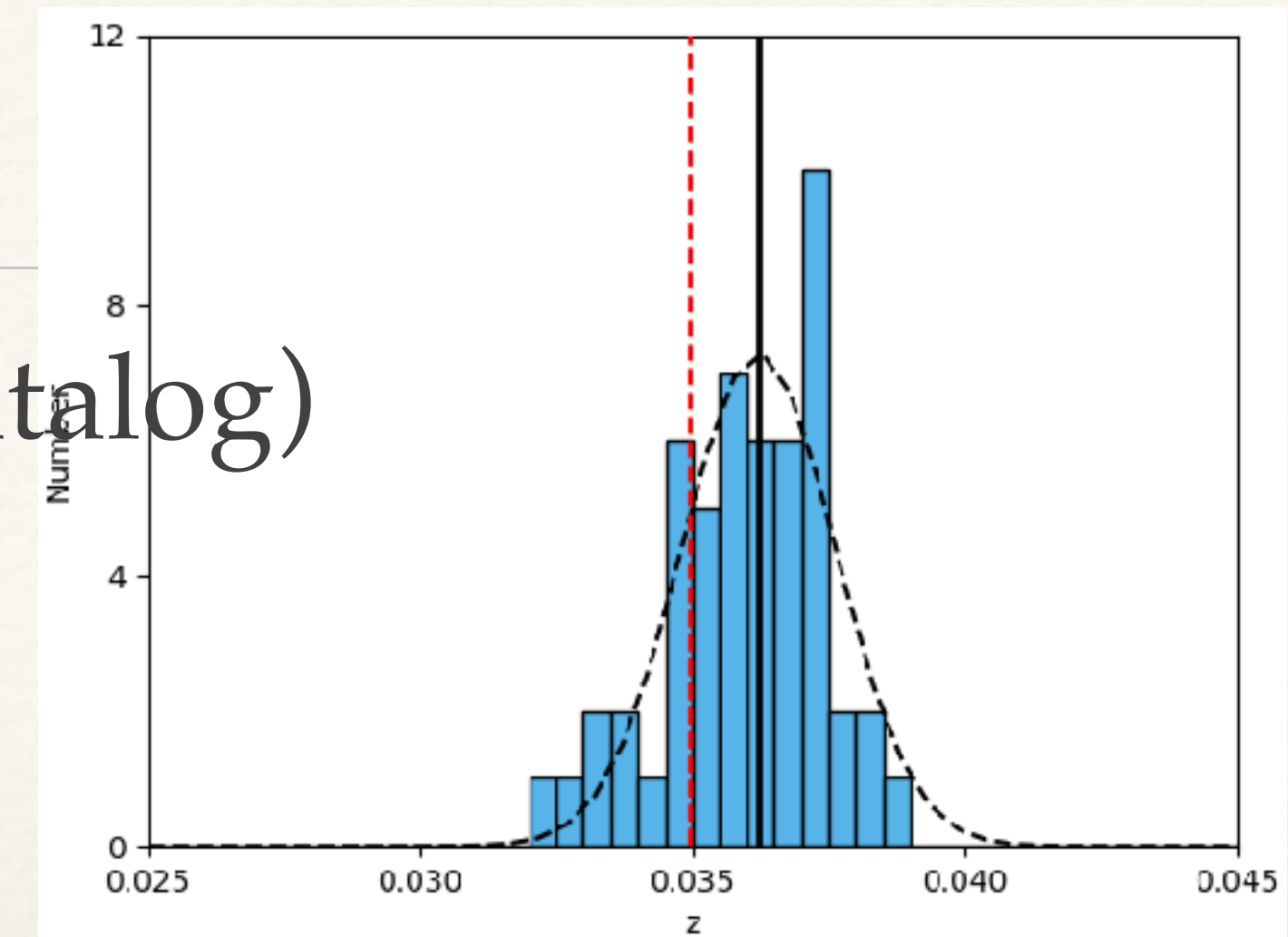
1. Wavelet: filter images with a multi-resolution wavelets to produce filtered images (erwavelet, from Florian Pacaud)
2. Source extraction (*SExtractor*, Bertin ea. 1996)
3. Maximum likelihood fitting (ML, From Miriam E. Ramos-Ceja):
 - A. point-like and extended source modelling;
 - B. important parameters: **extension likelihood and extent**
 - **point-like modeling**: PSF => detection likelihood of point source
 - **extended source modeling**: β model \otimes PSF => detection likelihood of extended source
 - **extension likelihood**: difference between detection likelihood of point source and extended source modeling.
 - **extent**: core radius of β model

$$S_X(r) \propto \left[1 + \left(\frac{r}{r_c} \right)^2 \right]^{-3\beta+1/2}$$



Pipeline of RXGCC

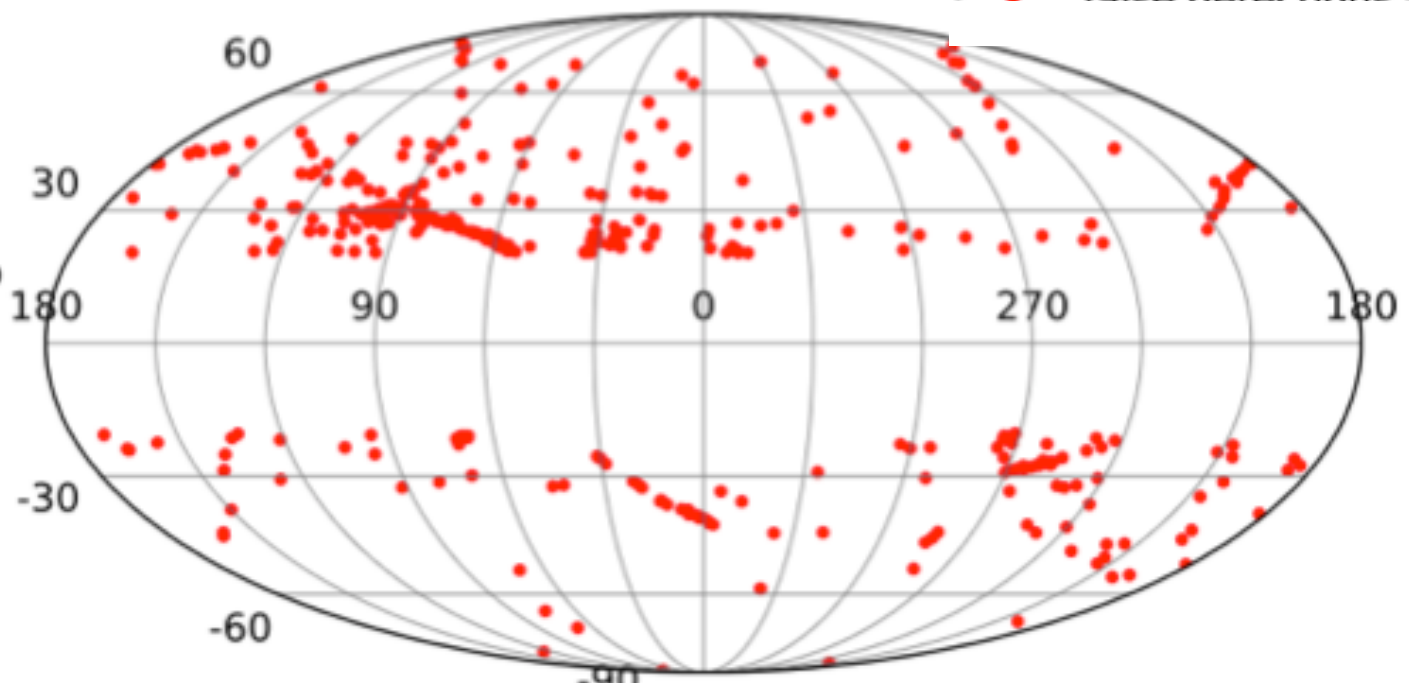
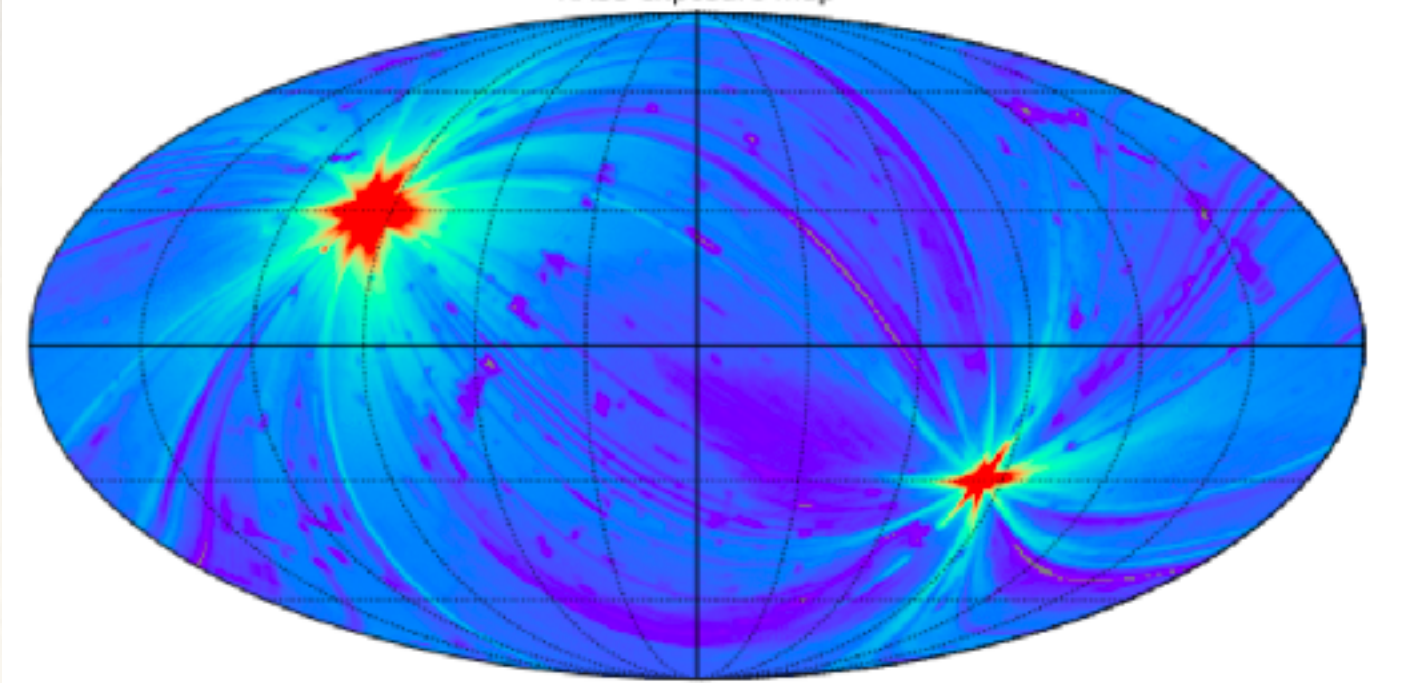
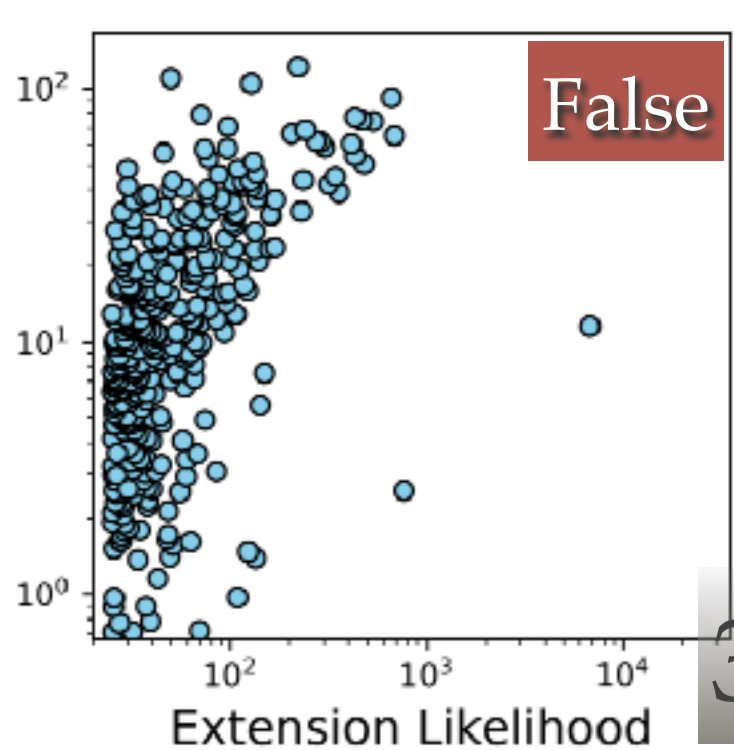
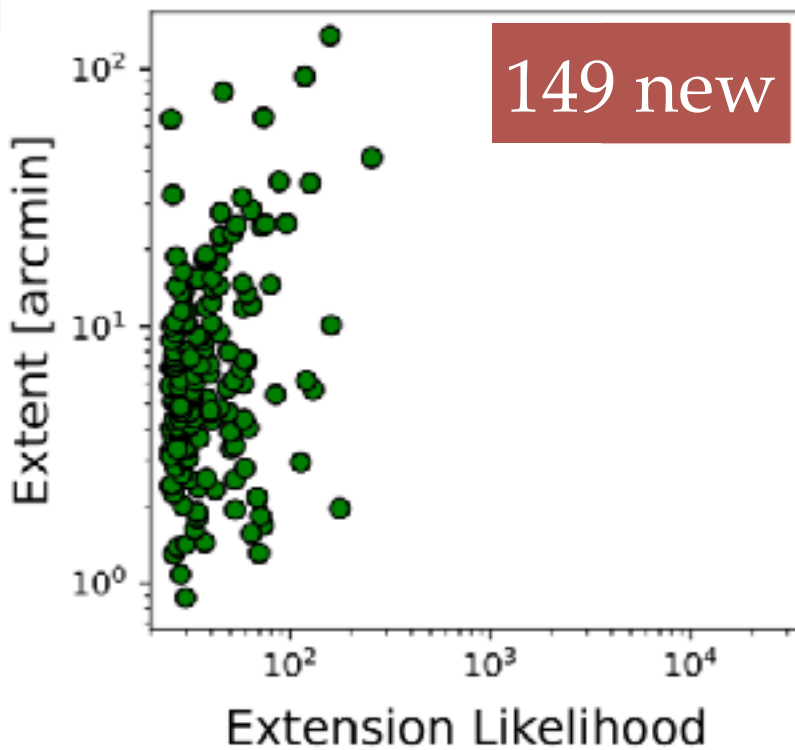
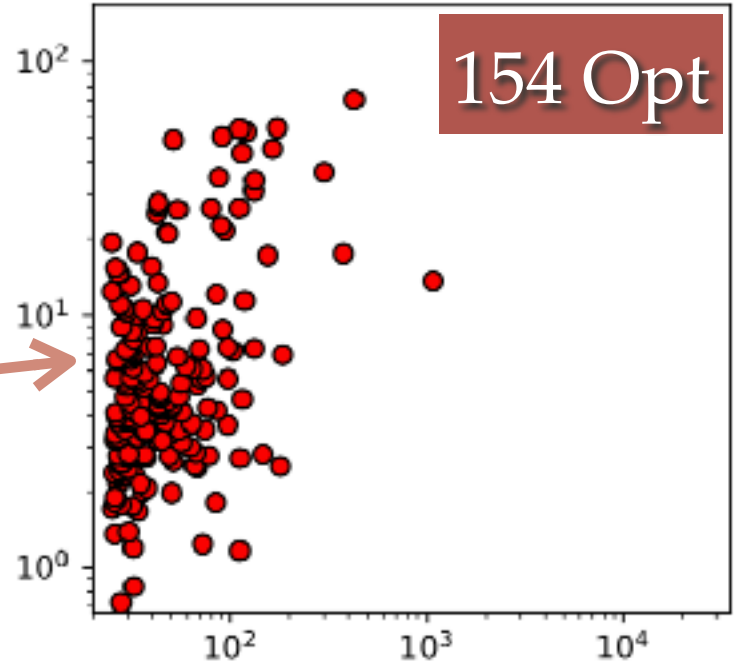
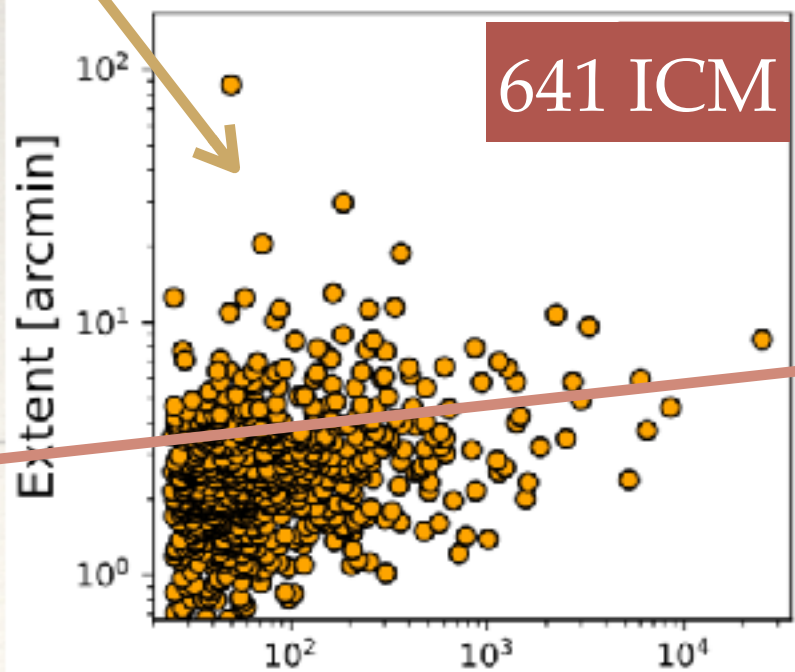
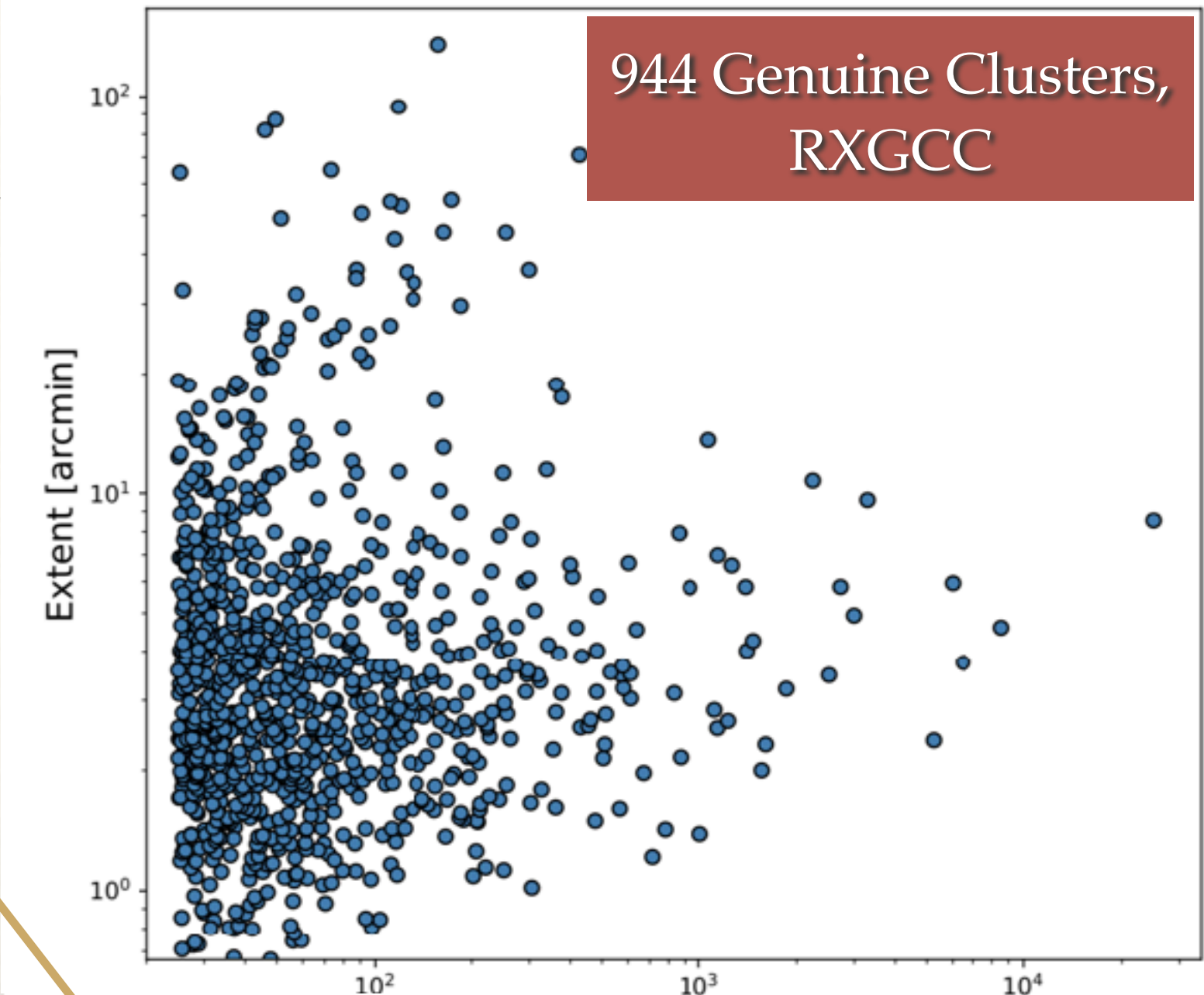
- ❖ RXGCC (RASS-based extended X-ray Galaxy Cluster Catalog)



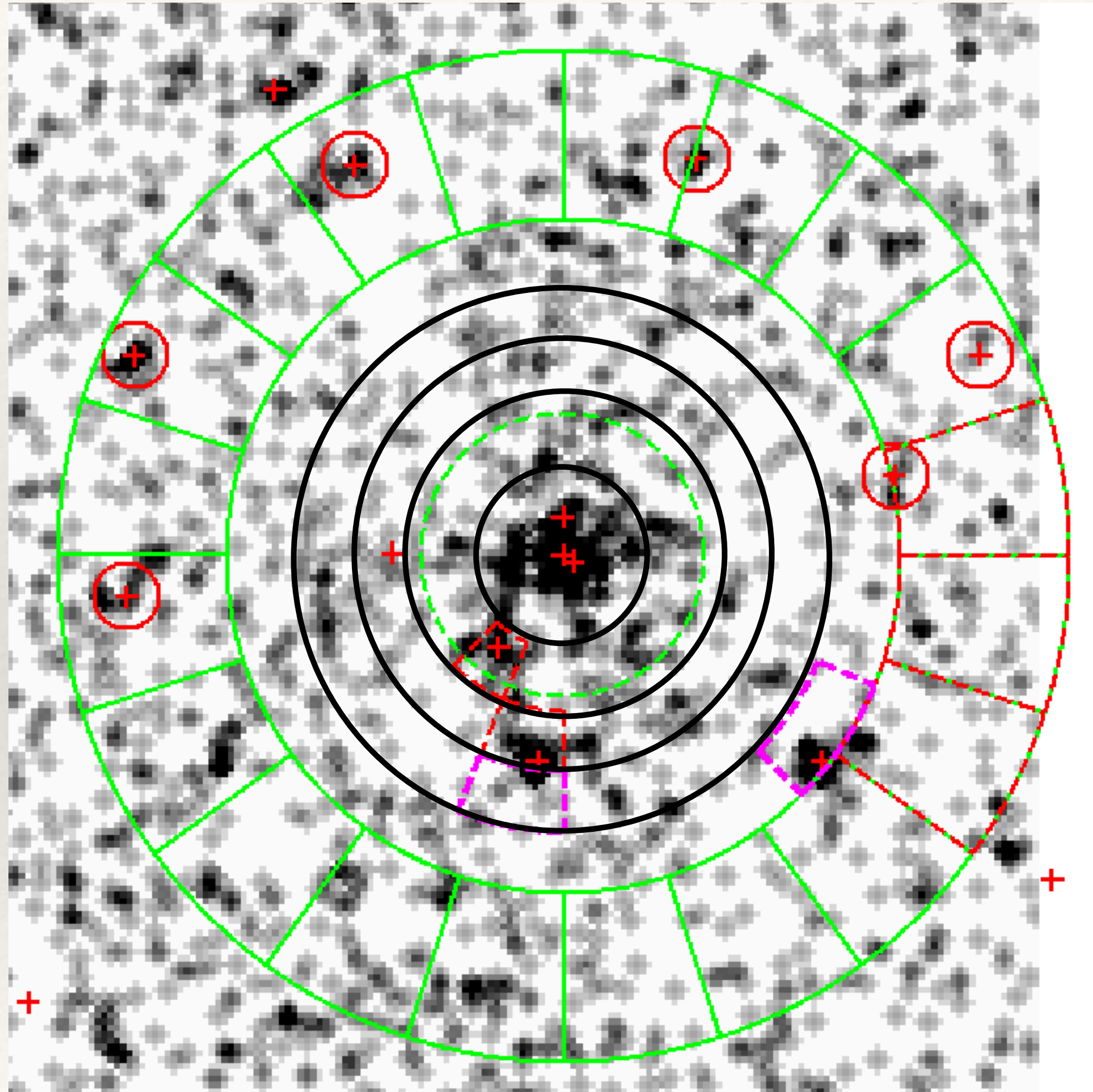
Classification

Table 1. Overview of cluster catalogs and X-ray point-source catalogs.

Catalogs	Reference	N _{gc}	N _{gc(with z)}	Survey
X-ray catalogs	Finoguenov et al. 2020	10 382	10 382	ROSAT
	Takey et al. 2011, 2013, 2014, 2016	904	904	XMM-Newton, SDSS
	Clerc et al. 2020; Kirkpatrick et al. 2021	2 740	2 740	ROSAT
	Clerc et al. 2016	240	240	ROSAT, XMM-Newton
	Clerc et al. 2012	422	176*	XMM-Newton XXL
	Pacaud et al. 2016	100	100	XMM-Newton XXL
	Liu et al. 2015	263	0	Swift
	Mehrtens et al. 2012	503	463	XMM-Newton
	Piffaretti et al. 2011	1 743	1 743	ROSAT
	Ledlow et al. 2003	579	579	ROSAT
Microwave catalogs	Ebeling et al. 1996	283	278	ROSAT
	Tarrío et al. 2019	2 323	1 459	Planck, RASS
	Tarrío et al. 2018	225	171	Planck, RASS
	Hilton et al. 2018	182	182	ACT
	Planck Collaboration et al. 2016	1 653	1 094	Planck
	Bleem et al. 2015	677	649	SPT
	Hasselfield et al. 2013	91	91	ACT
Optical & Infrared catalogs	Marriage et al. 2011	23	23	ACT
	Oguri et al. 2018	1 921	1 921	HSC
	Oguri 2014	71 743	71 743	SDSS
	Rykoff et al. 2016	26 898	26 898	SDSS
	Rykoff et al. 2014	25 325	25 325	SDSS
	Wen et al. 2018	47 600	47 600	2MASS, WISE, SuperCOSMOS
	Wen & Han 2015	25 419	25 419	SDSS
	Wen et al. 2012	132 684	132 684	SDSS
	Abell 1958; Abell et al. 1989	5524	875	-



Growth Curve Analysis - steps



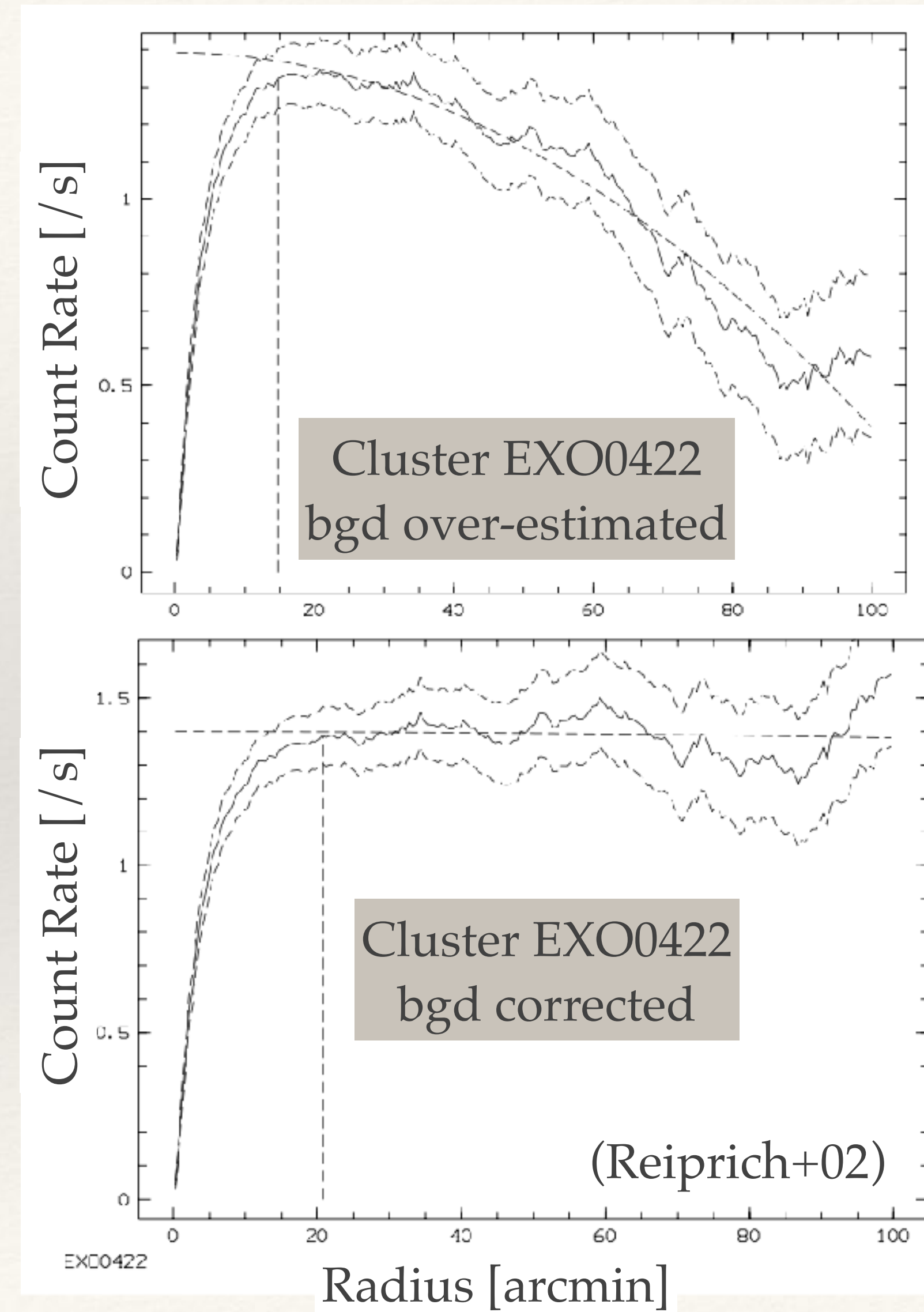
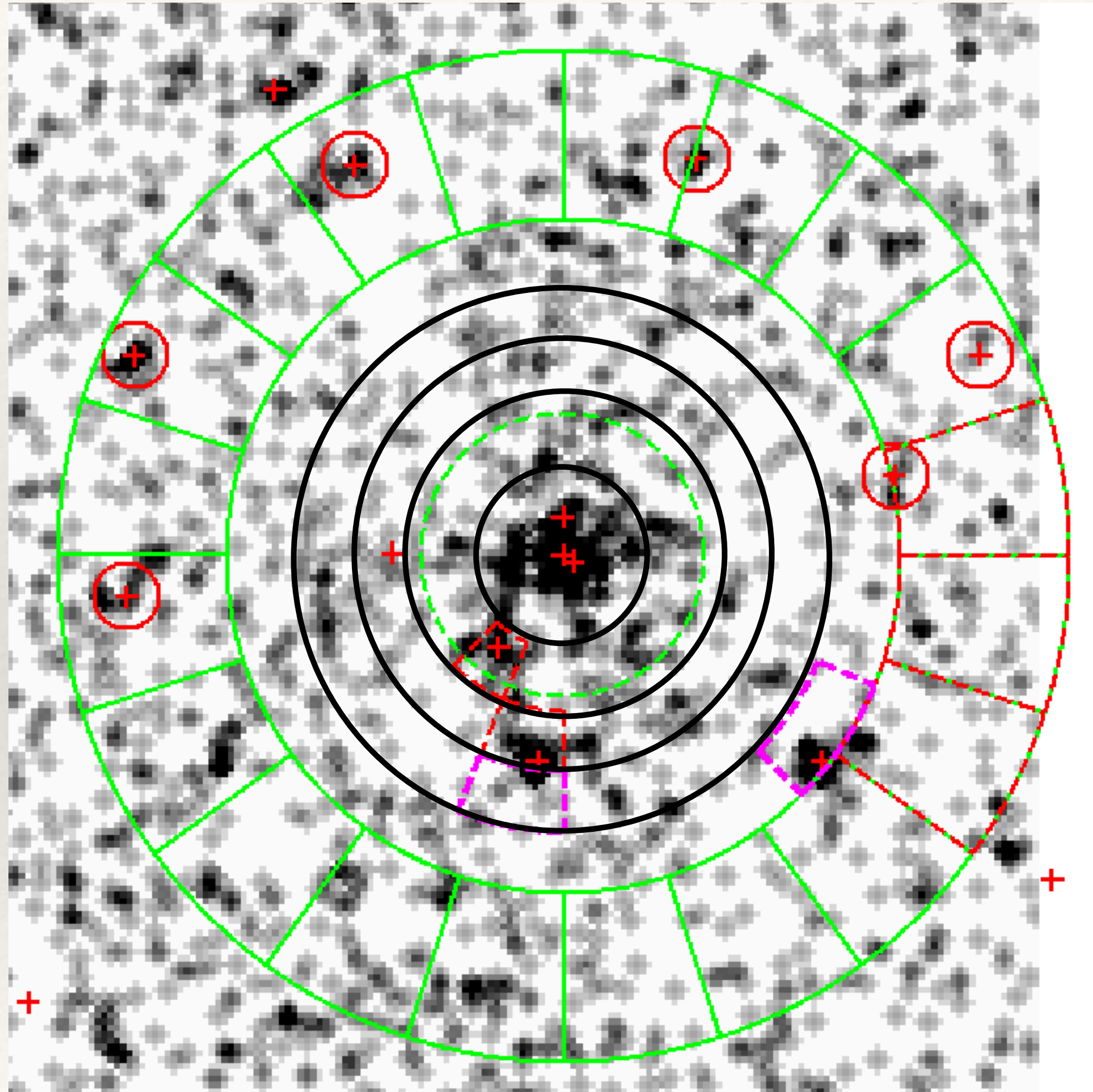
1. Background estimation in annulus, 20 sectors.

- ❖ Remove point sources,
- ❖ Remove sectors out of $\text{med} \pm 3\sigma$

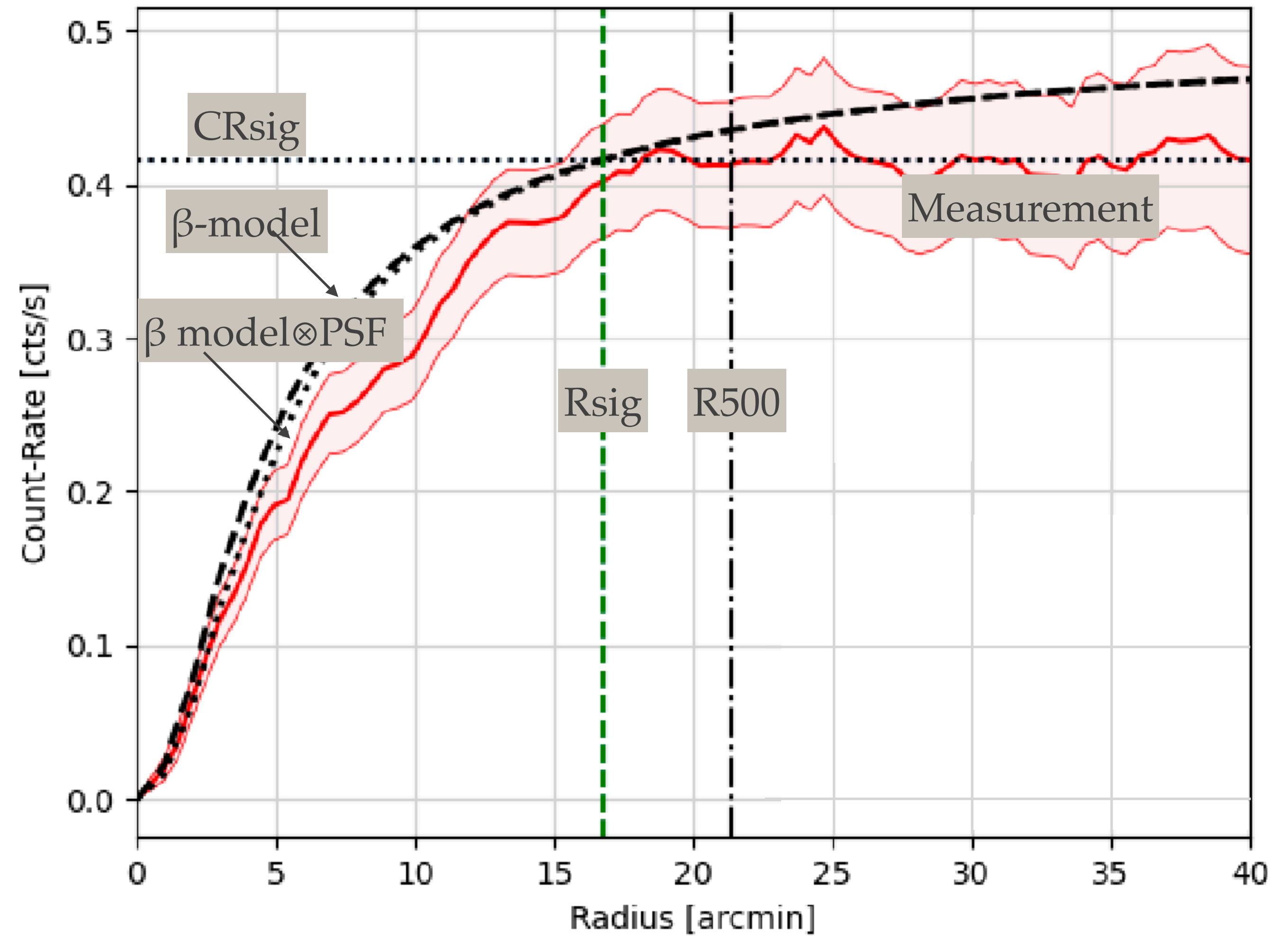
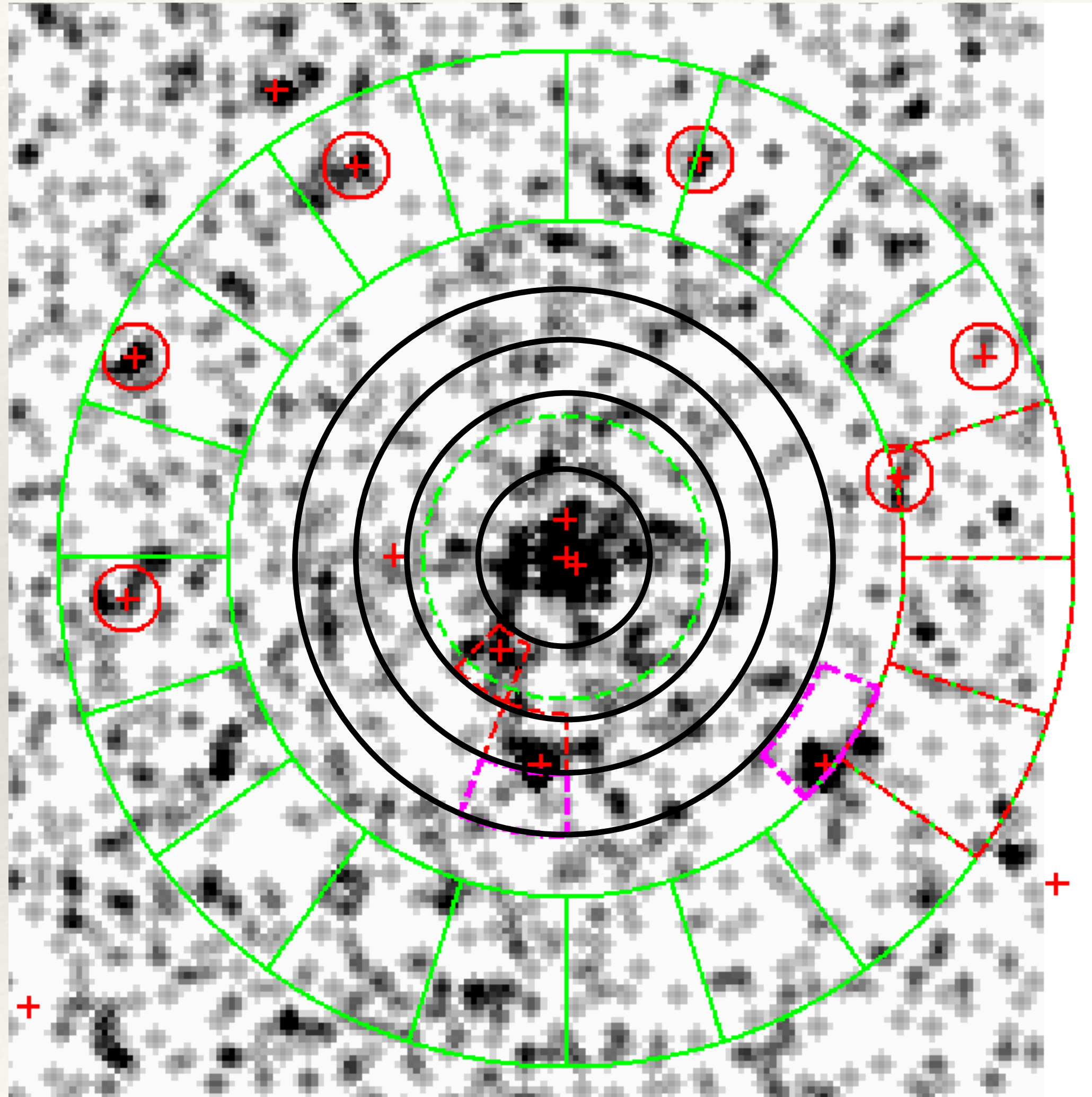
2. Growth curve of source

- ❖ 4 annulus, 16 sector each.
- ❖ Remove point sources,
- ❖ Remove sectors out of $\text{med} \pm 3\sigma$
- ❖ Remove more sectors manually.

Growth Curve Analysis - correction

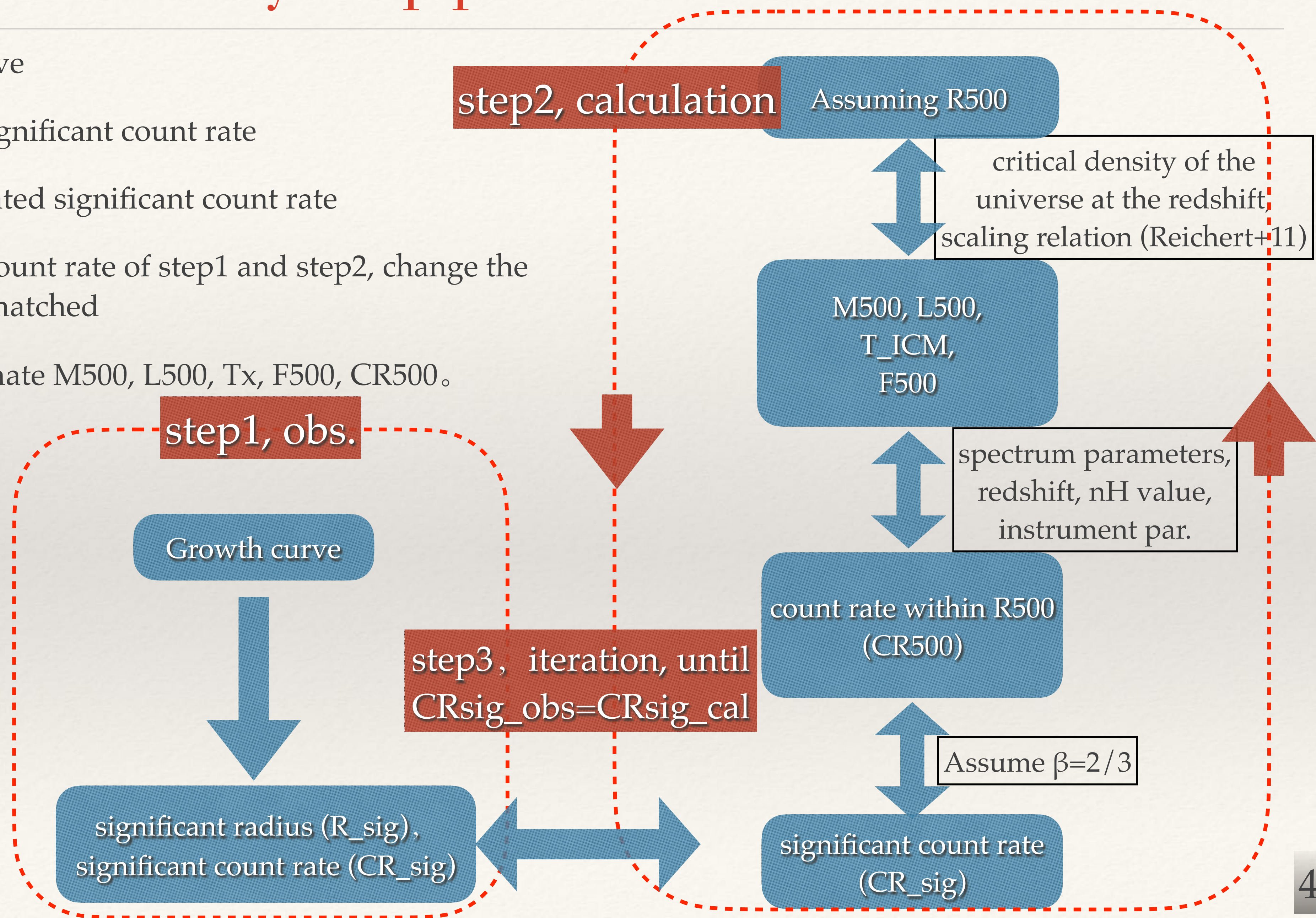


Growth Curve Analysis - example



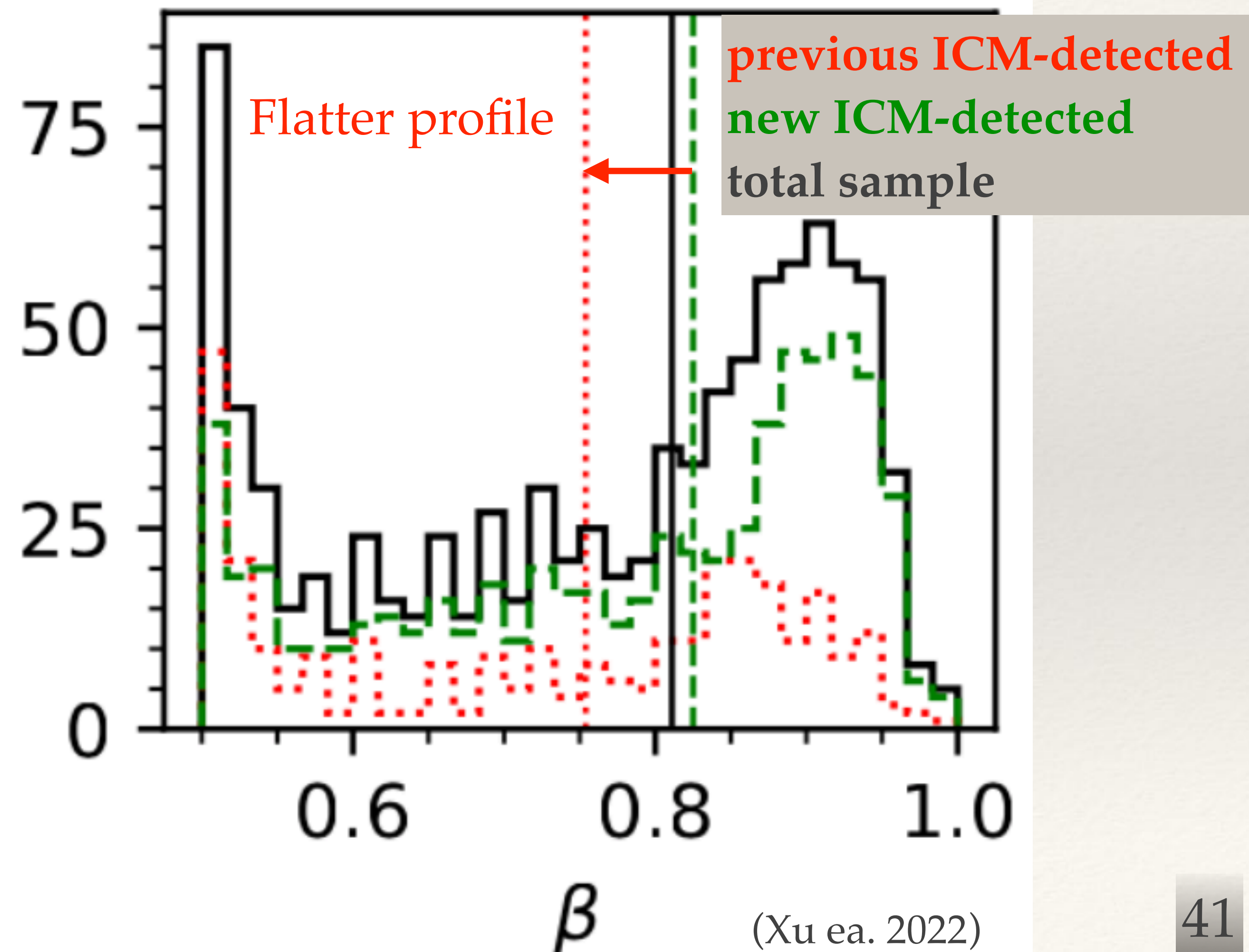
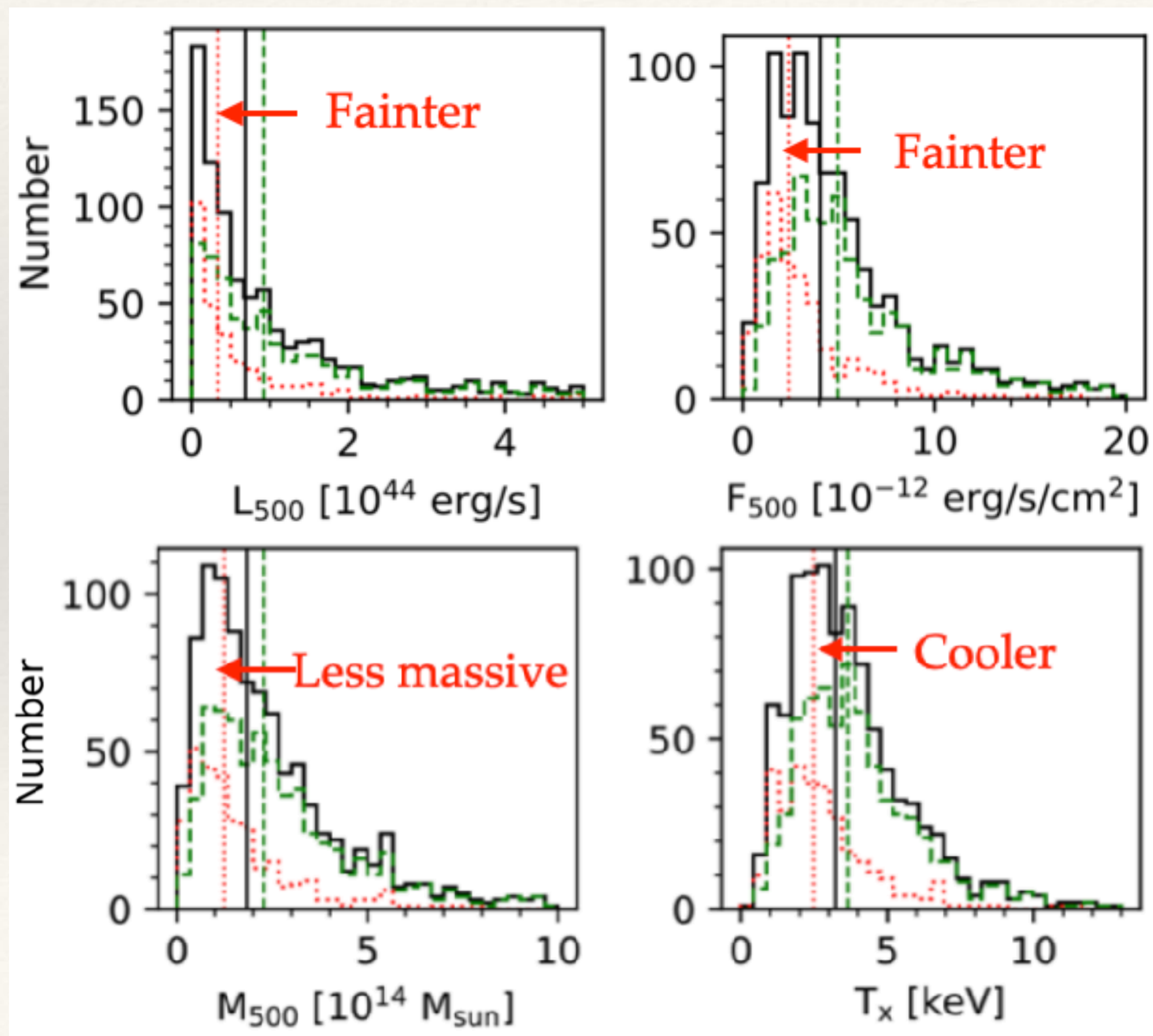
Growth Curve Analysis - pipeline for characterization

1. Plateau of the growth curve
=> significant radius, significant count rate
2. Assuming R500 => estimated significant count rate
3. Compare the significant count rate of step1 and step2, change the R500 of step2, until they matched
4. Using R500 of step2, estimate M500, L500, Tx, F500, CR500.

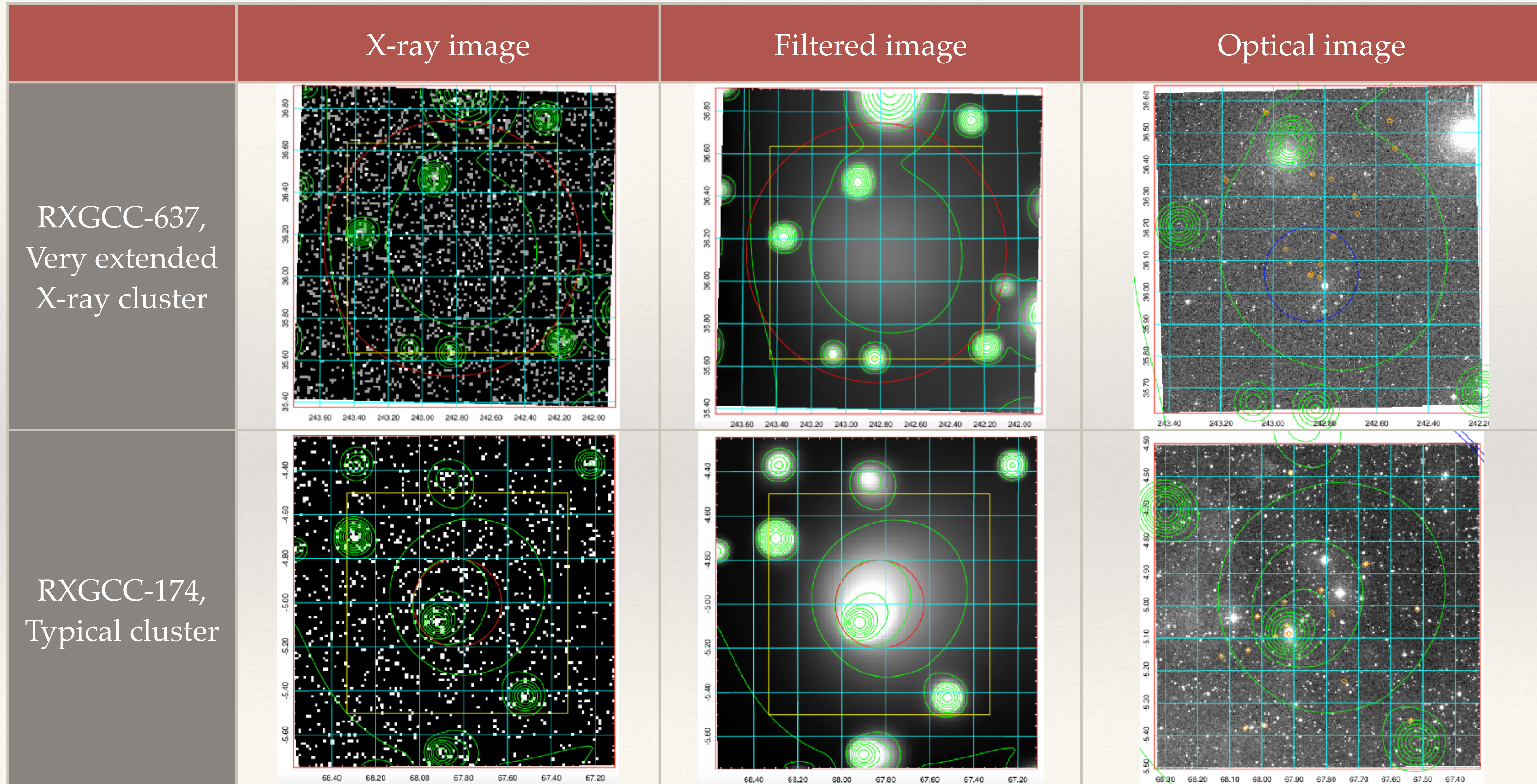


Parameter distribution of RXGCC clusters

- ❖ Compared with previous ICM-detected clusters, RXGCC new ICM-detected cluster systematically X-ray fainter, less massive, with lower temperature and flatter brightness profile.

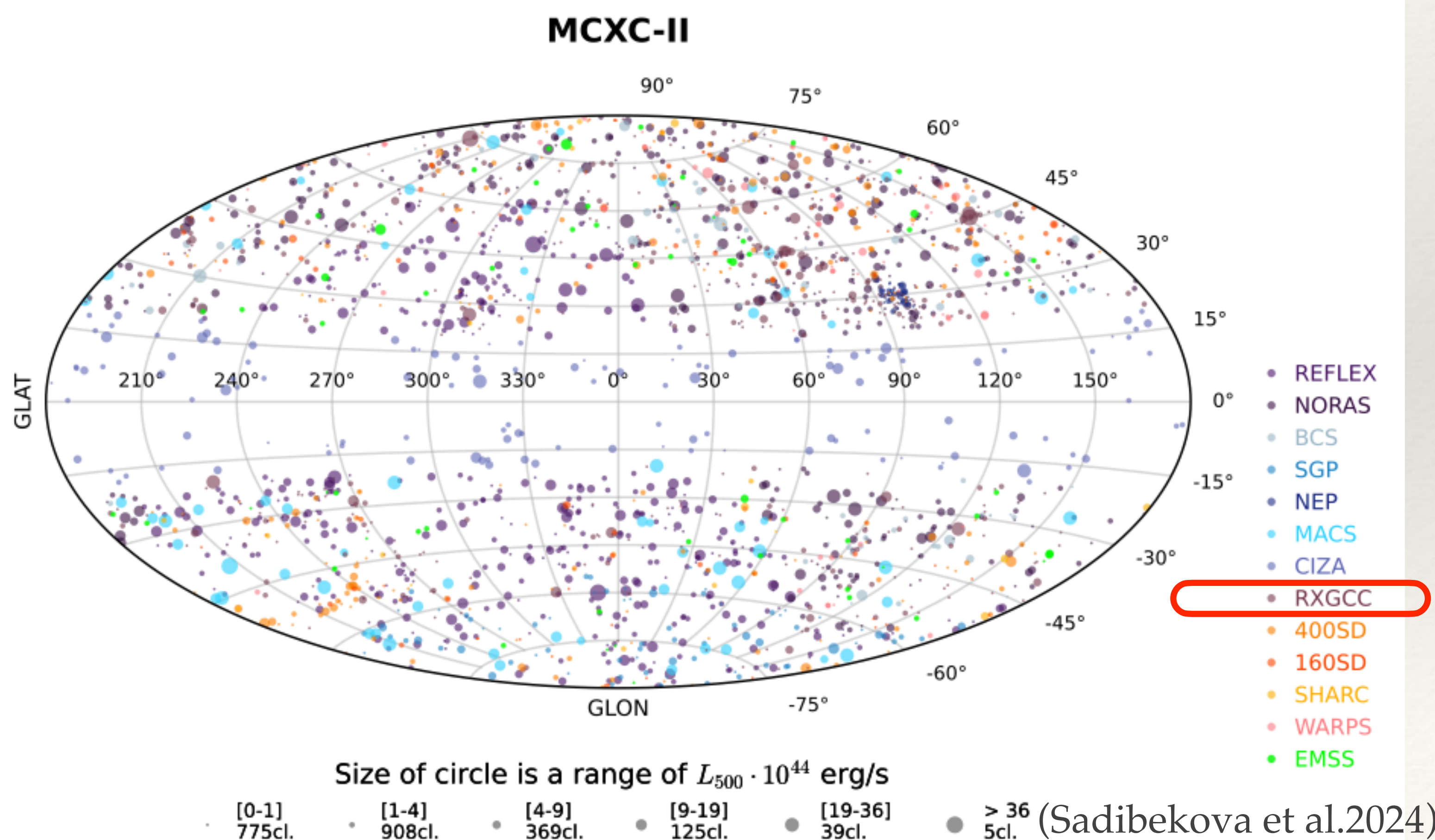
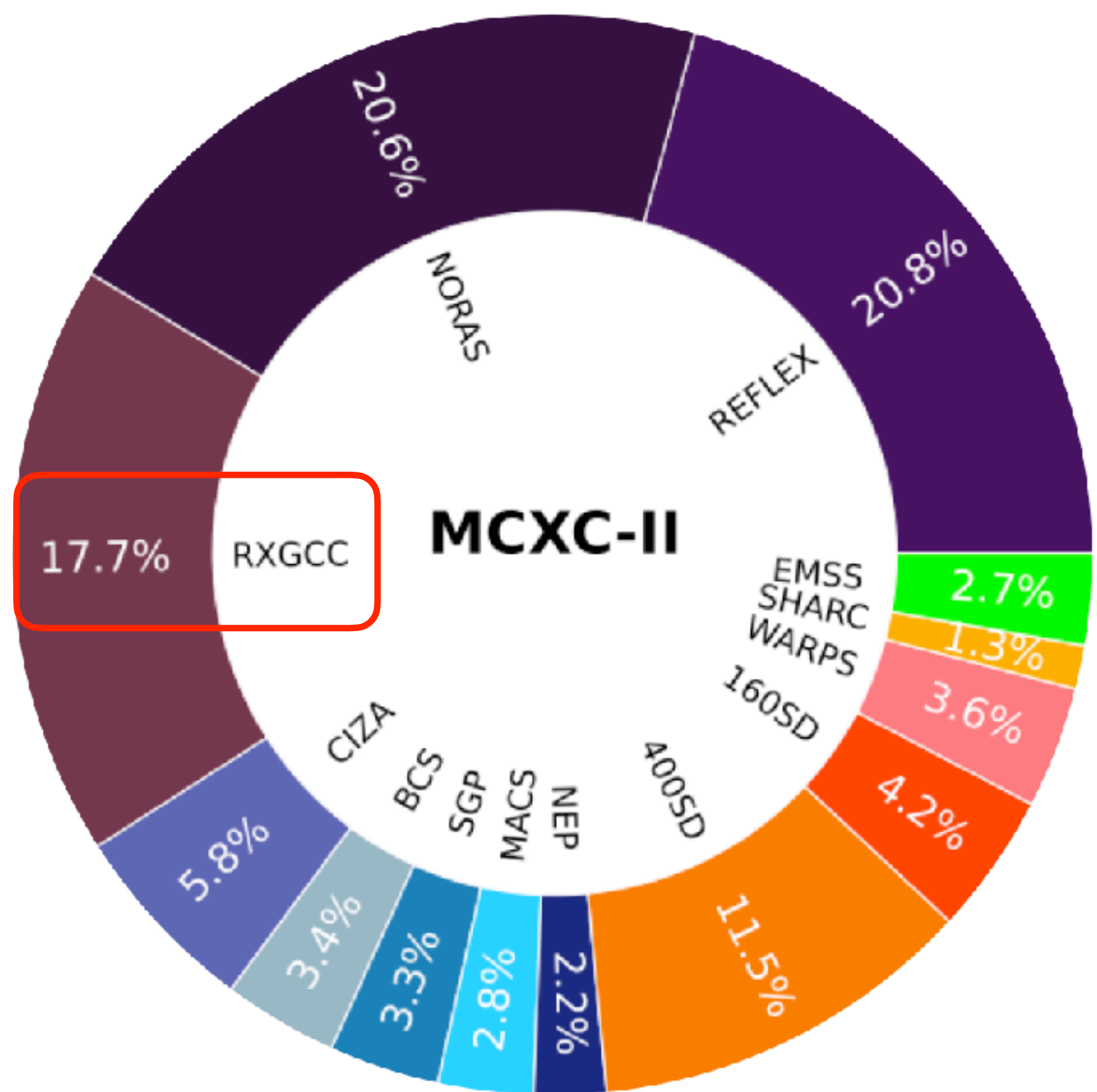


Example of comparison between extended/typical X-ray clusters

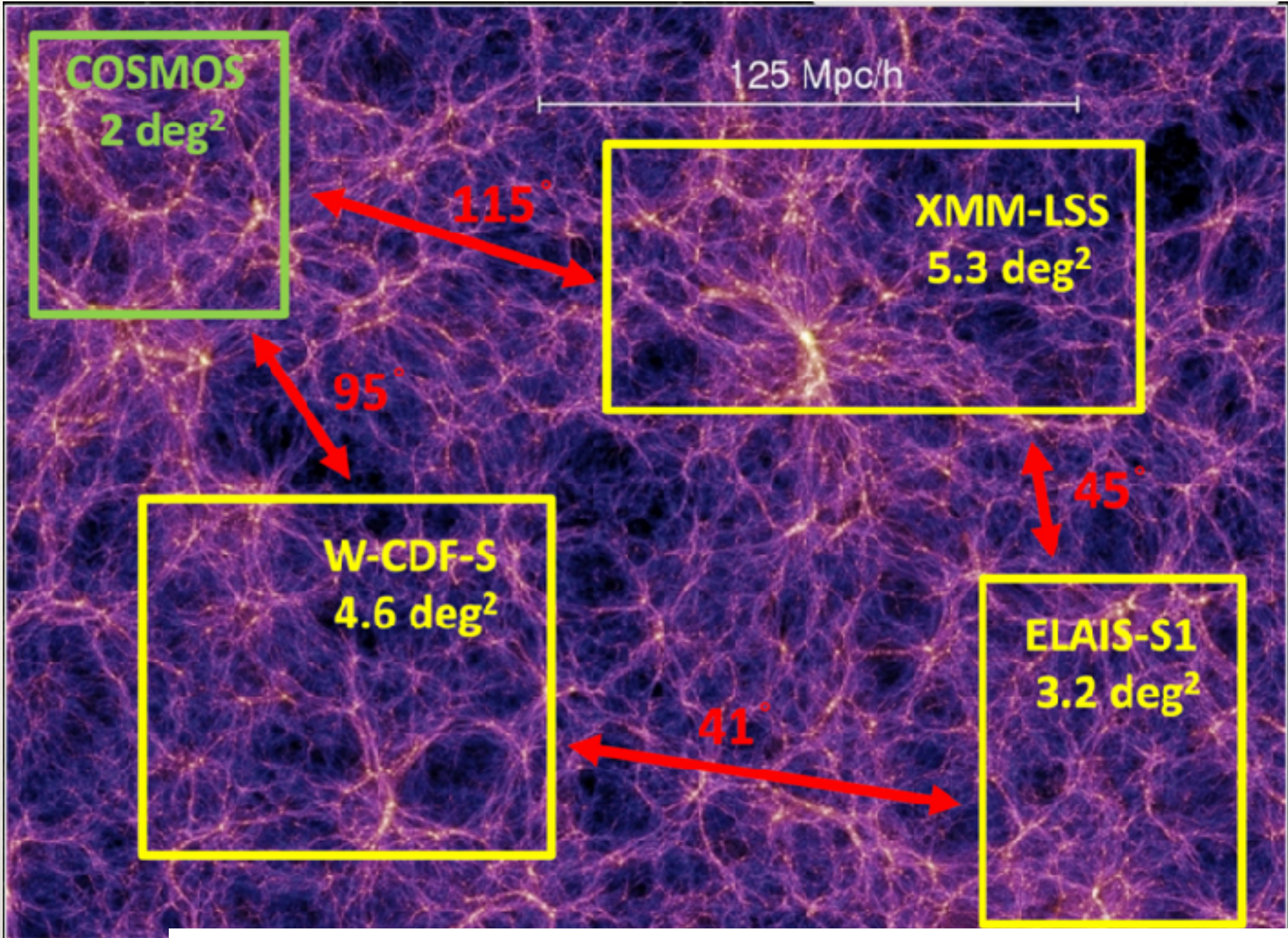


MCXC II

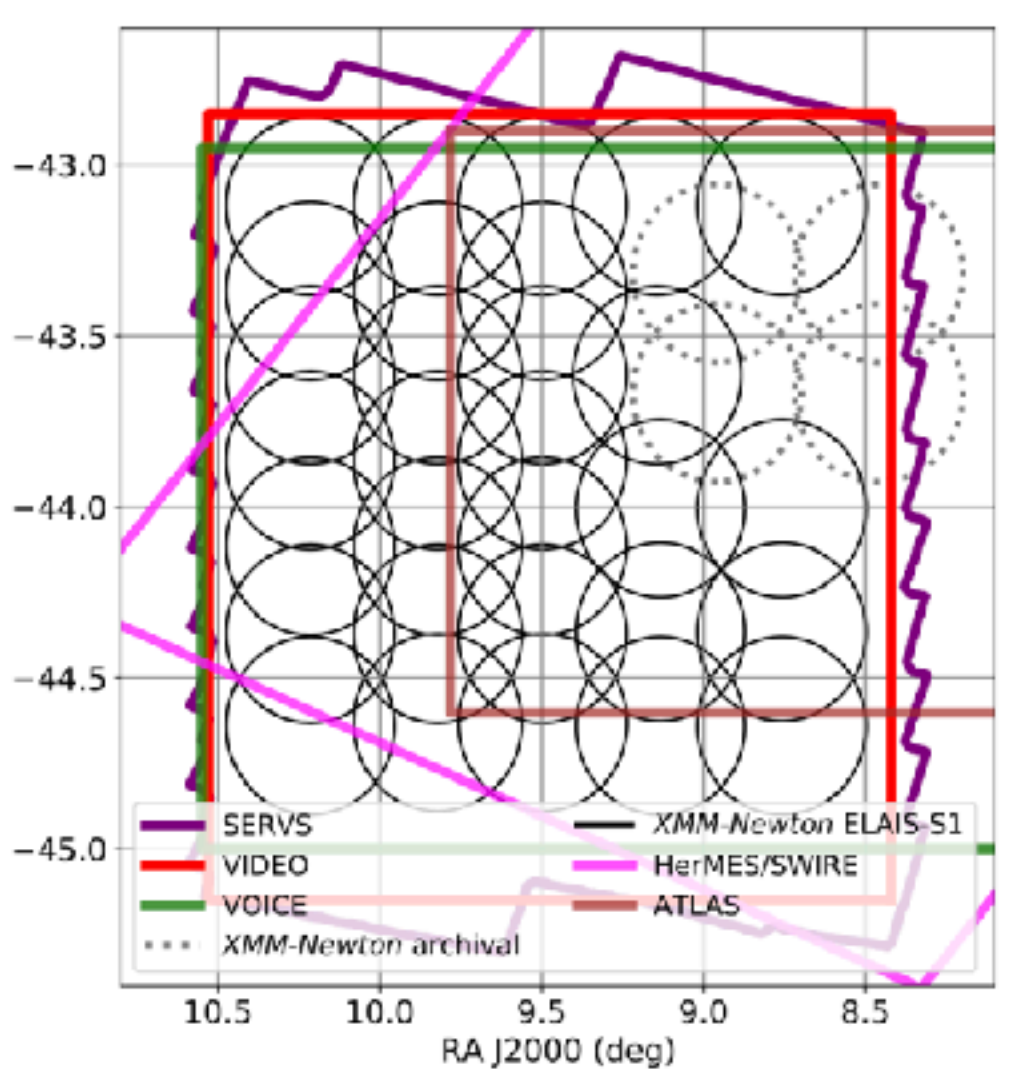
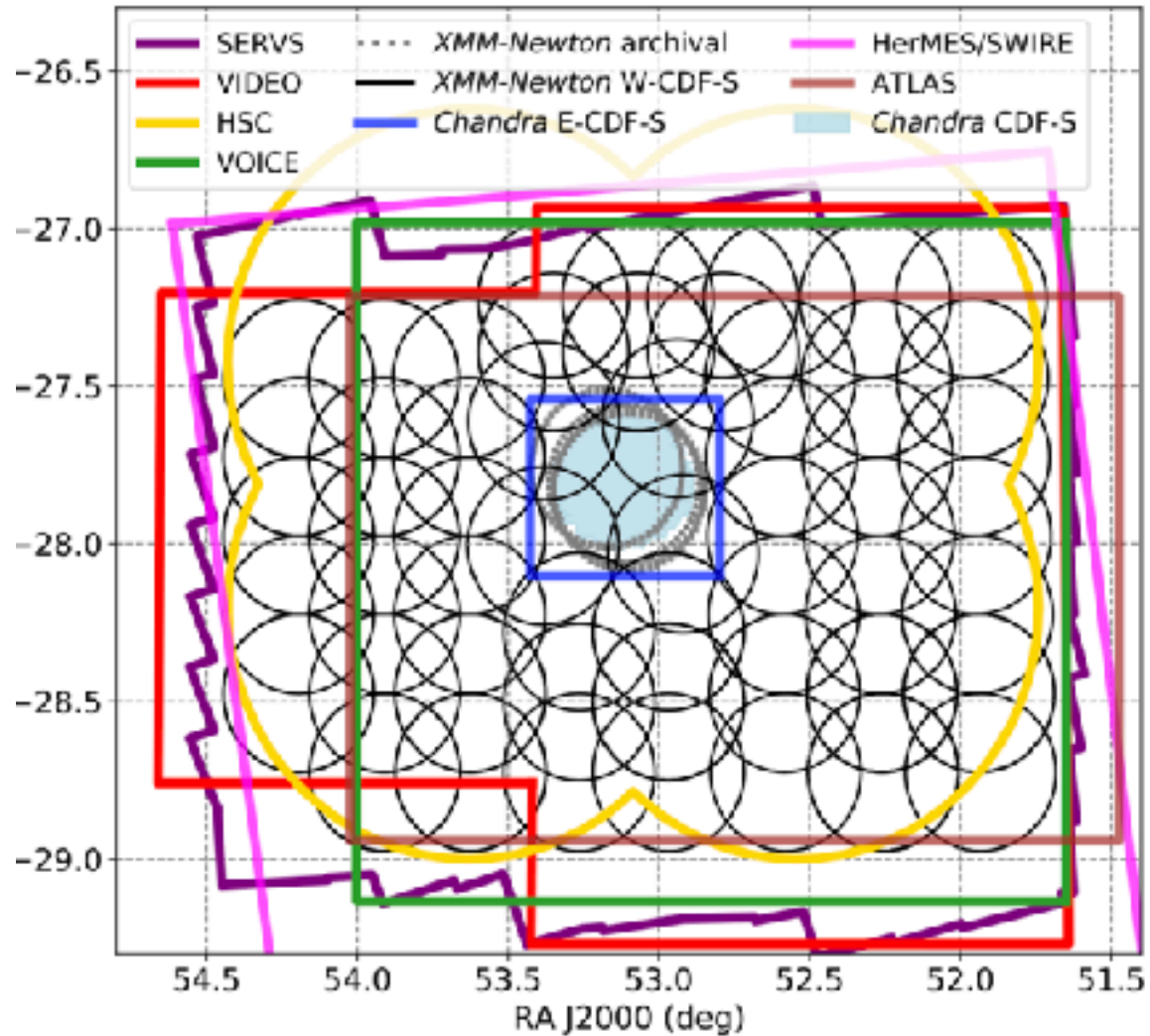
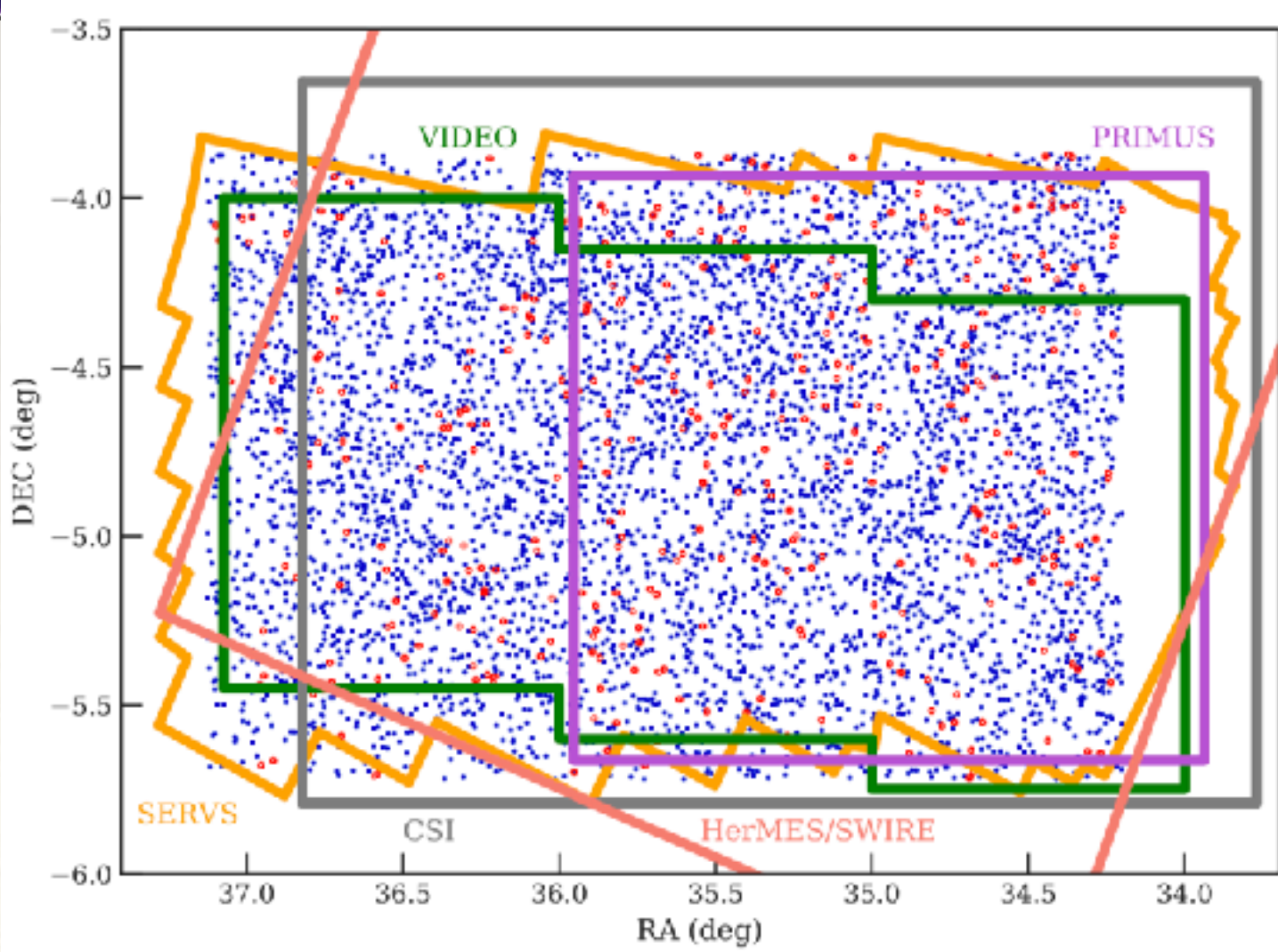
- ❖ MCXC-II, the second release of the Meta-catalogue of X-Ray detected Clusters of galaxies, is compiled from publicly available ROSAT All Sky Survey-based (NORAS, REFLEX, BCS, SGP, NEP, MACS, CIZA, and RXGCC) and serendipitous (160SD, 400SD, SHARC, WARPS, and EMSS) X-ray cluster catalogues.



XVXGC (XMM-SERVS X-ray eXtended Galaxy Cluster catalog)

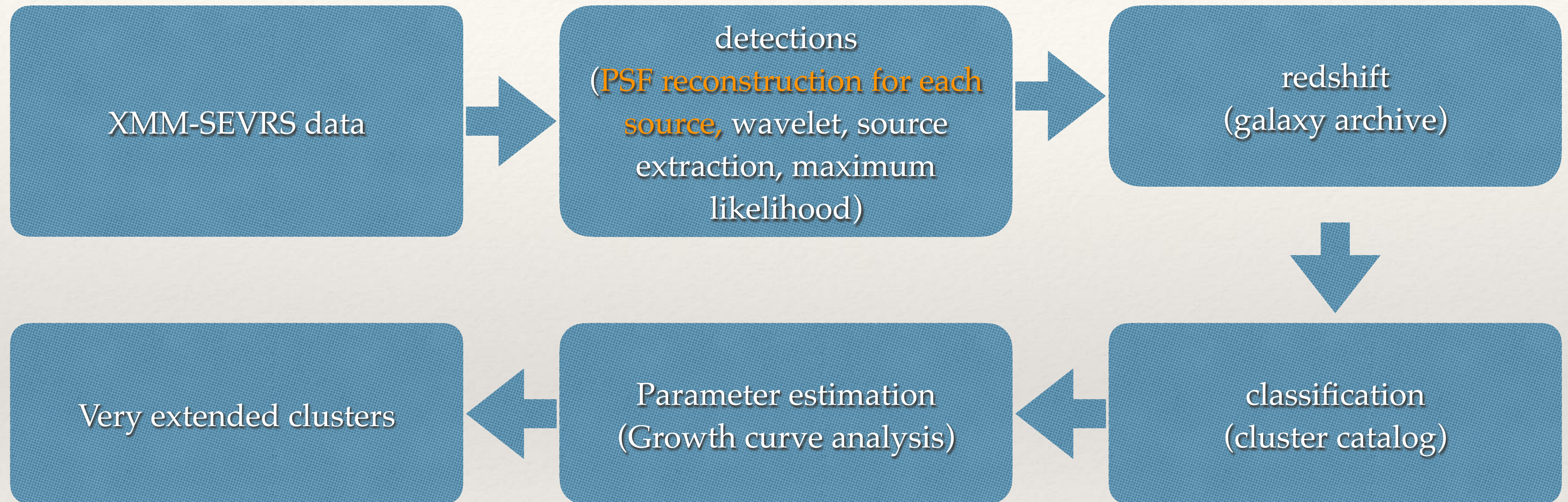


	XMM-LSS	W-CDF-S	ELAIS-S1
Coverage (deg ²)	5.3	4.6	3.2
Exposure (Ms, flare-filtered)	2.7	1.8	0.9
Flux limit (erg / s / cm ² , 0.5-10 keV)	6.5E-15	1.0E-14	1.3E-14



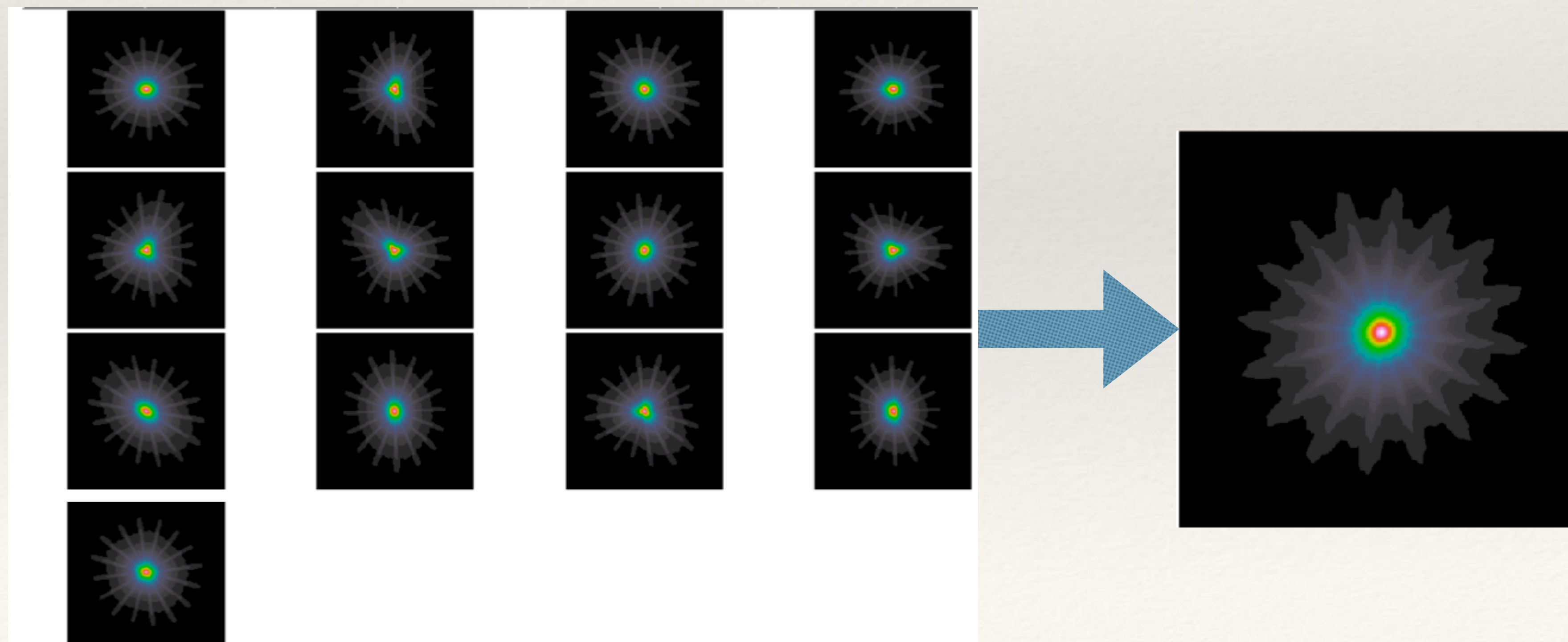
Pipeline for XVXGC

- ❖ XVXGC (XMM-SERVS X-ray eXtended Galaxy Cluster catalog)



PSF reconstruction - example

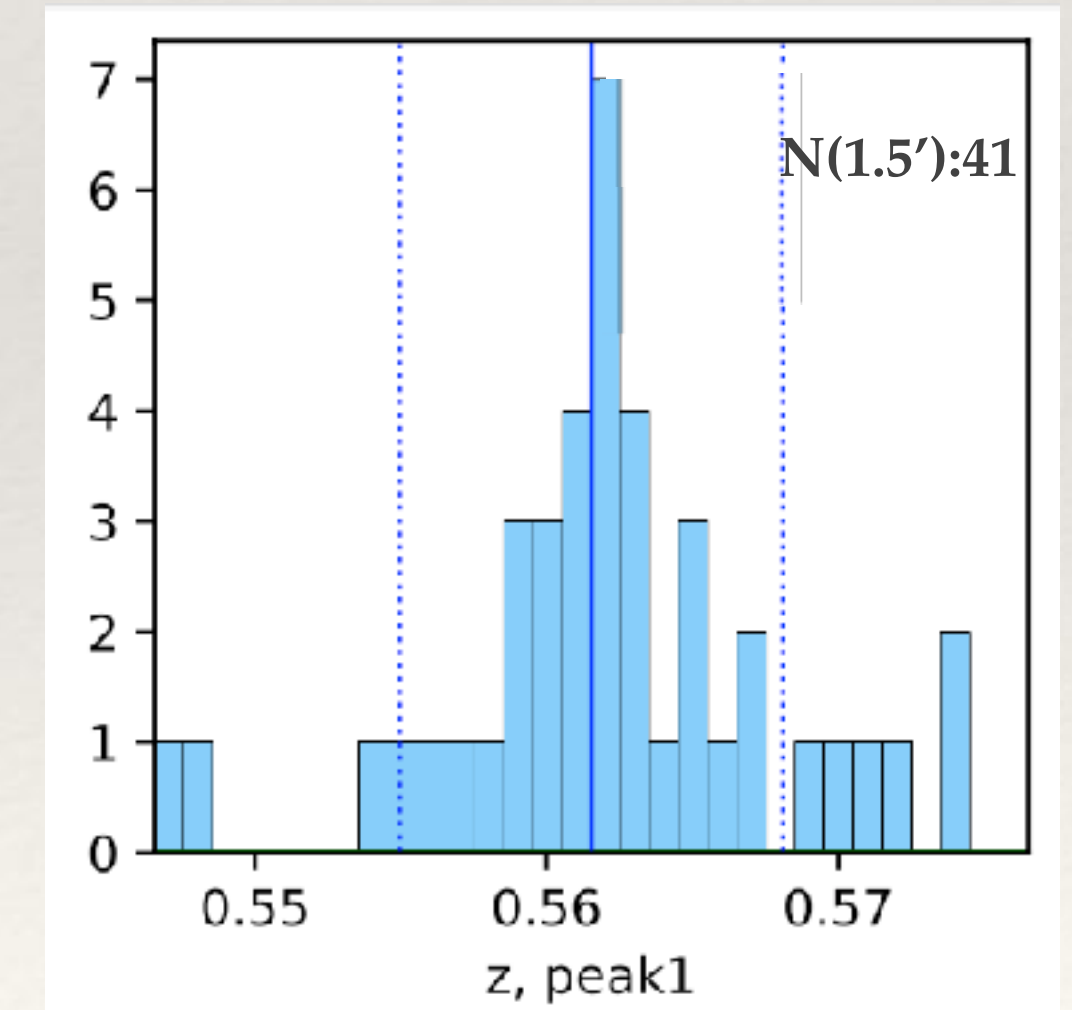
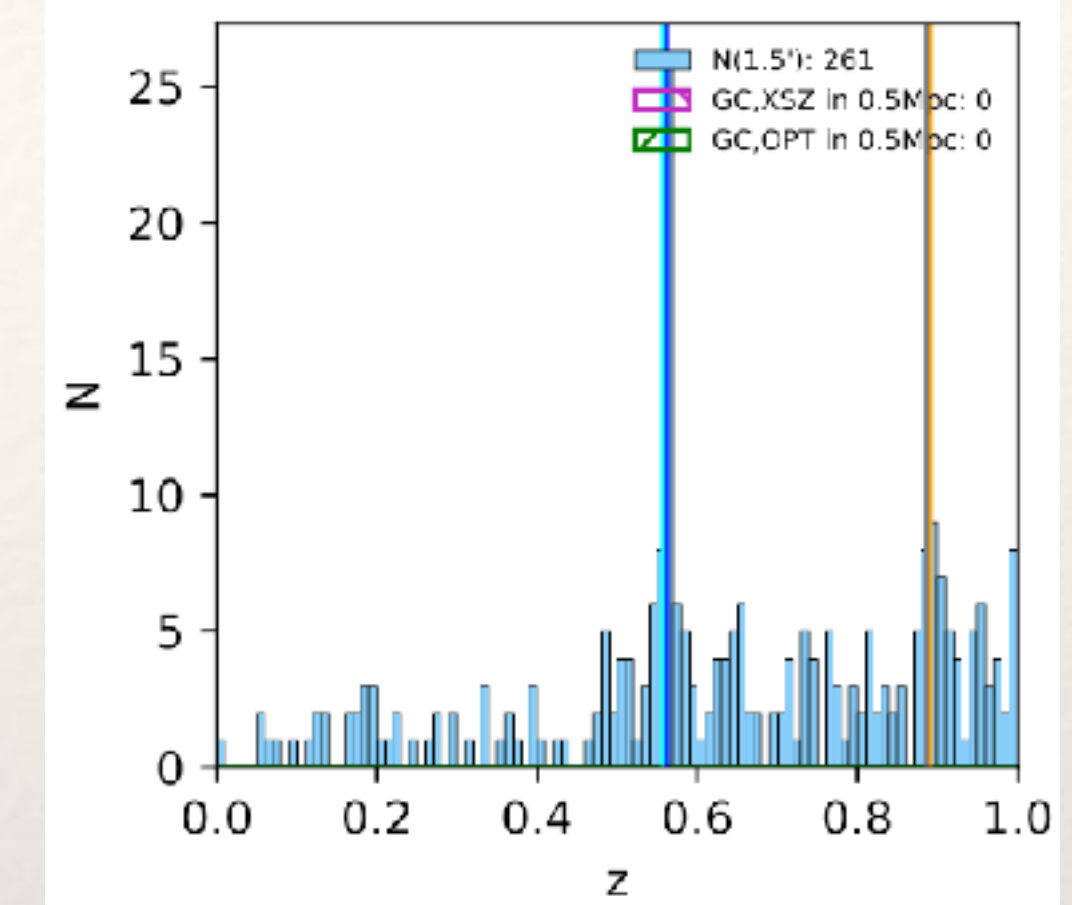
- ❖ PSF reconstruction for one source:
 - ❖ multiple detector (MOS1、MOS2、PN)
 - ❖ multiple exposures (offset and angle on the detector)
 - ❖ => the combined PSF weighted with exposure maps.
- ❖ The total PSF is taken as the input of third step (maximum likelihood fitting) , to estimation the parameters (extension likelihood, extend) to distinguish point sources and extended sources.



Redshift determination

Table 1. Overview of galaxy redshifts from literature and NED database*.

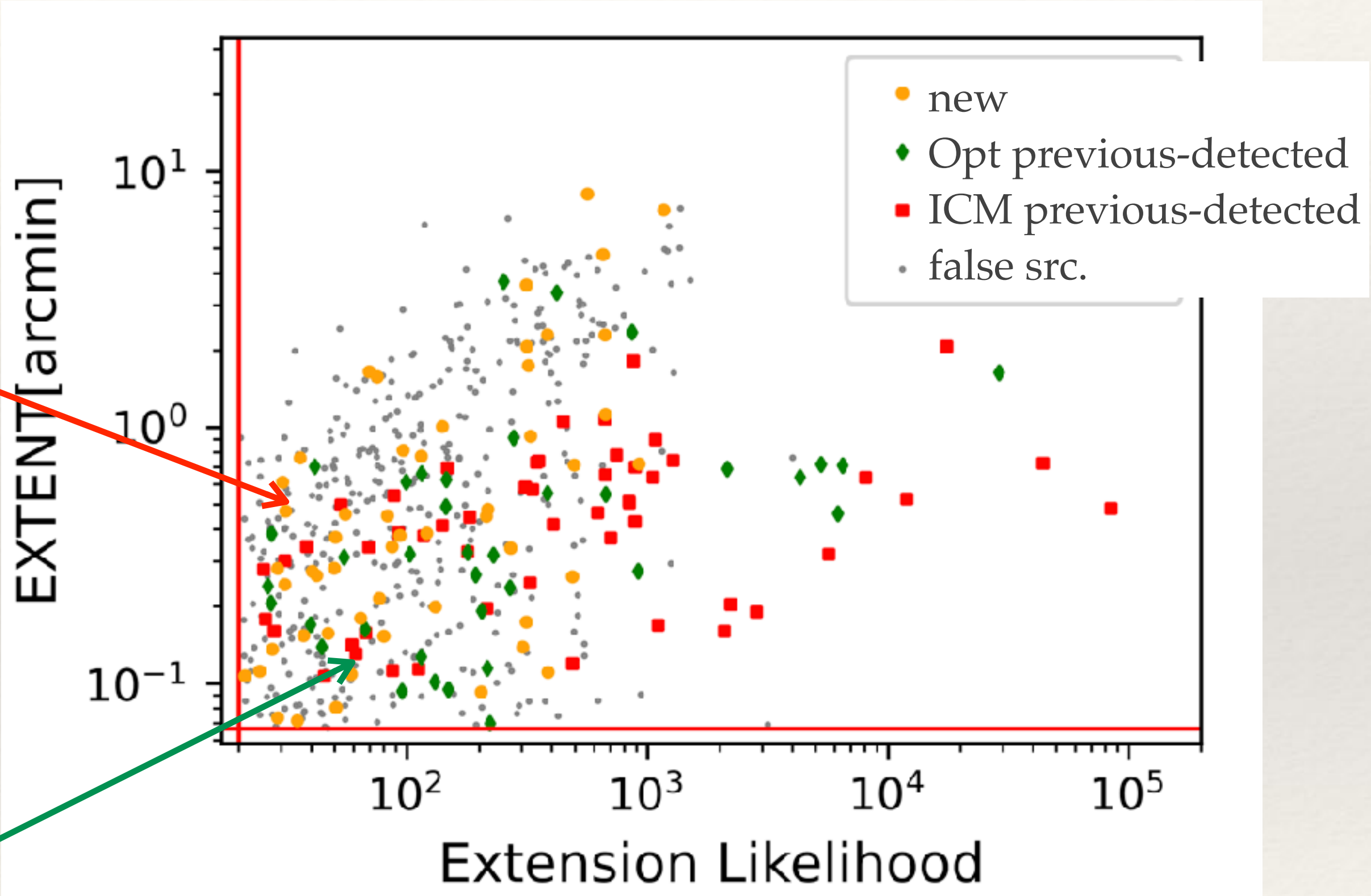
z	Catalogs	N(XMM-LSS) ^a	N(W-CDF-S) ^a	N(ES1) ^a	Reference
z_{sp}	-	0	29 888	10 579	Zou et al. (2021b)
	HELP	113 192	48 900	17 784	Shirley et al. (2021)
	SDSS DR17	10 893	0	0	Abdurro'uf et al. (2021)
	DESI	13 642	1 335	187	Zou et al. (2019)
	-	42 985	0	0	Chen et al. (2018)
	VIPER	24 963	0	0	Scodeggio et al. (2018)
	GAMA	10 108	0	0	Baldry et al. (2018)
	2MPZ ^b	167	231	70	Bilicki et al. (2014)
	PRIMUS	30 939	17 089	6 954	Coil et al. (2011)
	SXDF 100 μ Jy	315	0	0	Simpson et al. (2006, 2012)
	VVDS	8 472	1 160	0	Le Fèvre et al. (2013)
	6dFGS	139	53	79	Jones et al. (2004)
	2dFGRS	0	1 215	144	Colless et al. (2001)
	NED	3 589	2 191	437	-
	N _{sum} (z_{sp}) ^c	-	135 323	55 401	20 172
z_{ph}	-	0	755 714	806 695	Zou et al. (2021b)
	HELP	4 703 183	131 296	928 889	Shirley et al. (2021)
	SDSS DR17	164 521	0	0	Abdurro'uf et al. (2021)
	DESI	212 720	217 615	146 496	Zou et al. (2019)
	-	347 915	0	0	Chen et al. (2018)
	UDF	0	9 969	0	Rafelski et al. (2015)
	CFHTLS	1 673 935	0	0	Ilbert et al. (2006); Coupon et al. (2009)
	ISO	0	0	147	La Franca et al. (2004)
	NED	25 700	18 727	7 966	-
N _{sum} (z_{ph}) ^c	-	7 116 131	1 132 723	1 888 701	-



(Xu +24)

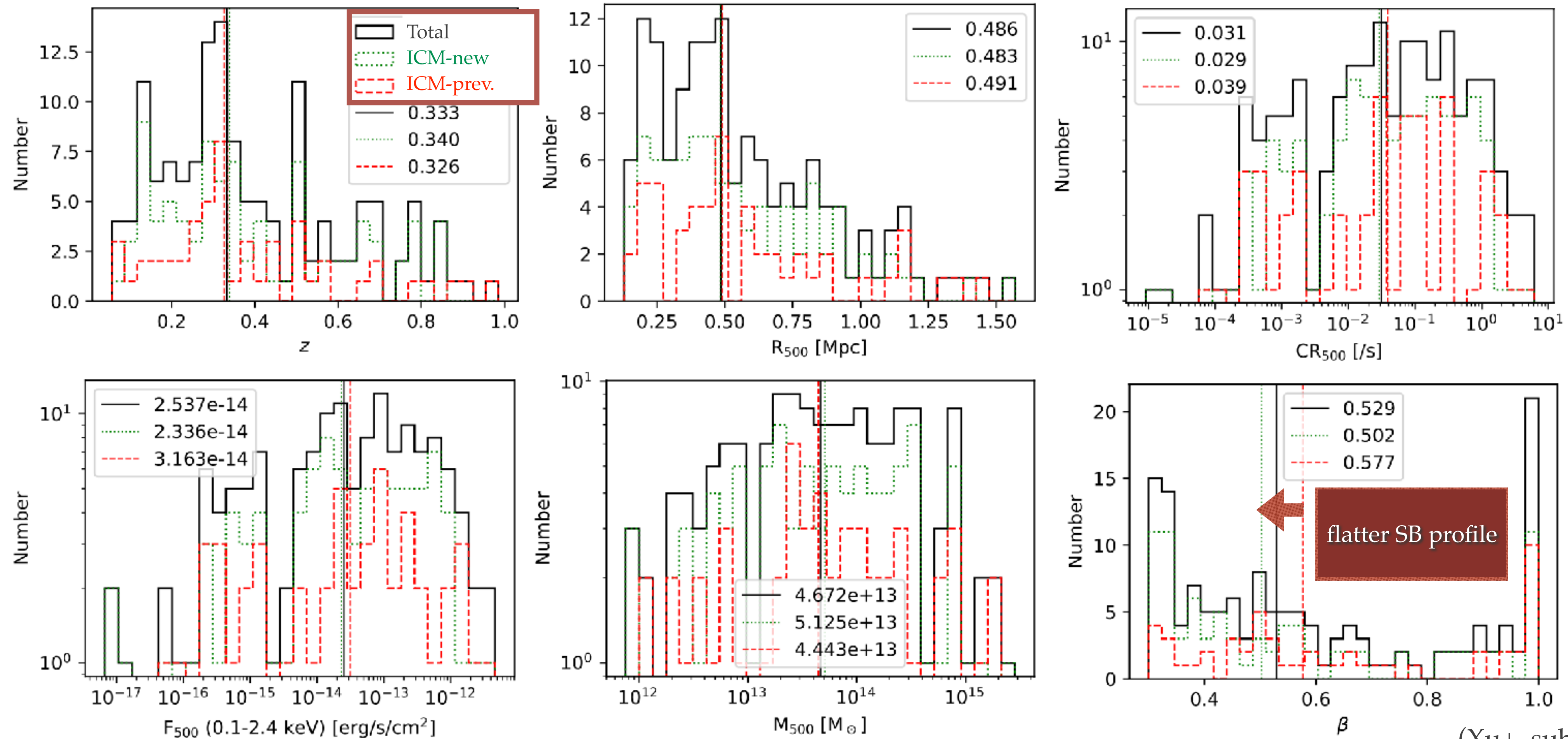
Classification with previous catalogs

		In XMM-LSS	W_CDF_S	ES1	Survey
Catalogs	Number	N(XMM-LSS)	N(W-CDF-S)	N(ES1)	
Xray GC	X-ray cluster	12 247	0	26	4
		944	0	0	0
		1 559	34	8	6
		10 382	11	0	0
		302	92	0	0
		1 490	5	0	1
		107	26	0	0
		46	0	46	111
		904	0	0	0
		503	32	0	5
		422	14	1	3
		1 743	1	4	0
		57	57	0	0
		242	0	4	0
		579	0	0	0
		283	0	0	0
		-	85	22	1
	N _{sum}	-	357	111	20
SZ GC	SZ cluster (detected in Microwave)	4 195	10	1	6
		2 323	1	0	2
		225	0	0	0
		182	8	0	1
		1 653	1	0	0
		1 227	1	0	1
		189	0	0	0
		677	0	0	4
		91	0	0	0
		23	0	0	0
		-	0	0	4
	N _{sum}	-	21	1	20
OPT GC	OPT/IR cluster (detected by members)	189	65	65	50
		1 921	135	0	0
		19	0	19	0
		71 743	76	0	0
		26 898	56	0	0
		25 325	36	0	0
		47 600	28	0	0
		25 419	25	0	0
		2 092	4	0	0
		132 684	150	0	0
		13 340	2	2	2
		-	577	94	21
	N _{sum}	-	1 154	229	112
Xsrc	X-ray source	6 683	0	4 053	2 630
		5 242	5 242	4 053	2 630
		5 572	5 161	4 053	2 630
	N _{sum}	-	10 404	4 053	2 630



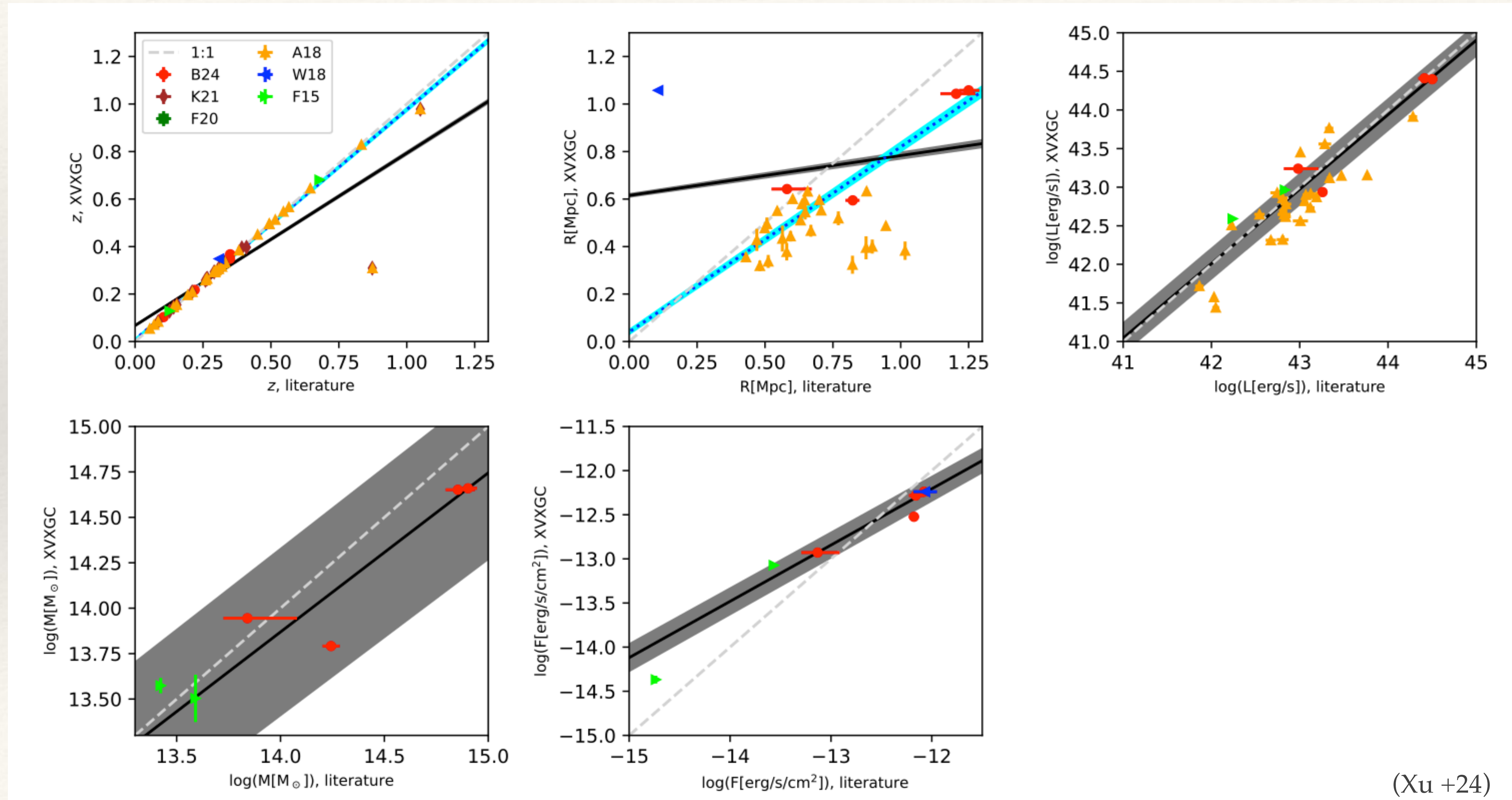
Parameter distribution

- ❖ Compared with previous ICM-detected clusters, the new ICM-detected XVXGC clusters tend to have flatter X-ray surface brightness profile.



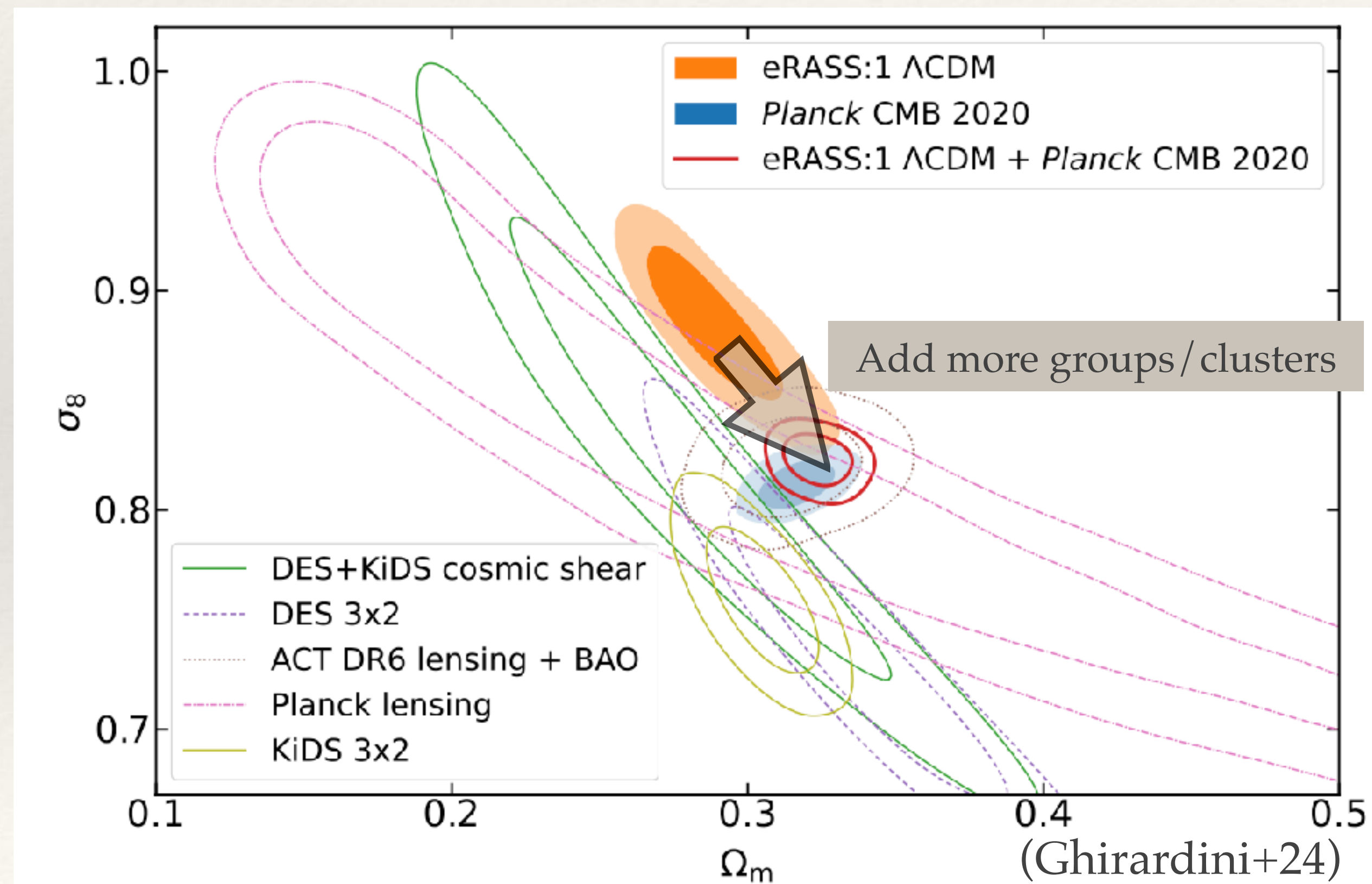
Parameter estimation

- ❖ consistent with previous works, no systematic bias.

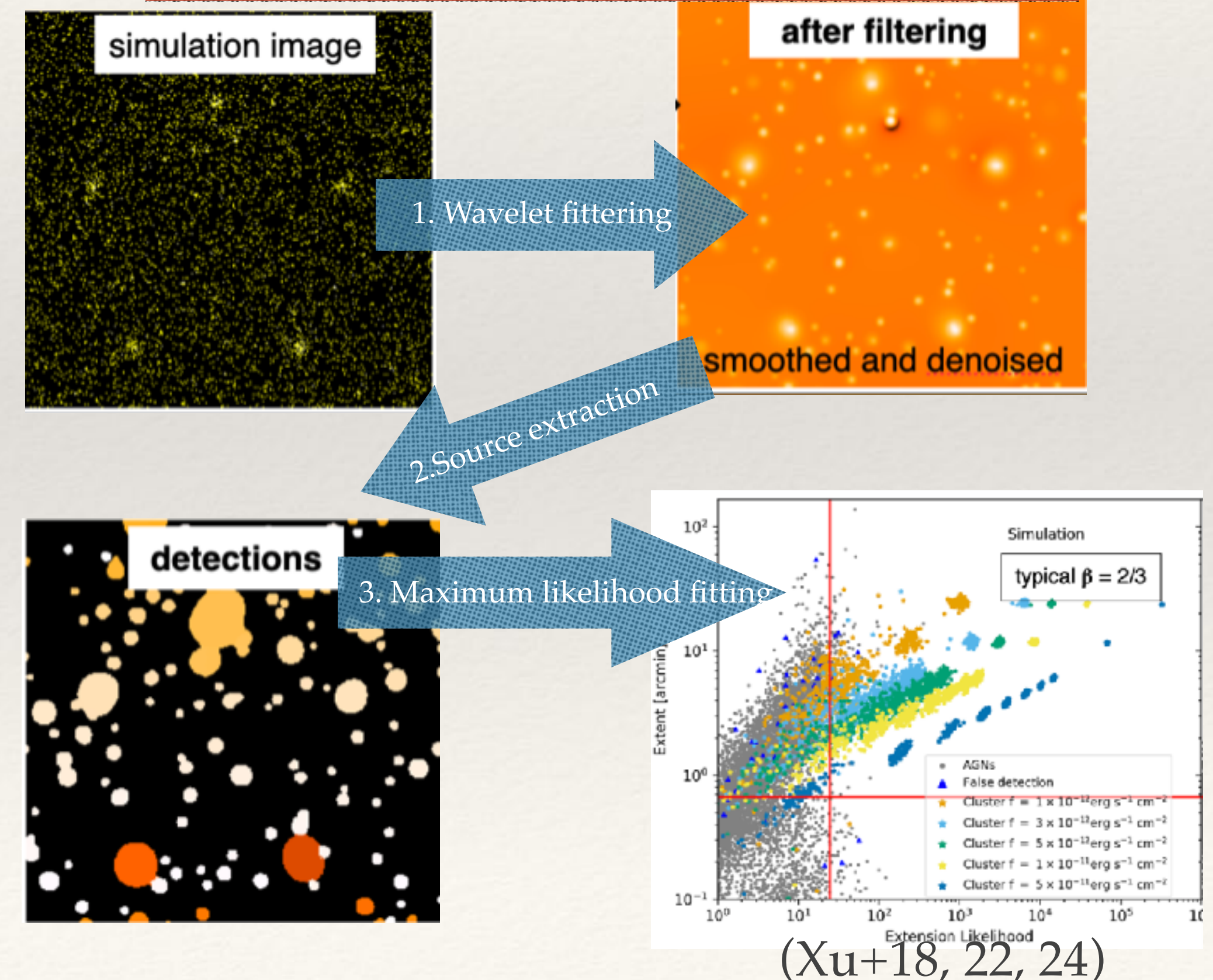


Summary: Detection of X-ray extended clusters

- Question: tension between cosmological parameters derived from cluster counts and the ones from primary CMB (Planck collaboration+14,15,20)
- One explanation: clusters samples might be incomplete.
- Our project: to search for very extended X-ray clusters that might be missed in previous ICM-based works.



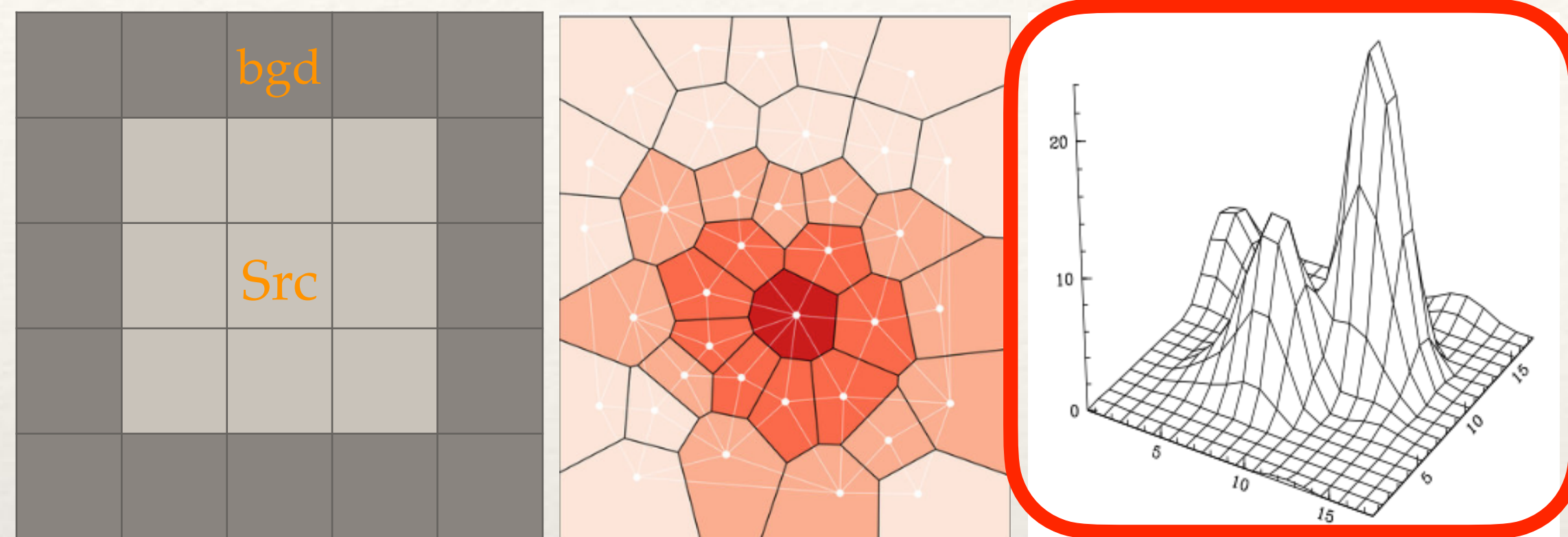
RXGCC/XVXGC catalog: wavelet-based, higher efficiency for extended src.



3.Summary

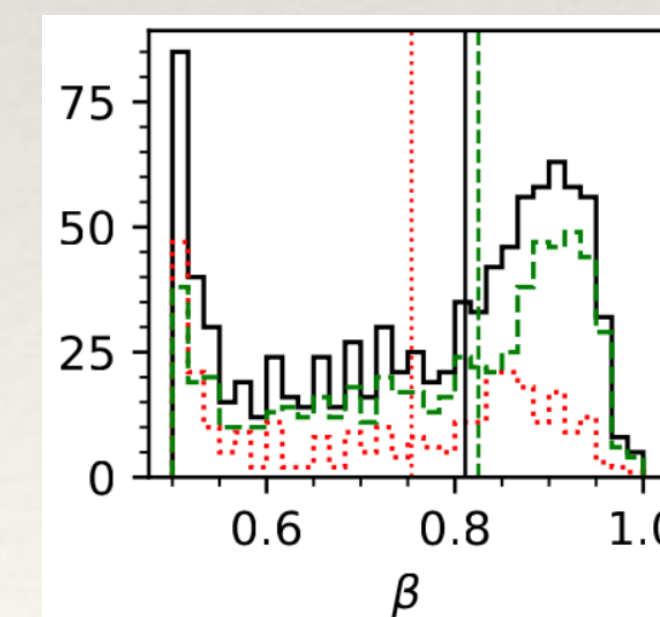
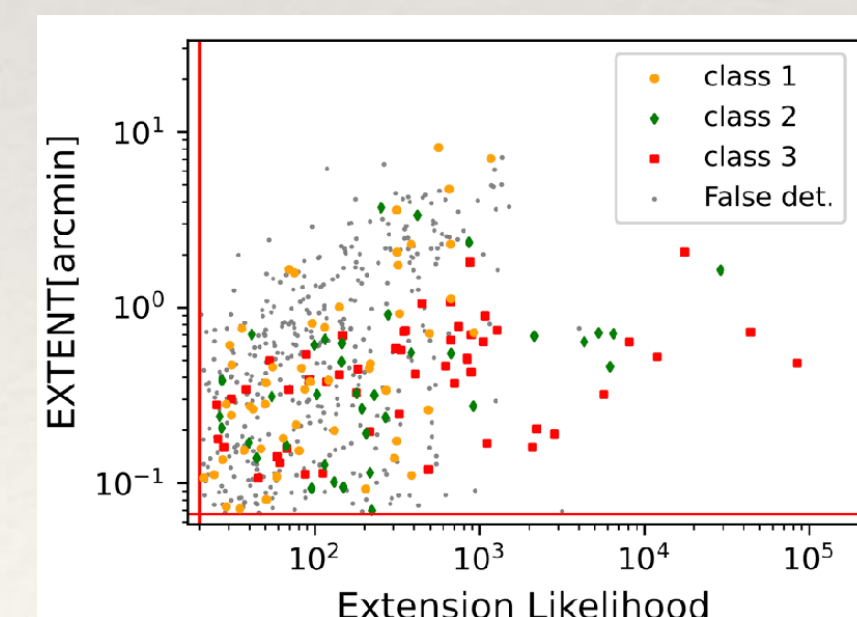
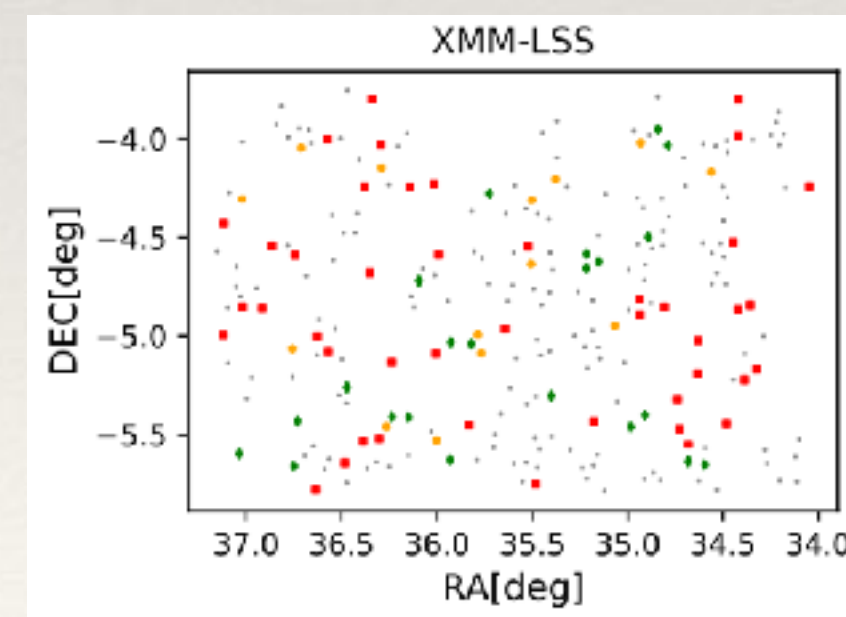
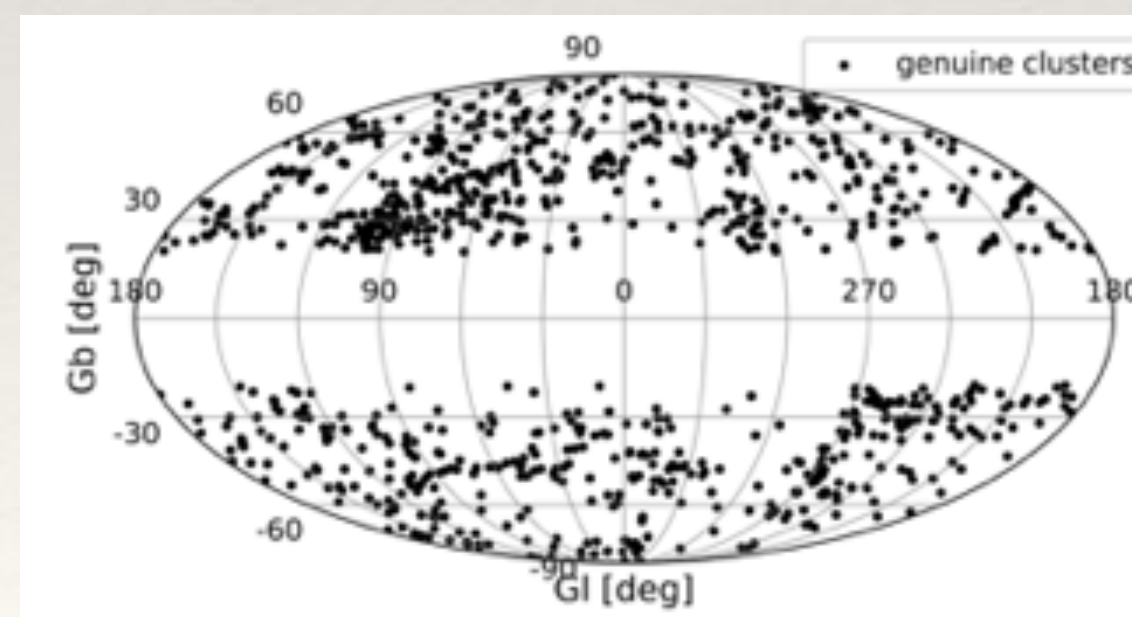
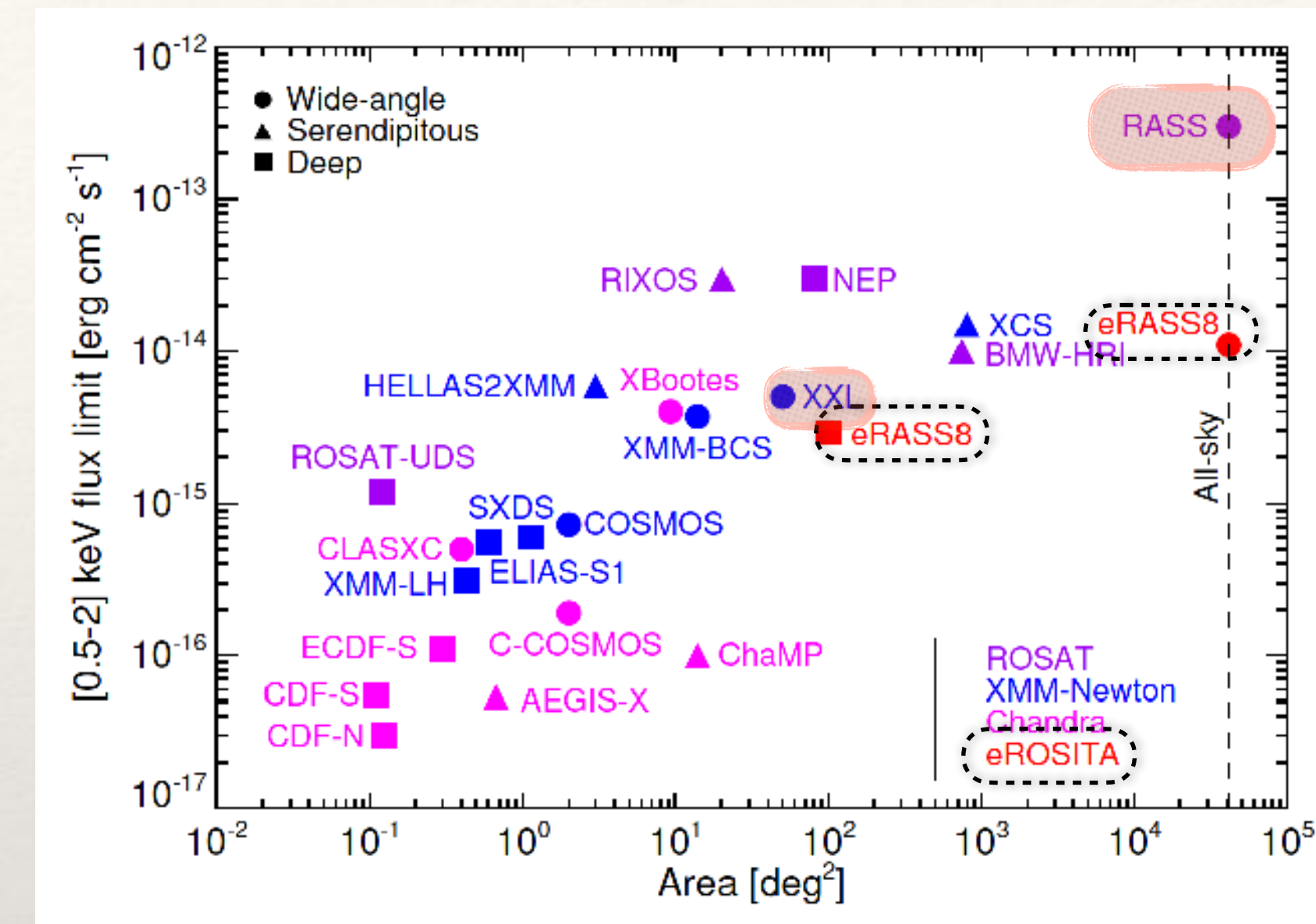
X-ray detection of galaxy clusters

- ❖ X-ray detection methods of galaxy clusters.



- ❖ The detection of X-ray extended clusters.

- RXGCC (RASS-based extended X-ray Galaxy Cluster Catalog)
- XVXGC (XMM-SERVS X-ray eXtended Galaxy Cluster catalog)



Contact me

- ❖ Weiwei Xu (徐伟伟)
- ❖ Computation Cosmological Group
- ❖ NAOC
- ❖ Orcid: 0000-0002-9587-6683
- ❖ Contact: wwxu@pku.edu.cn
- ❖ Research interest:
 - ❖ X-ray detection of clusters
 - ❖ Multi-bands researches of clusters
 - ❖ Dark matter halos
 - ❖ Cosmology
 - ❖ Filaments, gas bridge between clusters
 - ❖ Bullet-like clusters

Thanks